REALISTIC MODELS FOR POLARONS

by

Carl Joseph Chandler

A thesis submitted in partial fulfillment of the requirements for the degree of

Doctor of Philosophy

Department of Physics
University of Alberta

Abstract

Electrons interacting with the ions in a solid, or polarons, are some of the most basic condensed matter quasi-particles. They influence the electric conductivity in normal metals, but perhaps most fascinatingly, they mediate the formation of Cooper pairs in low temperature superconductors.

The details of this phonon mediation are poorly understood at the level of a microscopic Hamiltonian. The Hamiltonian for basic polaron models has only recently been solved for the single electron, and seems to predict that the polarons in low temperature superconductors would have very large effective masses. This is at odds with the measured small effective masses of many low temperature superconductors in the normal state.

In this thesis we examine extensions to the basic Holstein polaron Hamiltonian that provide a more realistic model of what happens in real materials. We also look at the BLF-SSH model, which is the appropriate Hamiltonian for superconductors without optical phonons such as the elemental superconductors.

We found that extending the Holstein model to include next nearest neighbour electron hopping and nearest neighbour electron-phonon interactions changed the effective mass slightly, but nowhere near enough to account for the low ef-

fective masses that must be present in real materials. The BLF-SSH model was examined in the adiabatic limit and with weak-coupling perturbation theory, but an exact solution was not found. It seems likely that the effective mass for this model is also very large, but an improved algorithm is necessary to prove this. A potential path forward is presented in the appendix.

"Dedicated to my wife, Leila"

Acknowledgements

Heartfelt thanks goes to my supervisor Dr. Frank Marsiglio for his support, guidance, and understanding in the dark nights of the soul of a PhD student. I also thank Dr. Kevin Beach for his help with the technical bits of C++ programing and valuable dicussions and explanations of Projector Monte Carlo.

The physics department office staff also deserve thanks for their helpful navigation of the University procedures, especially Sarah Derr. Burkhard Ritter was also a great help in making the data managment system I use, COndensed MAtter theory programing toolkit, and inspiring me to use python.

Contents

1 Introduction **1**

2 Holstein Model with Next Nearest Neighbour Hopping **6**

2.1 Model & Methods 8

2.1.1 Holstein Model 8

2.1.2 Weak-coupling Perturbation Theory 10

2.1.3 Modified Trugman Method for Exact Numerical Solutions 13

2.1.4 Heuristic Scaling 19

2.2 Summary and Conclusions 20

3 The Holstein Model with Extended Range Electron-Phonon Interactions **23**

3.1 Introduction 24

3.2 Model and Method 27

3.3 Results in Two Dimensions 31

3.4 Results in Three Dimensions 39

3.5 Summary 43

4 The BLF-SSH Model in the Adiabatic Limit **45**

4.1 Introduction 45

4.2 The Model 48

4.3 Methods 51

4.4 Analytical Results 54

4.5 Numerical Results 59
4.6 Summary 63
4.7 Supplemental Calculations for the adiabatic strong coupling limit in two and three dimensions 64

5 Weak Coupling Perturbation Theory for the BLF-SSH Model 67
5.1 Introduction 67
5.2 Perturbation Theory 71
5.2.1 Hamiltonian 71
5.2.2 Green's function analysis 72
5.2.3 Standard Perturbation Theory 74
5.3 Results and Discussion 74
5.3.1 Analytical Results in One Dimension 74
5.3.2 Comparison with other models 76
5.3.3 Numerical Results 77
5.3.4 Spectral function 82
5.4 Summary 85
5.5 Supplemental Perturbation Theory Calculations 86

6 Conclusions 90
6.1 Next Nearest Neighbour Hopping Holstein Model 90
6.2 Extended Range Interaction Holstein Model 91
6.3 Acoustic Phonons 92
6.4 Common Misconceptions 93
6.5 Final Remarks and Future Research Directions 94

A Variational Wavefunction for BLF-SSH 104
A.1 Introduction 104
A.2 Model 105
A.3 Future Directions 116

List of Tables

2.1 Electron dispersion relations for the Holstein model, allowing for next-nearest neighbour hopping. 10

2.2 Approximate ground state effective mass for small $\bar{\omega}_E \equiv \omega_E/t$ and small $\beta \equiv t_2/t$, from weak-coupling perturbation theory. . . 13

5.1 Self energy in the anti-adiabatic limit divided by coupling strength or: $\lim_{\omega_0 \to \infty} \Sigma(k = 0, \omega = \epsilon_k)/(\lambda t)$ 79

List of Figures

2.1 Numerically integrated perturbation theory, approximate perturbation theory, and exact numerical solution in one dimension. Note that the approximate perturbation theory is on top of the numerically integrated perturbation theory so here the approximation in Table II works very well. We used parameter values of $\omega_E/t = 0.1$ and $t_2/t = 0.025$. 14

2.2 Numerically integrated perturbation theory, approximate perturbation theory, and exact numerical solution in two dimensions. Here the approximate perturbation calculation fails quite badly even in the very small perturbative regime from $g^2 = 0$ to $g^2 = 1$. We used parameter values of $\omega_E/t = 0.2$ and $t_2/t = 0.025$. 14

2.3 Numerically integrated perturbation theory, approximate perturbation theory, and exact numerical solution in three dimensions. Again the approximate perturbation calculation fails even in the very small perturbative regime from $g^2 = 0$ to $g^2 = 3$. We used parameter values of $\omega_E/t = 0.3$ and $t_2/t = 0.025$. 15

2.4 Exact numerical results in one dimension for $t_2/t = 0, \pm 0.1$. Note that the effect of NNN hopping when the phonon frequency is scaled is smaller that that reported previously by Chakraborty et al. for identical values of NNN hopping. The scaling we have used also changes the direction of the scaling, as positive t_2 now raises the effective mass and negative t_2 lowers it. We use a relatively small value of $\omega_E/t = 0.1$ since phonon energies near the adiabatic regime are representative of real phonons in real materials. 17

2.5 Exact numerical results in two dimensions for $t_2/t = 0, \pm 0.025$. Note that the scaling of ω_E maps the NNN calculations back to the original. This is in agreement with our approximate perturbation theory results, though perhaps serendipitously since the approximate perturbation theory was not very close to the exact numerical perturbation theory. 18

2.6 Exact numerical results in three dimensions for $t_2/t = 0, \pm 0.025$. Note the change in the crossover coupling strength. Here it seems that the rescaling of ω_E *enhances* the effect of the NNN hopping on the effective mass beyond the crossover point, albeit reversed in sign as was the case in one dimension. 18

2.7 Exact numerical results in one dimension, with g scaling for $t_2/t = 0, \pm 0.1$. Note that the scale is much larger than that of Fig. (2.4) and the scaling works very well over the previous range, and improves the agreement with the numerical results at stronger couplings. 20

2.8 Exact numerical results in three dimensions, with g scaling for $t_2/t = 0, 0.025$, and 0.1. The scaling works remarkably well over the entire range, and matches up the crossover points very well. 21

3.1 Effective mass, m^*/m vs. coupling strength $\lambda_{\rm tot}$, using perturbation theory for both the extended and standard Holstein models. The perturbation theory are the solid lines the exact diagonalization results are the square and circle symbols. We have used $\omega_E = 0.2t$. Perturbation theory is less accurate for the extended model compared with the standard model. *Inset:* Ground state energy vs. $\lambda_{\rm tot}$. Note that the results for the energy are fairly accurate, in comparison to those for the effective mass. 31

3.2a m^*/m decreases as the accuracy of the calculation decreases. The curves with 5 and 3 phonons include states with phonons far from the electron, but never more than 5 or 3 phonons total respectively. 2^{nd} order perturbation theory includes excited states with at most a single phonon. $\omega_E = 0.2t$ 32

3.2b For the two dimensional extended Holstein model, m^*/m again decreases as the accuracy of the calculation decreases similar to the standard model. Here the effect is even more pronounced: many phonons are required even for moderate coupling strengths. Again, 2^{nd} order perturbation theory includes at most a single phonon. $\omega_E = 0.2t$ 33

3.3 Probability ($|d_n|^2$) of various basis states from the Lang-Firsov approximation and the standard model in two dimensions, with $\lambda = 0.62$ and $\omega_E = 0.2t$. The curve in black, labeled as 'Lang-Firsov' in the legend is the result obtained from the Lang-Firsov approximation given in Eq. (3.6). The other curves represent amplitudes obtained from the exact solution. The points denoted by triangle shaped symbols connected with a blue curve represent amplitudes with 'n' phonons on the same site as the electron, as denoted in the legend. These amplitudes are those of the true, numerically exact wavefunction, and are shifted compared to the Lang-Firsov approximation, as is evident from the figure. Also shown are amplitudes for wavefunction components representing an electron at some site, with 'n' phonons on the neighbouring site; these are indicated by circle shaped symbols connected with a green curve. Finally, the amplitudes for wavefunction components representing an electron with a single phonon on a neighbouring site and 'n' phonons on the same site as the electron are indicated by diamond shaped symbols and connected with a red curve. 35

3.4 m^*/m from 2^{nd} order perturbation theory vs ω_E. For definiteness, the value of λ_{tot} is 0.1. In the large ω_E limit all the curves approach 1.0 but the Extended model always has a larger m^*/m than the Standard model in both two and three dimensions. . . 37

3.5a For the two dimensional model, m^*/m as a function of λ_{tot} up to strong coupling with $\omega_E = 0.2t$. Note that beyond $\lambda_{\text{tot}} = 0.6$ the effective mass of both models is practically infinite, but at intermediate coupling strengths the extended model shows a significantly higher effective mass. *Inset:* Ground state energy vs. λ_{tot}. 38

3.5b For the two dimensional model, m^*/m as a function of $\lambda_{\rm tot}$ up to strong coupling with $\omega_E = t$. Note that the effective masses are all much smaller and at intermediate coupling strengths the extended model shows an effective mass only slightly higher than the standard model. The coupling strength is also much larger before the effective masses rise to unphysical values. *Inset:* Ground state energy vs. $\lambda_{\rm tot}$. 38

3.6 For the three dimensional model, m^*/m as a function of $\lambda_{\rm tot}$, with $\omega_E = 0.3t$, to compare exact and perturbative results. Similar to the two dimensional the region of validity for perturbation theory is much smaller in the extended model though it is not particularly large for the standard model either. *Inset:* Ground state energy vs. $\lambda_{\rm tot}$. Again, perturbation theory works better for the ground state energy than for the effective mass. 40

3.7 For the three dimensional case, m^*/m vs. λ_{tot}, with $\omega_E = 0.3t$. The effective mass increases as more and more states with more than one phonon excitation are included. The curves with 4 and 5 phonons include states with phonons far from the electron, but there are never more than a total of 4 or 5 phonons, respectively. The calculation with 2^{nd} order perturbation theory includes basis states with at most a single phonon. 41

3.8 For the three dimensional case, m^*/m vs. λ_{tot} with various values of $f(1)$. These results are from numerically exact calculations. The extended model can shift the onset of unphysically high effective masses to stronger coupling, though the extra range of tenable coupling strengths is rather small. 41

4.1 A one dimensional depiction of the variables used to describe ionic motion. The full blue circles are ions at their equilibrium positions, and the grey dotted circles are ions displaced from their equilibrium positions. The $u_{x\mathbf{i}}$ variables are then seen to be the displacements from equilibrium and $\tilde{x}_{\mathbf{0}} = u_{x\mathbf{0}} - u_{x\mathbf{1}}$ so $\tilde{x}_{x\mathbf{0}}$ can be thought of as the distance change between the two ions after subtracting the equilibrium distance spacing. 49

4.2 The ground state energy for the one dimensional BLF-SSH model in the adiabatic limit. The solid curve with (blue) squares is the numerical solution, while the various strong-coupling expansions are shown as indicated in the legend. The divergence in weak-coupling is due to the finite expansion in $t/\lambda W$ and not from some effect of the model itself. 57

4.3 The two possible configurations for stretched bonds in the two dimensional strong-coupling limit. The square has the electron amplitude equal on all four sites while the star configuration has half of the electron probability on the centre site and one eighth on each of the four surrounding sites. 58

4.4 The energy for the two dimensional BLF-SSH model from numerical calculations (periodic boundary conditions) for a wide range of coupling strengths and using both possible starting configurations. Finite size effects have been converged to the thermodynamic limit by using larger and larger clusters. The previous results of Miyasaka and Ono[64] have been extracted from their 2001 paper to show that our energies are somewhat lower. 61

4.5 The electron and ion distortion configuration at $\lambda = 0.1$ for the two configurations discussed in the text. In (a) and (b) we show the 'star' and 'square' configurations, respectively. The energies of both these configurations are degenerate. The width of the black rectangles connecting the ion sites is proportional to the amount that a bond is compressed. The green circles have an area proportional to the electron density on that site. Both of these configurations differ qualitatively from the quasi-one-dimensional configuration found in Ref. (64). 62

4.6 The energy for the three dimensional SSH model from numerical calculations (periodic boundary conditions) for a wide range of coupling strengths. 63

5.1 Electron self energy for the ground state ($k = 0$), normalized to λ (or λ_H) vs. characteristic phonon frequency ω_0 (this is ω_E for the Holstein model), for both the BLF-SSH and Holstein models, in one, two, and three dimensions, as indicated. Alternatively, the ordinate is simply the second order (in g) correction to the ground state energy within Rayleigh-Schrödinger perturbation theory. In all cases the magnitude of the correction increases with increasing ω_0. At low ω_0 the magnitudes of the the results are ordered three, two, and one dimensions (lowest to highest) whereas at high frequency the ordering is just the opposite. All six cases have non-zero limiting values as $\omega_0 \to \infty$, given in Table 1. 78

5.2 The electron effective mass, normalized to the 2^{nd} order correction to the energy for the anti-adiabatic limit, vs. characteristic phonon frequency, ω_0, for both the BLF-SSH and Holstein models, in one, two, and three dimensions, as indicated. In one dimension the effective mass diverges for both models, though the divergence is stronger for the BLF-SSH model, as indicated by Eq. (5.20). In two dimensions the effective mass approaches a constant as $\omega_0 \to 0$ for both models, while in three dimensions the effective mass ratio approaches unity in the same limit. At the opposite extreme, both one dimension results give $m^*/m \to 1$ as $\omega_0 \to \infty$, while in both two and three dimensions the effective mass remains above unity in this limit. Note that in all three dimensions, for a given reduction in energy as given by the 2^{nd} order correction to the energy, the BLF-SSH model results in significantly higher effective masses. 80

5.3 Spectral function for the BLF-SSH model, for $\lambda_{BLF} = 0.2$ for three different characteristic phonon frequencies, as a function of frequency. All three spectra are similar as one would find for the Holstein model, and consist of quasiparticle peak with weight $z_0 = 0.766, 0.727, 0.724$, for $\omega_0/t = 0.1, 0.5, 2.0$, respectively, followed by an incoherent piece. 81

5.4 Quasiparticle residue, z_0 vs. ω_0/t for both the BLF-SSH and Holstein models in all three dimensions. Note that while the result for the Holstein model tends to be inversely proportional to the effective mass, this is not the case for the BLF-SSH model at low phonon frequency in one and two dimensions. In one dimension in particular, the effective mass diverges, while z_0 also turns upward. 82

5.5 Comparison of the quasiparticle residue (upper panel) with the electron effective mass (lower panel) as a function of ω_0/t, for the BLF-SSH model in one dimension. The behaviour noted in Fig. 5.4 is clear here. Moreover, note the scales; while the effective mass ratio is very large (≈ 4) for $\lambda_{BLF} = 0.01$ and small values of ω_0/t, the quasiparticle residue remains within 15% of unity. 84

A.1 Here we plot the variational energies for $\omega_0 = 0.1$ and $\omega_0 = 0.5$ along with the adiabatic results for a 10 site cluster. The general trend is similar to the Holstein model, the energy decreasing with increasing ω_0 and it appears to be always polaronic, in agreement with the perturbation results. Note that the variational method fails at low lambda, that is, for the data point at $\lambda = 0.02$ the variational energies are not lower than the adiabatic. This means a comparison with the perturbation theory is unhelpful. 115

Chapter 1

Introduction

The polaron, an electron coupled to ionic distortions or phonons, was first postulated by Landau in 1933 and was one of the first problems addressed by Feynman after his invention of the path integral formulation of quantum mechanics. Despite this pedigree, only the most basic model Hamiltonians have been solved for the single electron ground state and a proper understanding of the interaction between two polarons and other few electron systems is still lacking. Even in systems that are unambiguously governed by electron-phonon coupling, the theory has not reached the point of predictive power. Improvements in these materials have come more from experimental intuition than a comprehensive theory.

The early work on polarons in the 50's and 60's did not attempt a complete solution of the quantum mechanical model on the lattice but instead often used a continuum approximation for the electron or ions or both. The continuum model for ions was justified by the idea that each electron would influence many lattice sites through the long range Coulomb interaction, and the continuum electron model was justified for materials with small electron filling in each band such as doped semiconductors. The Fröhlich model is the prototypical model of this, a continuum electron, independent simple harmonic oscillators for ionic degrees of freedom, and an extended range dipole r^{-3} interaction. This model

was solved with path integrals by Feynman in the limit of weak electron-phonon coupling.[1][2] Others did calculations in the adiabatic continuum limit which treats the phonons classically. [3] The success of these models was explaining the larger effective mass of electrons in semiconductors.

Another avenue pursued was the thermally activated polaron, which is still considered today for some higher temperature applications. This assumes that the electron has become locally trapped by the conspiring of an impurity and large effective mass from the electron-phonon interaction. Then only at non-zero temperature may the electron move from site to site, producing a system similar to a tunneling problem. [4]

Later, as numerical computations became possible, much of the focus changed to small lattice polarons. Here a tight-binding model is used for the electrons and the ions are described by individual or collective quantum degrees of freedom which are coupled to the electrons in some way. The Holstein model is the prototypical example of these[5], with others including the BLF-SSH[6][7] and modifications to include Jahn-Teller interactions[8] . Work has continued on the Fröhlich model as well, with numerical solutions giving good approximations to the ground state energy. [9]

Accurate numerical methods for the single electron Holstein and Fröhlich models have been developed [10][9] but the materials of interest are far more complex than dilute semiconductors, almost always involving electron-electron interactions. Both low and high temperature superconductors, Manganites exhibiting colossal magnetoresistance and organic conductors are the new targets and are still poorly understood.

The paths to improving the situation are to either improve the realism of individual polaron models, include electron-electron interactions, or eventually to do both. None of these are simple tasks: even a single electron polaron is a difficult quantum many-body problem since there are many ions with which the electron may interact.

Improving the polaron models can be simply adding more terms to model magnetic interactions as in Jahn-Teller Hamiltonians or refining the existing terms such as improving the electron-phonon coupling to have a linear and quadratic component. [11] Each of these modifications is generally tuned to examine a particular physical phenomenon since including an ever growing number of corrections would quickly become computationally intractable. By examining each correction individually, it is hopefully possible to tease out what is essential to model a polaron. In the words of Albert Einstein: "Everything should be made as simple as possible, but not simpler."

The other avenue of including many-electron effects has been to use dynamical mean field theory (DMFT) or quantum Monte Carlo (QMC) along with a single polaron model. Here the Hamiltonian is modified with a Hubbard U electron-electron interaction. Work has been done on a spinless electron Holstein-Hubbard model with Monte Carlo simulations for finite electron filling in a band[12, 13, 14, 15, 16], but the sign problem limits the accuracy even with very sophisticated sampling methods. There have also been studies of real materials using Dynamical Mean Field Theory (DMFT) and local density approximation (LDA) [17] which have had a good deal of success. These models have been able to successfully reproduce T_c and other experimentally observed quantities and are an important part of the tool kit. Unfortunately, the methods used to deal with the complex many-body wavefunction obscure the microscopic details in the results, so there is still a gap in our understanding of real materials.

An accurate single electron solution will not solve all the mysteries of the electron-phonon coupling in real materials, but it will greatly improve our understandings of the microscopic actors. With the basic building blocks understood, cluster DMFT and other many-electron methods may be applied more intelligently. It also gives a good opportunity to examine the many-body wavefunction in a more tractable situation and develop techniques that may be

useful for other many-body problems.

With these goals in mind this thesis will present novel research of the single electron polaron models beyond the standard well-studied Holstein model. The Holstein model is the obvious place to start since the single electron problem is well understood, even near the adiabatic limit, which is importantly the physically relevant regime. [18] [10] The model is completely solved in 1,2, and 3 dimensions, yet still exhibits an effective mass far larger than that which can be reconciled with mobile Cooper pairs in bulk superconductors.

In the second chapter the effect of next nearest neighbour hopping is discussed. This is a relatively simple modification to the standard model and realistic since many real material band structures can be approximated with a tight-binding model that includes significant next nearest neighbour and beyond hopping amplitudes. [19] We use the same new algorithm as in the first chapter to confirm previous results in one dimension, and then expand to two and three dimensions again with the ability to choose realistic near adiabatic parameters. We also found an interesting heuristic scaling that allows one to predict the effect of next nearest neighbour hopping on the effective mass. These were previously published in Ref. 20.

In the third chapter we look into the single electron Fröhlich model which includes the effect of the long range coulumb interaction between the electron and the ions, going beyond the simple on-site iteration of the Holstein model. We present a modification of the full extended Fröhlich model including only the nearest neighbour ions, which, given the exponential decay of the interaction in the full Fröhlich model, should dominate the results. We confirm previous two dimensional work done with Quantum Monte Carlo with a Krylov space exact diagonalization method. This new algorithm also allowed us to look at the three dimensional case, which is the most relevant for bulk superconductors, and to do it in the near adiabatic limit, which is the most physically relevant. These results were previously published in Ref. 21.

In the fourth chapter we switch from improvements to the Holstein model to the BLF-SSH model. While the Holstein model is well suited to materials that have a dominating optical phonon mode, this is only a subset of the known bulk superconductors. The elemental superconductors, for instance, have only acoustic phonon modes. While Eliashberg theory can be used to understand these materials, the Holstein model is often implicit in these calculations, casting some doubt onto their trustworthiness. Unfortunately treating the acoustic phonons in the BLF-SSH model is much more difficult than the Holstein model so we start with a study of the semi-classical adiabatic model. We perform the calculations in one, two, and three dimensions and correct previous inaccurate calculations of the two dimensional. The true shape of the ionic distortion is presented and simple analytic calculations for the strong-coupling regime are included as well. These were previously published in Ref. 22.

The appendix includes research results of a variational wavefunction for the fully quantum BLF-SSH model. A derivation is presented in detail to benefit future research and the variational ground state energies are also included.

Chapter 2

Holstein Model with Next Nearest Neighbour Hopping

In the realm of BCS theory, it is well known that electron-phonon interactions in solid materials are integral to the emergence of superconductivity, as they are responsible for the effective attraction that leads to the formation of Cooper pairs.[24] On the other hand, the importance of electron-phonon interactions in high temperature superconductivity is not yet clear.[25] Since polarons are simply quasiparticles consisting of electrons dressed with the net effect of these electron-phonon interactions, it is important to understand this basic building block, and the related bipolaron problem of the attraction between polarons. This will allow a full understanding of conventional superconductivity, and possible extensions to nonconventional superconductors.[26] To this end, the problem of a single electron in the conduction band of a crystal lattice has been extensively studied.[27] Specifically, a numerically exact algorithm for solving the Holstein model with tight-binding electron bands in the thermodynamic limit was formulated in Ref. 28, and now that problem is effectively solved. Several extensions were subsequently reported, including ones to better manage disparate electron (t) and phonon (ω_E) energy scales (in particular, $\omega_E << t$),[10, 29], higher dimensionality,[30, 31, 32] extended interaction range

[18, 21] and inclusion of next-nearest neighbour (NNN) single-particle hopping amplitude.[33] In this last study it was found that including NNN hopping in the one dimensional Holstein model altered significantly the electron's effective mass in strong-coupling.

The purpose of this chapter is to follow up on this study. Thus far studies of polaron properties within the Holstein model have revealed that the effective mass becomes very large with rather modest electron-phonon coupling strength. This is incompatible with experiment, specifically with the evidence that some conventional superconductors have a large electron-phonon coupling strength, and yet show almost no sign of single-electron polaronic behaviour.[34] Chakraborty *et al.* [33] found that including NNN hopping in the one-dimensional Holstein model could decrease the polaron effective mass significantly, particularly at strong-coupling. This is potentially very important since this is a means for lowering the polaron effective mass to a realistic level, such that an Eliashberg treatment [35, 36, 37, 38, 39] makes sense.

To more fully understand the effects due to NNN electron hopping we will first present our perturbation theory calculations for the energy and effective mass of the NNN Holstein model in one, two, and three dimensions. We use square and simple cubic lattices for two and three dimensions, respectively. These results agree for sufficiently low coupling strength with our exact numerical calculations using our previously refined algorithm for the Holstein model [21] extended to include NNN interactions. We note that quantitative agreement with perturbation theory extends over a surprisingly limited range of electron-phonon interaction strength, even in three dimensions, which is the most applicable to bulk superconductors. A low phonon frequency approximation to the perturbation theory results suggests a scaling of the phonon frequency with the low energy effective bandwidth, which explains the results obtained as a function of NNN electron hopping. We also note an additional scaling factor that accounts for the results with non-zero NNN hopping with

respect to those with nearest-neighbour hopping only, over a more extended coupling strength range.

Since including NNN electron hopping also modifies the 'effective' electronic bandwidth (to be defined more precisely below), we should account for this in using the appropriate phonon frequency. That is, since altering the adiabatic ratio ω_E/t, even in the case with NN hopping only, is known to lead to changes in the polaronic effective mass for the same coupling strength, then we should be careful to use an appropriately scaled phonon frequency.

After a brief introduction we use perturbation theory to determine the polaron effective mass in weak-coupling. Since these expressions are analytical, they are well-suited to examine the various scaling factors. We then present exact solutions, in one, two, and three dimensions, to examine the effect on polaron mass over the entire coupling range. We also note a heuristic scaling, found numerically, that very accurately maps the parameters with NNN hopping back to the original Holstein Model.

2.1 Model & Methods

2.1.1 Holstein Model

The Holstein model [5] is perhaps the simplest model for describing electron-phonon interactions; it treats (optical) phonons as local ion vibrations, and assumes that each atomic site oscillates with the same characteristic frequency ω_E. With NNN hopping included, the Hamiltonian that describes such a system is:

$$\hat{H} = -t\sum_{\mathbf{j},\delta}(\hat{c}^{\dagger}_{\mathbf{j}}\hat{c}_{\mathbf{j}+\delta} + \hat{c}^{\dagger}_{\mathbf{j}+\delta}\hat{c}_{\mathbf{j}}) - t_2\sum_{\mathbf{j},\gamma}(\hat{c}^{\dagger}_{\mathbf{j}}\hat{c}_{\mathbf{j}+\gamma} + \hat{c}^{\dagger}_{\mathbf{j}+\gamma}\hat{c}_{\mathbf{j}}) + \hbar\omega_E\sum_{\mathbf{j}}\hat{a}^{\dagger}_{\mathbf{j}}\hat{a}_{\mathbf{j}} + \hbar\omega_E g\sum_{\mathbf{j}}(\hat{a}_{\mathbf{j}} + \hat{a}^{\dagger}_{\mathbf{j}})\hat{c}^{\dagger}_{\mathbf{j}}\hat{c}_{\mathbf{j}}. \tag{2.1}$$

Here, t and t_2 are the nearest neighbour and NNN hopping integrals respectively with δ and γ being the vectors to the nearest neighbour and NNN sites, respectively. The sum over the vector of site positions $\mathbf{j}$ covers all sites. The electron creation and phonon creation operators at site $\mathbf{j}$ are $\hat{c}^{\dagger}_{\mathbf{j}}$ and $\hat{a}^{\dagger}_{\mathbf{j}}$, respectively, and $g \equiv \sqrt{\frac{\alpha^2}{2\hbar M\omega_E^3}}$ is a dimensionless measure of the electron-phonon coupling strength, with M being the atomic mass and α being the coupling strength as defined in real space.

In order to diagonalize this Hamiltonian, we transform into k-space, according to the equation:

$$\hat{c}_j = \frac{1}{\sqrt{N}}\sum_k e^{i\vec{k}\cdot\vec{R}_j}\hat{c}_k \tag{2.2}$$

where $\vec{R}_j$ points to lattice site j, and $\vec{k}$ is a wave vector summed over the First Brillouin Zone (FBZ). The relation for $\hat{c}^{\dagger}_j$ may be obtained simply by taking the Hermitian conjugate of the above expression, and the bosonic Fourier transforms are defined almost identically. In the FBZ there are N distinct k values within $(-\pi/a, \pi/a)$ in each direction. The transformed Hamiltonian then becomes

$$\hat{H} = \sum_k \epsilon(\vec{k})\hat{c}^{\dagger}_k\hat{c}_k + \hbar\omega_E\sum_k\hat{a}^{\dagger}_k\hat{a}_k + \hbar g\omega_E\sum_{k,q}(\hat{a}_q + \hat{a}^{\dagger}_{-q})\hat{c}^{\dagger}_{k+q}\hat{c}_k, \tag{2.3}$$

Dim.	$\epsilon(\vec{k})$
1D	$-2t\cos ka - 2t_2\cos 2ka$
2D	$-2t(\cos k_x a + \cos k_y a) - 4t_2\cos k_x a\cos k_y a$
3D	$-2t(\cos k_x a + \cos k_y a + \cos k_z a)$
	$-4t_2(\cos k_x a\cos k_y a + \cos k_x a\cos k_z a + \cos k_y a\cos k_z a)$

Table 2.1: Electron dispersion relations for the Holstein model, allowing for next-nearest neighbour hopping.

and holds for all dimensions with dispersion relations $\epsilon(\vec{k})$ given in Table 2.1.

In this chapter, we will examine various properties of the ground state, which for $\frac{t'}{t} > -\frac{1}{4}$ is at zero total crystal momentum p. For all dimensions this results in a low energy dispersion E_p quadratic in $p = |\mathbf{p}|$, so that the ground state effective mass of the electron is given by:

$$\frac{1}{m^*} = \frac{1}{\hbar^2}\left.\frac{\partial^2 E_p}{\partial p^2}\right|_{p=0}. \tag{2.4}$$

2.1.2 Weak-coupling Perturbation Theory

Beginning with the perturbative approach (in the weak-coupling regime), we consider the electron-phonon interaction to be the perturbation, so that the unperturbed energy is simply $E_p^{(0)} = \epsilon(\vec{p}) \equiv \epsilon_p$. The unperturbed ground state for arbitrary p is therefore

$$|\phi_p^{(0)}\rangle = \hat{c}_p^\dagger |0\rangle . \tag{2.5}$$

Here, $|0\rangle$ is simply the electron-phonon vacuum state. Unperturbed excited states include all states with a single electron and any number of phonons such that the total crystal momentum still adds to p. It is easy to check that given these definitions, $E_p^{(1)} = 0$, independent of the choice of total crystal momentum. Under these conditions, the energy correction to second order (in α or g) is:

$$E_p^{(2)} = \sum_{k,q} \frac{\left| \langle \phi_p^{(0)} | \, \hat{V}_{pert} \hat{c}_k^\dagger \hat{a}_q^\dagger \, |0\rangle \right|^2}{\epsilon_p - (\epsilon_k + \hbar\omega_E)} \tag{2.6}$$

In this case, $\hat{V}_{pert}$ is the electron-phonon interaction term of the Hamiltonian in Eq. 2.3. Note that only one phonon is considered in the unperturbed excited states because $\hat{V}_{pert}$ only creates (annihilates) one phonon. Upon evaluating this sum, we may apply Eq. 2.4 to find the effective mass. In order to do so, we convert the sum in Eq. 2.6 to an integral over k-values, since the thermodynamic limit ($N \to \infty$) implies a continuum of k values between $-\pi/a$ and π/a.

In the one-dimensional case, the corrected energy according to second order perturbation theory (in g) is

$$\begin{aligned} E_p^{1D} = & -2t\left(\cos\left(pa\right) + \beta\cos\left(2pa\right)\right) \\ & -\frac{(\hbar g\omega_E)^2}{4W}\frac{1}{\sqrt{(\frac{\overline{\omega}_E}{2} - \beta + 1 + \cos pa + \beta\cos 2pa)b^2}} \\ & \times\left[\frac{4\beta - 1 + b}{\sqrt{3\beta + \frac{\overline{\omega}_E}{2} + \cos pa + \beta\cos 2pa + b}}\right. \\ & \left. -\frac{4\beta - 1 - b}{\sqrt{3\beta + \frac{\overline{\omega}_E}{2} + \cos pa + \beta\cos 2pa - b}}\right] \end{aligned} \tag{2.7}$$

where we have defined dimensionless parameters $\overline{\omega}_E \equiv \frac{\hbar\omega_E}{t}$, $\beta = t_2/t_1$, and

$$b \equiv \sqrt{1 + 8\beta(\beta + \frac{\overline{\omega}_E}{2} + \cos pa + \beta\cos 2pa)}$$

The above result, substituted into Eq. (2.4), gives an expression for the effective ground-state electron mass m^* at $p = 0$:

$$\left(\frac{m_b}{m^*}\right)_{\text{1D}} = 1 - \lambda\overline{\omega}_E \left\{ \frac{8\beta^2 + 12\beta + 4\beta\overline{\omega}_E + \frac{1}{2}}{((4+\overline{\omega}_E)b^2)^{\frac{3}{2}}} \right.$$
$$\times \left[\frac{4\beta - 1 + b}{\sqrt{8\beta + 2 + \overline{\omega}_E + 2b}} - \frac{4\beta - 1 - b}{\sqrt{8\beta + 2 + \overline{\omega}_E - 2b}} \right]$$
$$+ \frac{1}{\sqrt{(4+\overline{\omega}_E)b^2}} \left[\frac{-2\beta}{b} \left(\frac{1}{\sqrt{8\beta + 2 + \overline{\omega}_E + 2b}} \right.\right.$$
$$\left.\left. + \frac{1}{\sqrt{8\beta + 2 + \overline{\omega}_E - 2b}} \right) \right.$$
$$+ \frac{4\beta - 1 + b}{\sqrt{2}(8\beta + 2 + \overline{\omega}_E + 2b)^{\frac{3}{2}}} \left(\frac{4\beta}{b} + 1 \right)$$
$$\left. + \frac{4\beta - 1 - b}{\sqrt{2}(8\beta + 2 + \overline{\omega}_E - 2b)^{\frac{3}{2}}} \left(\frac{4\beta}{b} - 1 \right) \right] \right\} \tag{2.8}$$

where b is evaluated at $p = 0$, and with $\lambda \equiv \frac{2g^2\omega_E}{W}$, where W is the electronic bandwidth. This definition for λ applies for three dimensions as well, though in two dimensions, $\lambda \equiv \frac{g^2\omega_E}{2\pi t}$ is used.[1] Note that in the above equation, we have normalized by the inverse of the electron band mass (unperturbed effective mass):

$$\frac{1}{m_b} = \frac{1}{\hbar^2} \frac{\partial^2 \epsilon_p}{\partial p^2}\bigg|_{p=0} = \frac{(2t + 8t_2)a^2}{\hbar^2}. \tag{2.9}$$

More generally, evaluating for the second-order energy correction in two or three dimensions proves tedious, and has a cumbersome, unenlightening answer (as in eq. (2.8)). For these cases, we have also integrated the result numerically to check our analytical results. In the figures that follow, these are referred to as "numerically integrated perturbation theory."

For an approximate analytical result, we observe that the integrand in the energy correction expression decays more or less to 0 by some $k_0 < \pi$ for most small values of the parameters β and ω_E. Cutting the integral off at this k_0

[1] This definition is preferred by the authors since it captures better the density of states for a single electron in the band, and only differs by an integral multiple of $\pi/2$ anyway.

Dim.	Eff. Mass Ratio: $\frac{m_b}{m^*}$	$\frac{m_b}{m^*}$ (as a function of g)
1D	$1-\frac{1}{2}\frac{\lambda}{\sqrt{1+4\beta}}\frac{1}{\sqrt{\overline{\omega}_E}}$	$1-\sqrt{\frac{\overline{\omega}_E}{(1+4\beta)}}\frac{g^2}{4}$
2D	$1-\frac{1}{2}\frac{\lambda}{(1+2\beta)}$	$1-\frac{\overline{\omega}_E}{(1+2\beta)}\frac{g^2}{4\pi}$
3D	$1-\frac{3}{4\pi}\frac{\lambda}{(1+4\beta)^{\frac{3}{2}}}\sqrt{\overline{\omega}_E}$	$1-\frac{\overline{\omega}_E^{\frac{3}{2}}}{(1+4\beta)^{\frac{3}{2}}}\frac{g^2}{8\pi}$

Table 2.2: Approximate ground state effective mass for small $\bar{\omega}_E \equiv \omega_E/t$ and small $\beta \equiv t_2/t$, from weak-coupling perturbation theory.

and making the approximation that $k \ll 1$ for $k \leq k_0$, we achieve the analytic approximations shown in Table 2.2. Unfortunately, these approximations prove to be rather crude in two and three dimensions, which limits their usefulness. Regardless, we present them alongside our numerically integrated results for completeness in Figs. (2.1 - 2.3). The approximations do work better for smaller ω_E; however we have tested them in a reasonably physically representative regime of small ω_E [21] and even here the agreement is poor.

Secondly, it is important to note that even without approximations, the range of coupling strengths over which the numerical perturbation theory is valid is very small. This feature is similar to our results for the standard Holstein model [21] so we do not recommend using the perturbation calculations for physical predictions but only as a check on more powerful numerical calculations such as the Trugman Method.

2.1.3 Modified Trugman Method for Exact Numerical Solutions

The single polaron problem is solved here with the variational exact diagonalization method described in Bonča et al. [28] and revised by the authors as described in [10, 21] to account for a rapidly growing Hilbert space from the additional terms in the Hamiltonian. For the data included in these plots 20 -

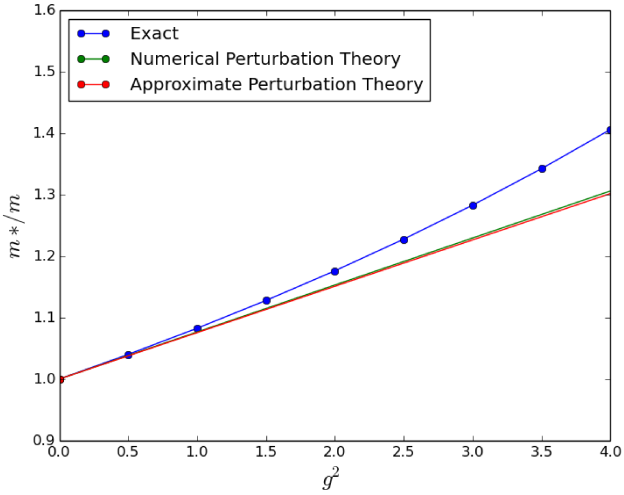

Figure 2.1: Numerically integrated perturbation theory, approximate perturbation theory, and exact numerical solution in one dimension. Note that the approximate perturbation theory is on top of the numerically integrated perturbation theory so here the approximation in Table II works very well. We used parameter values of $\omega_E/t = 0.1$ and $t_2/t = 0.025$.

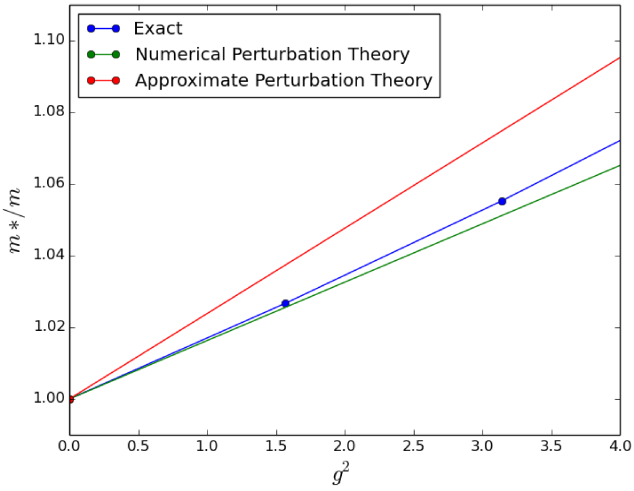

Figure 2.2: Numerically integrated perturbation theory, approximate perturbation theory, and exact numerical solution in two dimensions. Here the approximate perturbation calculation fails quite badly even in the very small perturbative regime from $g^2 = 0$ to $g^2 = 1$. We used parameter values of $\omega_E/t = 0.2$ and $t_2/t = 0.025$.

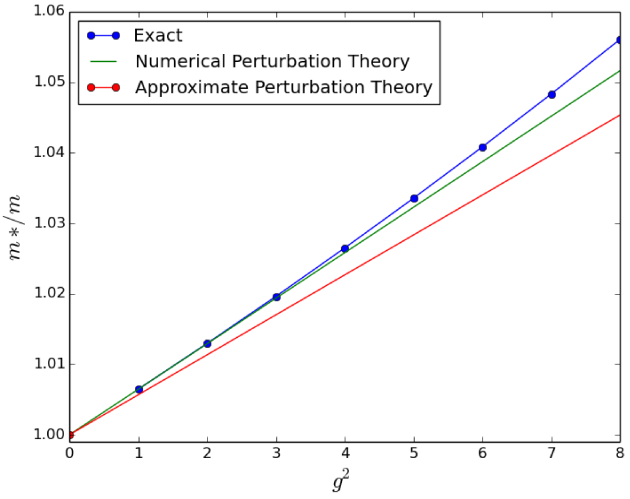

Figure 2.3: Numerically integrated perturbation theory, approximate perturbation theory, and exact numerical solution in three dimensions. Again the approximate perturbation calculation fails even in the very small perturbative regime from $g^2 = 0$ to $g^2 = 3$. We used parameter values of $\omega_E/t = 0.3$ and $t_2/t = 0.025$.

100 preliminary diagonalizations were performed with the most strongly contributing basis states selected at each iteration to seed the next iteration. All results were converged for the effective mass. While our algorithm for generating basis states differs significantly from that of Chakraborty et al., [33] our one dimensional results are in agreement with theirs and our algorithm permits efficient calculations in higher dimensions and for realistic values of ω_E/t.

Note that the introduction of non-zero t_2 leaves the bandwidth invariant; however it does alter the curvature of the dispersion relation near $k = 0$. The result is a different bare electron mass (see Eq. (2.9)) and, correspondingly, a different *effective* bandwidth. The different bare electron mass and different normalization of the effective mass has been noted before,[33] but the different effective bandwidth was not considered. If we take some small $k_0 \ll 1/a$, and calculate the bandwidth in the region $[-k_0, k_0]$ up to second order accuracy in k_0, then we find the ratio of next-nearest neighbour bandwidth to nearest

neighbour bandwidth to be:

$$\left(\frac{W_{NNN}}{W_{NN}}\right)_{1D} \approx (1+4\beta) \approx \left(\frac{W_{NNN}}{W_{NN}}\right)_{3D} \tag{2.10}$$

and:

$$\left(\frac{W_{NNN}}{W_{NN}}\right)_{2D} \approx (1+2\beta). \tag{2.11}$$

This suggests the the phonon energy scale $\hbar \cdot \omega_E$ also should be rescaled by the same factors to keep the ratio of phonon energy to effective bandwidth constant. The interaction strength parameter g is dimensionless and thus remains unchanged, though the electron-phonon interaction term in the Hamiltonian is rescaled since it is proportional not simply to g, but to $g\hbar\omega_E$. It can be seen from the result in table 2.2 that rescaling $\overline{\omega}_E$ by the effective bandwidth change would transform the NNN approximate effective mass onto that for NN hopping only. In other words, if we use a renormalized phonon frequency with the same value with respect to the effective electronic bandwidth, then the addition of next nearest neighbour hopping has no effect on the effective mass (according to Table 2.2). However these are only approximate perturbation calculations and the exact results show that the NNN effective mass is substantially different from the NN effective mass even when the proper scalings have been taken into account.

On the other hand, this rescaling of ω_E (which was not done by Chakraborty et al. [33]), definitely reduces the effect of the NNN hopping on the polaron effective mass.

In Fig. 2.4 we compare the data with and without the scaling of ω_E to the original Holstein model in one dimension with $t_2/t = \pm 0.1$. The one dimensional case has no crossover coupling strength in the standard Holstein model, where the polaron effective mass suddenly begins to increase exponentially with coupling strength, and while $t_2 > 0$ did decrease the effective mass somewhat,

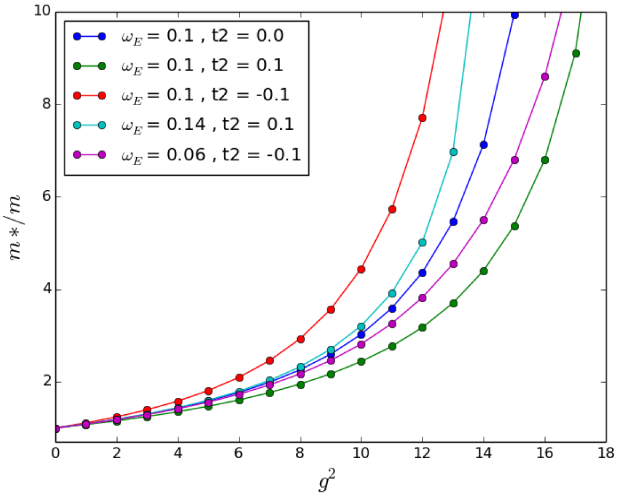

Figure 2.4: Exact numerical results in one dimension for $t_2/t = 0, \pm 0.1$. Note that the effect of NNN hopping when the phonon frequency is scaled is smaller that that reported previously by Chakraborty et al. for identical values of NNN hopping. The scaling we have used also changes the direction of the scaling, as positive t_2 now raises the effective mass and negative t_2 lowers it. We use a relatively small value of $\omega_E/t = 0.1$ since phonon energies near the adiabatic regime are representative of real phonons in real materials.

no crossover point was found for the NNN Holstein model in 1D either. Our results are in agreement with Chakraborty et al. [33] for the same value (i.e. unscaled) of ω_E. However, including the correction described in the preceding paragraph decreases the effective mass change and even the direction of the change. The one dimensional case is not very realistic for bulk materials so we continue with two and three dimension calculations.

In two and three dimensions we find that for small NNN hopping parameters the effective mass deviates from the standard Holstein model only slightly until the crossover coupling strength in two and three dimensions is reached. At this point the effective masses increase sharply for both models. However, the introduction of non-zero t_2 changes the crossover point slightly. We have included the unscaled results with the ω_E/t scaled results for the sake of completeness in Fig. 2.5 and Fig. 2.6 for two and three dimensions, respectively.

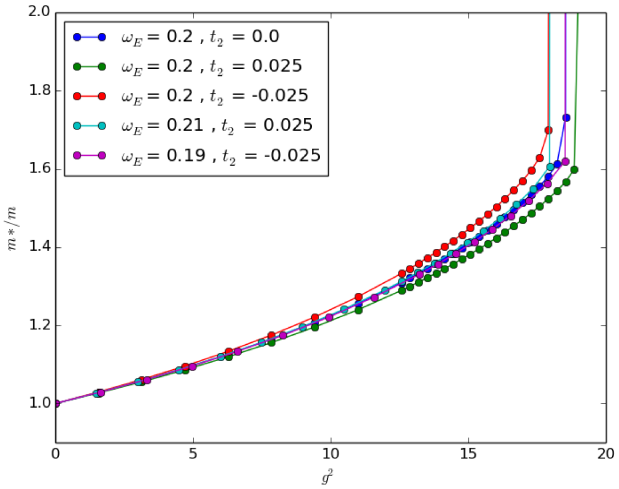

Figure 2.5: Exact numerical results in two dimensions for $t_2/t = 0, \pm 0.025$. Note that the scaling of ω_E maps the NNN calculations back to the original. This is in agreement with our approximate perturbation theory results, though perhaps serendipitously since the approximate perturbation theory was not very close to the exact numerical perturbation theory.

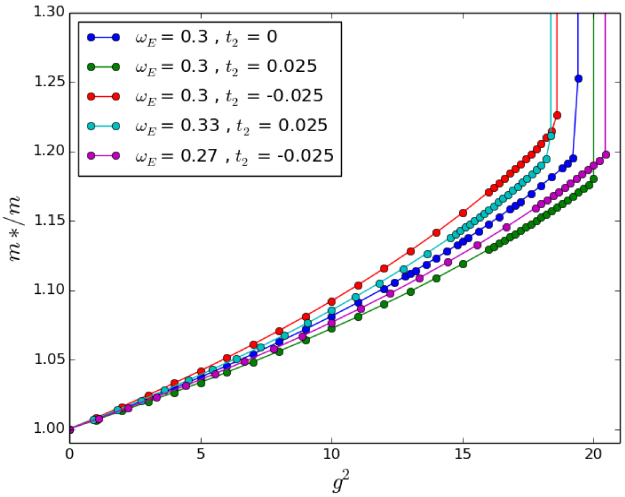

Figure 2.6: Exact numerical results in three dimensions for $t_2/t = 0, \pm 0.025$. Note the change in the crossover coupling strength. Here it seems that the rescaling of ω_E *enhances* the effect of the NNN hopping on the effective mass beyond the crossover point, albeit reversed in sign as was the case in one dimension.

While our approximate perturbation theory suggests that the scalings of ω_E/t given in Table 2.2 would map the NNN effective masses onto the NN effective mass, Figs. 2.4, 2.5, and 2.6 make it clear that this scaling does not work very well except in the two dimensional case. The approximate perturbation theory only agrees exactly with the numerical perturbation theory in one dimension and there is no reason to trust even the numerical perturbation theory for the effective mass outside of very small coupling strength as we have remarked on other occasions.[21] In two dimensions the approximate ω_E scaling suggested in Table 2.2 mapped the effective masses back close to that obtained with no NNN hopping, but in one and three dimensions it over-corrected the change in the effective mass. Also, not surprisingly, in all three dimensions a simple scaling does not work well in the very strong-coupling regime. So in agreement with Chakraborty et al., [33] NNN hopping does introduce changes in the properties of the polaron, and leads to a decreased effective mass for some additional (positive) t_2 hopping if no phonon frequency scaling is introduced. But NNN hopping leads to an *increased* effective mass if the phonon frequency is also increased to account for the increase in the 'local' bandwidth. Most importantly for our understanding of the conventional framework for superconductivity, the inclusion of NNN hopping changes the critical coupling strength in three dimensions at which the effective mass increases sharply towards infinity (see the large coupling regime of Fig. 2.6).

2.1.4 Heuristic Scaling

In the course of our investigations we further found a heuristic scaling of the coupling strength that, combined with the bandwidth-inspired scaling, works very well; however, the underlying physical motivation is still rather unclear. We introduce a scaling factor in the dimensionless interaction param-

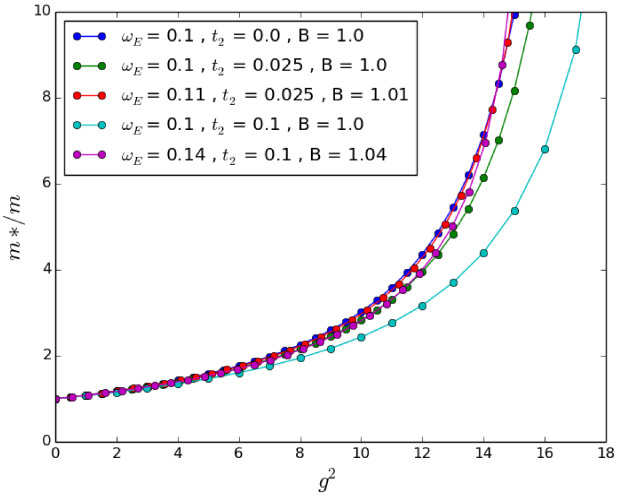

Figure 2.7: Exact numerical results in one dimension, with g scaling for $t_2/t = 0, \pm 0.1$. Note that the scale is much larger than that of Fig. (2.4) and the scaling works very well over the previous range, and improves the agreement with the numerical results at stronger couplings.

eter $g_{original} \cdot B = g_{scaled}$ such that the new term in the Hamiltonian is:

$$\hbar\omega_E g_{scaled} \sum_{\mathbf{j}} (\hat{a}_{\mathbf{j}} + \hat{a}^\dagger_{\mathbf{j}}) \hat{c}^\dagger_{\mathbf{j}} \hat{c}_{\mathbf{j}} \tag{2.12}$$

By experimenting with different values of B we found that in one dimension, $B = 1 + 4\beta$ and in three dimensions, $B = 1 + \beta$ work very well. These statements are validated in Figs. (2.7 , 2.8) and at least for three dimensions is very accurate, even in the crossover regime.

2.2 Summary and Conclusions

We have performed weak-coupling perturbation calculations for the Holstein model with next nearest neighbour (NNN) hopping and compared them with exact calculations in one, two, and three dimensions. We confirmed previous results obtained in one dimension by Chakraborty et al.; [33] however, we point

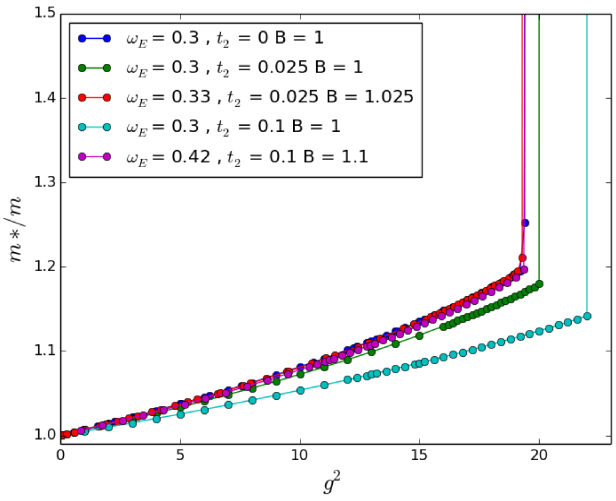

Figure 2.8: Exact numerical results in three dimensions, with g scaling for $t_2/t = 0, 0.025$, and 0.1. The scaling works remarkably well over the entire range, and matches up the crossover points very well.

out that a more appropriate comparison, at least in weak-coupling, requires a change of the phonon frequency, ω_E, as given in Table 2.2, for the case with NNN hopping. With this change accounted for we find that the effect of NNN hopping on the effective mass is opposite to the change without a phonon frequency change. Including t_2 with the same sign as t reduces the polaron effective mass, when the same phonon frequency is used, whereas including a change in the phonon frequency according to the changes in effective bandwidth as in Eqs. (2.10) and (2.11) *increases* the effective mass in one and three dimensions. We feel that including the change in phonon frequency is the more physically correct procedure. In two dimensions NNN hopping has very little effect on the effective mass in weak-coupling.

In one and three dimensions we have also found a heuristic scaling factor for g, the dimensionless electron-phonon coupling strength, that maps the results for the polaron effective mass of the NNN Holstein model back onto the standard model without NNN hopping. While the physical reason for this effect is not known, this heuristic scaling allows us to crudely estimate how increasing

t_2 impacts the coupling strength at which the (sharp) crossover occurs for polaronic behaviour. For small values of t_2/t the crossover remains in the regime of moderate electron-phonon coupling. Therefore it remains difficult to reconcile the fairly strong-coupling attributed to some real metals/superconductors with the diverging effective mass predicted for a single polaron at the same coupling strength.

Chapter 3

The Holstein Model with Extended Range Electron-Phonon Interactions

We present numerically exact solutions to the problem of a single electron interacting through an extended interaction with optical phonons in two and three dimensions. This is another possible avenue to reconciling the large electron effective mass at strong coupling to the mobile Cooper pairs or superconductors. Comparisons are made with results for the standard Holstein model, and with perturbative approaches from both the weak-coupling and strong coupling sides. We find, in agreement with earlier work, that the polaron effective mass increases (decreases) in the weak (strong) coupling regime, respectively. However, in two dimensions, the decrease in effective mass still results in too large an effective mass to be relevant in realistic models of normal metals. In three dimensions the decrease can be more relevant, but exists only over a very limited range of coupling strengths.

3.1 Introduction

The standard theoretical framework for superconductivity is known as BCS-Eliashberg theory,[24, 35, 36, 37, 38, 39] and, as catalogued in the cited reviews, accurately describes many experimentally known properties of the so-called conventional superconductors, like Pb. BCS theory itself is almost universal, and confirmation of this theory, achieved with unprecedented accuracy for weak-coupling superconductors like Aluminium, serves to vindicate the"pairing formalism", utilized to construct BCS theory, but does little to confirm the mechanism.[40]

The mechanism for pairing in conventional superconductors is believed to be virtual phonon exchange, in complete analogy to the virtual photon exchange which is responsible for the direct Coulomb interaction between two charged particles. The primary evidence for this belief comes from the isotope effect and a comparison of tunnelling data with the *deviations* from BCS theory captured in Eliashberg theory, and again, a considerable body of evidence that confirms the virtual phonon exchange mechanism for pairing is described in Refs. [24, 35, 36, 37, 38, 39].

At a more microscopic level, for the past several decades the Holstein model[5, 27] has served as the chief paradigm to describe electron-phonon interactions in solids. In part this paradigm choice has been driven by the physics, and the realization that in the single polaron problem the interaction can be very local and the (optical) phonons are well-described by Einstein oscillators. In addition, however, computational techniques for understanding the properties of a polaron have evolved in a manner conducive to lattice models with local interactions; this has led to an abundance of studies of the properties of this particular model. Many of these properties are at odds with the Eliashberg description; early work[14, 15] using Quantum Monte Carlo (QMC) methods suggested a dominance of charge ordering phenomena in lieu of superconductiv-

ity, while more recent work relying on hybrid Migdal-Eliashberg and Dynamical Mean Field Theory (DMFT) [41] provided some reconciliation, though the competitive charge-ordered phase was not included. In any event we currently lack a microscopic description of the many-body Fermi sea of electrons interacting with phonons with an intermediate to strong coupling strength, *in terms of* the basic building block, i.e. a *single* electron coupled to phonons. The problem is that, in this same coupling strength regime, a single electron is highly polaronic,[42, 43, 28, 44] particularly when the phonon frequency is small compared to the electronic bandwidth.[10, 29, 45] In other words, either we have to understand how electrons become *less polaronic* as many of them assemble to form a a degenerate Fermi sea, or we have to understand how weakly interacting (non-polaronic) electrons, when assembled to form a Fermi sea, become more strongly interacting, presumably through phonon renormalization.

Alongside these developments the Fröhlich model[46, 47, 48] for electron-phonon interactions describes a screened but long-range interaction between an electron and the (positively charged) ions in a crystal. In fact, it is for this model that much of the early analytical work on the polaron was done.[1, 49, 50, 51, 52] This model has only one energy scale, the phonon frequency, which makes a comparison with the Holstein model, for example, difficult. In the Holstein model and other lattice models like it, there are two energy scales, one corresponding to the phonon frequency and the other corresponding to the (bare) electron bandwidth. Polaronic effects depend significantly on the ratio of these two energy scales, $\omega_{\rm ph}/t$, sometimes known as the adiabatic ratio. Here, t is the bare electron hopping amplitude. Until recently,[10, 29] much of the work done on microscopic models used an adiabatic ratio close to unity; the more physical regime, and the one required by the Migdal approximation when many electrons are considered, is $\omega_{\rm ph}/t << 1$.

In an effort to draw comparisons between the short-range Holstein model and the longer-range Fröhlich model, Alexandrov and Kornilovitch[53] defined

a Fröhlich polaron problem on a discrete lattice. They examined the behaviour of the effective mass as a function of coupling strength, primarily on one and two dimensional lattices. They concluded that with extended range interactions, the effective mass can be much smaller than for the Holstein polaron. Thus, a microscopic model with long-range electron-phonon interactions is a possible means of reconciling exact single electron "building-block" calculations with the Migdal approximation that underlies the Eliashberg theory of electron-phonon-mediated superconductivity.

However, as mentioned earlier, the single electron longer-range interaction studies were carried out with an adiabatic ratio of order unity. Here we wish to re-examine this problem with more physical values of the adiabatic ratio, and extend their calculations[53] to three dimensions. We will also adopt the truncated (in range) interaction subsequently adopted by a number of authors — see e.g. Refs. 18, 32 — and include nearest neighbour interactions only, in addition to the on-site interaction included in the standard Holstein model. Following these latter two papers we will refer to this is as the extended Holstein model. In fact this interaction better represents the expected screening in a real metal; this effect has been studied in, for example, Ref. 54. We find that while the conclusion of Ref. 53 that the effective mass can be much smaller for the extended than for the Holstein model is correct, this statement applies for a very restrictive range of the coupling strength. We also note that the behaviour in two dimensions is not representative of what occurs in either one or three dimensions. In fact, even in what is normally considered the perturbative regime, low-order perturbation theory is not very accurate. Their initial conclusions are actually more representative for the three dimensional case.

The rest of the chapter proceeds as follows. First, following Ref. [53], we define the model, and we outline the method of solution. We have exact results for all our calculations, based on refinements of the method introduced by

Bonča et al.[28] This controlled method of solution becomes somewhat more difficult for three dimensions, but we present converged results for phonon frequencies as low as $\omega_E/t = 0.3$. Considering that this is achieved in three dimensions, where the electronic bandwidth is $W \equiv 12t$, this phonon energy scale represents 2.5% of the electronic bandwidth.

Results are first presented in two dimensions. We first re-assess some older results,[10] and note that, even for the standard Holstein model, perturbative calculations, either in weak or strong coupling, are actually not very accurate. In weak-coupling for example, multi-phonon excitations lead to a significantly enhanced effective mass. This phenomenon is amplified when extended interactions are included, so in fact we find the conclusions of Ref. [53] somewhat misleading. The effective mass does decrease due to longer range interactions in the strong coupling regime, but in two dimensions, the resulting effective mass is still much too high to be relevant for normal (i.e. non-polaronic) metals.

The following section treats the three dimensional case, where we find that a lower effective mass, *to realistic values*, is indeed achieved by including extended interactions. However, even here the range of coupling strengths over which this is achieved is very narrow; in terms of the dimensionless coupling constant λ (to be defined below), this range is very close to unity, and not in the range associated with so-called Eliashberg strong coupling superconductors.

3.2 Model and Method

The lattice Fröhlich ("extended Holstein") model is defined as[53]

$$\begin{aligned} H = & - t \sum_{i,\delta} \left[c_i^\dagger c_{i+\delta} + c_{i+\delta}^\dagger c_i \right] \\ & - g\omega_E \sum_{\langle \mathbf{i},\mathbf{j} \rangle} f(\mathbf{j}) n_{\mathbf{i}} (a_{\mathbf{i}+\mathbf{j}} + a_{\mathbf{i}+\mathbf{j}}^\dagger) \\ & + \omega_E \sum_i a_i^\dagger a_i, \end{aligned} \tag{3.1}$$

where the range of the interaction is given by

$$f(\mathbf{j}) = \frac{1}{(|\mathbf{j}|^2 + 1)^{3/2}}. \tag{3.2}$$

In Eq. (3.1) t is the electron hopping parameter, ω_E is the characteristic phonon frequency, taken to be a constant here, and $g\omega_E f(\mathbf{j})$ is the coupling strength between an electron at a particular site and a phonon at a site a distance $a_0|\mathbf{j}|$ away, where a_0 is the lattice spacing (taken to be unity hereafter) and $\mathbf{j}$ is the vector connecting the electron and phonon. The case $f(\mathbf{j}) = \delta_{\mathbf{j},\mathbf{0}}$ reduces to the usual Holstein model. The other symbols are defined as follows: $c_i^\dagger$ (c_i) creates (annihilates) an electron at site i, and $a_i^\dagger$ (a_i) creates (annihilates) a phonon at site i. The electron number operator is given by $n_i \equiv c_i^\dagger c_i$, and the spin index has been suppressed since we are dealing with only one electron. Note that the sum over δ in the electron hopping part of the Hamiltonian is over nearest-neighbour sites on the positive side only, to avoid double counting, whereas the sum over $\mathbf{j}$ in the interaction term in principle includes the on-site term ($\mathbf{j} = 0$) along with neighbouring sites in *all* directions. As mentioned earlier, we will follow Refs. [18, 32], and we will terminate the sum at nearest neighbour interactions.

We will use Eq. (3.2) for all dimensions, but, with interactions truncated to nearest neighbour distances. In reality this form is motivated by the three dimensional case, where the long range interaction follows a $1/r^3$ decay. At short distances a potential divergence is cut off by the constant '1' in the denominator of Eq. (3.2); this corresponds to a characteristic decay length of the lattice spacing, and in principle this can be varied as well. Here, for simplicity, we keep the constant fixed at unity. This Hamiltonian contains a dimensionless coupling constant, namely g, which becomes most important in the strong coupling regime. In practice we also define another dimensionless coupling constant, λ, which becomes important in the weak-coupling regime.

Specifically for the coupling of the electron to the phonons at the same site we use, following Li et al.,[10] $\lambda_c \equiv \omega_E g^2/(W/2)$ in one and three dimensions, where W is the bare electron bandwidth, $W = 4t$ in one dimension and $W = 12t$ in three dimensions for the tight-binding model on a linear or cubic lattice with nearest neighbour hopping, respectively. In two dimensions we use a definition where the electron density of states at the bottom of the bare band is used [$\equiv 1(4\pi t)$] instead of the average value of the density of states across the entire band [$\equiv 1/(8t)$], so $\lambda_c \equiv \omega_E g^2/(2\pi t)$. For the Holstein model the entire coupling would be that of the on-site coupling.

To define the coupling strength for the extended model, $\lambda_{\rm tot}$, we follow the definitions of Alexandrov and Kornilovitch,[53] with the total coupling being the sum of the couplings to the different sites. This definition is physically based on the ratio of the polaronic shift to the electron kinetic energy. For example, in two dimensions we obtain the on-site contribution along with four equally weighted nearest neighbour contributions, reduced by $[1/2^{3/2}]^2 = 1/8$ compared to the on-site value:

$$\lambda_{\rm tot} = \sum_{\mathbf{j}} \lambda_c f^2(\mathbf{j}) = \lambda_c \left(1 + 4\frac{1}{8}\right). \tag{3.3}$$

The single polaron problem is solved here with the variational exact diagonalization method described in Bonča et al[28] with the same refinements for low frequency calculations as developed by Li et al.[10] The modifications required for the extended model fit nicely into this computational framework, with the cost of a denser Hamiltonian matrix, and a Hilbert space that grows faster with each application of Hamiltonian, compared to similar calculations for the standard (i.e. on-site) Holstein model. This rapid growth makes it difficult to converge results using an extended version of the adaptive method of Li et al.

We therefore further refined the method by producing a list of the most

important basis states for each point in parameter space. Starting with a list of basis states from a nearby parameter point previously diagonalized, or a truncated coherent state from the strong coupling Lang-Firsov solution[55, 56, 10] we diagonalized the Hamiltonian in this basis. These basis states in turn were ranked according to the magnitude of their contribution to the ground state, and the top N_1 contributions were kept. We then acted on these N_1 states with the Hamiltonian to produce more basis states and diagonalized the Hamiltonian in this new space. The resulting eigenvector was then sorted, the top N_1 contributions were kept, and the process repeated. Once this procedure converged, we sorted one last time, and kept the top N_2 states ($N_2 > N_1$) and did the final diagonalization. While this was a time-consuming calculation, it allowed for much better results with a finite amount of computer memory since it selected out the basis states that were the most important for describing the ground state.

Using this method at small λ should reduce to weak-coupling 2^{nd} order perturbation theory. Using straightforward Rayleigh-Schrödinger perturbation theory in two dimensions with on-site and nearest-neighbour interactions only results in a second-order correction to the ground state energy,

$$E^{(2)}(k_x, k_y) = -\frac{2\pi\lambda_{\rm tot} t\omega_E}{1+4f^2(1)}\frac{1}{N}\sum_{k'}\frac{\left(1-\frac{f(1)}{t}\epsilon_{k'-k}\right)^2}{\epsilon_{k'}+\omega_E-\epsilon_k}, \tag{3.4}$$

where $\epsilon_k \equiv -2t[\cos(k_x a_0) + \cos(k_y a_0)]$ is the bare energy for the nearest-neighbour tight-binding model. This expression can be evaluated in terms of complete elliptic integrals — for example [$f_1 \equiv f(1)$],

$$\begin{aligned} &E^{(2)}(0,0) = \\ &-\lambda_{\rm tot}\omega_E\left\{\frac{(1+4zf_1)^2}{1+4f_1^2}\frac{1}{z}K\big[\frac{1}{z^2}\big] - 4\pi f_1\frac{1+2zf_1}{1+4f_1^2}\right\}, \end{aligned} \tag{3.5}$$

where $z \equiv 1+\omega_E/(4t)$, but for most of our perturbation results we have simply

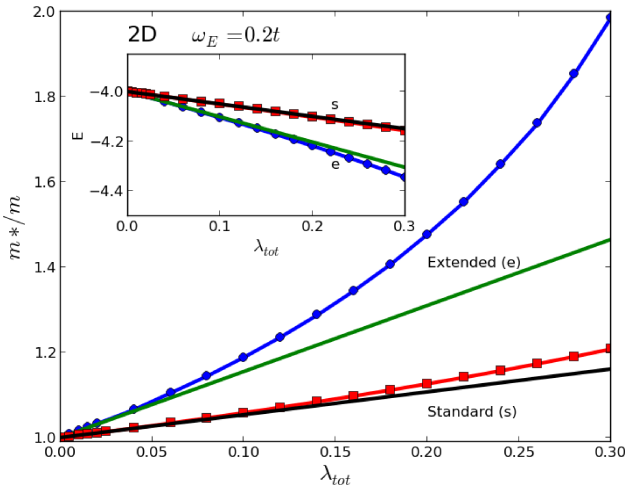

Figure 3.1: Effective mass, m^*/m vs. coupling strength $\lambda_{\rm tot}$, using perturbation theory for both the extended and standard Holstein models. The perturbation theory are the solid lines the exact diagonalization results are the square and circle symbols. We have used $\omega_E = 0.2t$. Perturbation theory is less accurate for the extended model compared with the standard model. *Inset:* Ground state energy vs. $\lambda_{\rm tot}$. Note that the results for the energy are fairly accurate, in comparison to those for the effective mass.

evaluated the effective mass numerically. Results are shown for the effective mass in the k_x direction although of course there is a $k_x - k_y$ symmetry.

3.3 Results in Two Dimensions

While others have studied the standard Holstein model in detail,[28, 10, 29] there are a few results here that should be emphasized, and which are important for a more complete understanding of the extended Holstein model. The perturbative regime for the two dimensional Holstein model is actually very small. While the ground state energy from perturbation theory matches the exact ground state energy well, the wavefunction and effective mass do not, as seen in Fig. 3.1. Perturbation theory does not work very well because the wavefunction, even at weak-coupling, needs to include states with multiple

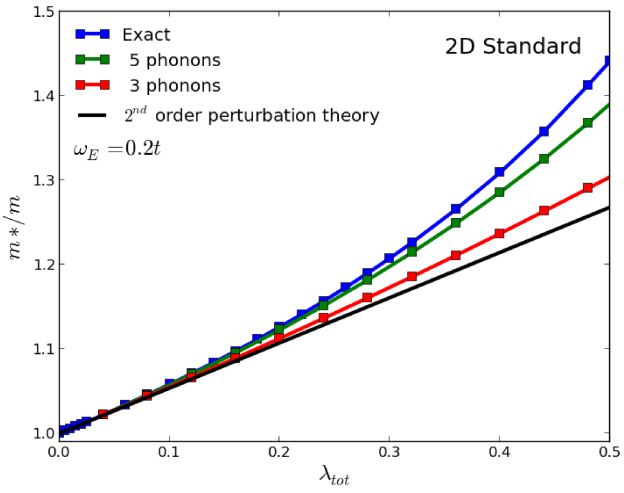

Figure 3.2a: m^*/m decreases as the accuracy of the calculation decreases. The curves with 5 and 3 phonons include states with phonons far from the electron, but never more than 5 or 3 phonons total respectively. 2^{nd} order perturbation theory includes excited states with at most a single phonon. $\omega_E = 0.2t$

phonons, *especially* when the phonon frequency is small compared to the electron hopping parameter, t. Even for the standard Holstein model, restricting our exact diagonalizations to a subspace with a limited number of phonons gives quantitatively inaccurate results for the effective mass, even if the energy was not strongly affected, as illustrated in Fig. 3.2a. For the extended model, the discrepancies are even more pronounced, as shown in Fig. 3.2b.

A second point we wish to make concerning the standard model is that, contrary to what the (fairly accurate) results for the ground state energy might imply, the strong coupling solution is not simply the single Lang-Firsov coherent state:

$$|\psi\rangle = e^{-g^2/2}\frac{1}{\sqrt{N}}\sum_{\ell} e^{ikR_\ell} e^{g\hat{a}_\ell^\dagger}\hat{c}_\ell^\dagger|0\rangle. \tag{3.6}$$

We have done an exact calculation and compared the resulting exact wavefunction to the Lang-Firsov coherent state in Fig. 3.3. The exact solution has a large coherent state component which has a peak somewhat shifted from the

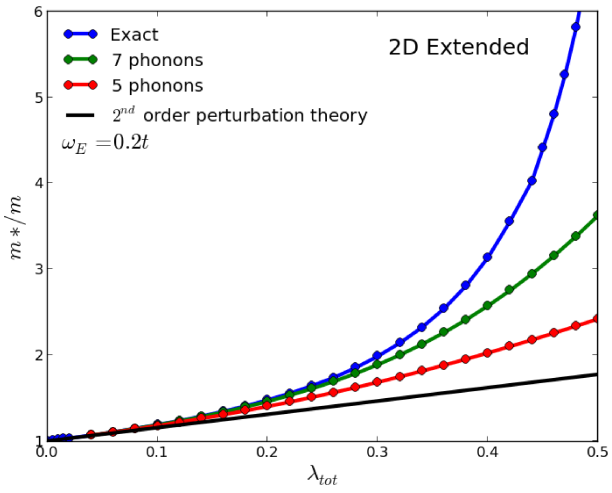

Figure 3.2b: For the two dimensional extended Holstein model, m^*/m again decreases as the accuracy of the calculation decreases similar to the standard model. Here the effect is even more pronounced: many phonons are required even for moderate coupling strengths. Again, 2^{nd} order perturbation theory includes at most a single phonon. $\omega_E = 0.2t$

Lang-Firsov coherent state. The really important difference is the contribution of states with phonons that are not on the same site as the electron. While these states do not have a large probability in the overall wavefunction, they are important for calculating an accurate effective mass. These states increase the size of the phonon cloud so that neighboring sites are "more prepared" to receive the electron and thus lower the overall effective mass. Using only the Lang-Firsov coherent state gives an effective mass that is too high by orders of magnitude. The same principle reduces the effective mass in the extended model; a nearest neighbour coupling produces phonons on the neighbouring sites, preparing them to receive the electron and lowering the effective mass.

As illustrated in Fig. 3.3 the crucial addition of extended phonons can be grouped with great precision into multiple coherent states, and coherent states modified with a few other phonons. So, in general, the wave function could be

expanded into multiple coherent components:

$$\begin{aligned}|\psi\rangle &\approx b_0 e^{-g_0^2/2}\frac{1}{\sqrt{N}}\sum_\ell e^{ikR_\ell}e^{g_0\hat{a}_\ell^\dagger}\hat{c}_\ell^\dagger|0\rangle \\ &+ b_1 e^{-g_1^2/2}\frac{1}{\sqrt{4N}}\sum_{\ell,\delta} e^{ikR_\ell}e^{g_1\hat{a}_{\ell+\delta}^\dagger}\hat{c}_\ell^\dagger|0\rangle \\ &+ b_2 e^{-g_2^2/2}\frac{1}{\sqrt{4N}}\sum_{\ell,\delta} e^{ikR_\ell}e^{g_2\hat{a}_\ell^\dagger}\hat{a}_{\ell+\delta}^\dagger\hat{c}_\ell^\dagger|0\rangle + ..., \end{aligned} \tag{3.7}$$

where δ designates neighbouring sites in all directions. Based on how orderly Fig. 3.3 looks one could imagine using a variational approach with these coherent states as well. For this paper, however, we kept with the simple Bloch states which, though far more numerous, are easier to handle as they are guaranteed to be orthogonal. We express the exact wavefunction $|\psi\rangle$ in terms of those states:

$$|\psi\rangle = \sum_n d_n \left(\frac{1}{\sqrt{N}}\sum_\ell e^{ikR_\ell}|\phi_{n\ell}\rangle\right) \tag{3.8}$$

where the $|\phi_{n\ell}\rangle$ are orthonormal product states consisting of an electron at site ℓ and product states of phonons at all sites $\ell+\delta$. For example, for the Lang-Firsov state given by Eq. (3.6), $d_n = e^{-g^2/2}g^n/\sqrt{n!}$.

The main message of this is that while the standard Holstein model may be the simplest polaron model, its solution is still a fairly complicated many-body wavefunction, even in the weak and strong coupling limits. Without accurate characterization of this wavefunction, it may still be possible to calculate some expectation values, like the ground state energy, accurately, but others, such as the effective mass, need a more precise wavefunction. When measuring expectation values with any numerical method, it is important to converge these values on their own as they may need a much larger basis space than, for example, the ground state energy, to be accurately described.

The first qualitative difference found between the extended and on-site Holstein models is at weak-coupling. In the standard model, we find a very slight

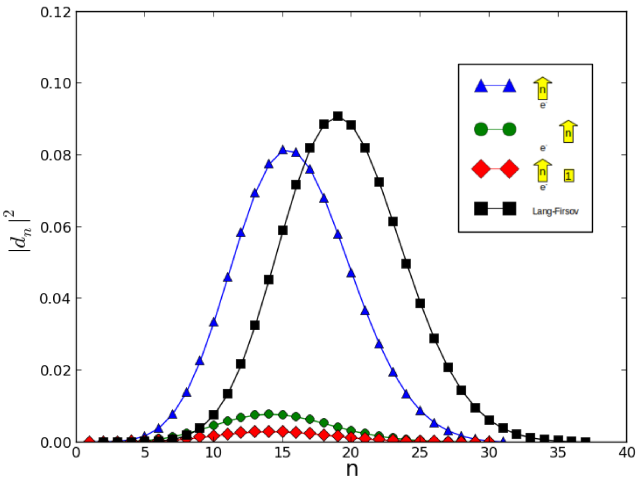

Figure 3.3: Probability ($|d_n|^2$) of various basis states from the Lang-Firsov approximation and the standard model in two dimensions, with $\lambda = 0.62$ and $\omega_E = 0.2t$. The curve in black, labeled as 'Lang-Firsov' in the legend is the result obtained from the Lang-Firsov approximation given in Eq. (3.6). The other curves represent amplitudes obtained from the exact solution. The points denoted by triangle shaped symbols connected with a blue curve represent amplitudes with 'n' phonons on the same site as the electron, as denoted in the legend. These amplitudes are those of the true, numerically exact wavefunction, and are shifted compared to the Lang-Firsov approximation, as is evident from the figure. Also shown are amplitudes for wavefunction components representing an electron at some site, with 'n' phonons on the neighbouring site; these are indicated by circle shaped symbols connected with a green curve. Finally, the amplitudes for wavefunction components representing an electron with a single phonon on a neighbouring site and 'n' phonons on the same site as the electron are indicated by diamond shaped symbols and connected with a red curve.

increase of the effective mass with increasing phonon frequency (see Fig. 3.4), while in the extended model, we find the opposite; the effective mass decreases as a function of increasing frequency. Note that the analytical result for the effective mass in the adiabatic limit is obtained from perturbation theory, and not from the semi-classical adiabatic calculations.[57] The adiabatic calculation reveals in weak-coupling a regime in which there are *no* ion deformations, which one might possibly interpret as indicating an effective mass equal to the non-interacting electron mass. However, this is not what is obtained when the full quantum calculation is performed in the limit of vanishingly small phonon frequency. Moreover, perturbation theory calculations correctly yield an effective mass ratio equal to $(1 + \lambda/2)$ for the standard Holstein model in two dimensions, in agreement with the full quantum calculations.

For the extended model used here, one can show that the perturbative effective mass is given by

$$m^*/m = 1 + \frac{\lambda_{\rm tot}}{2}\frac{[1+4f(1)]^2}{1+4f^2(1)}. \tag{3.9}$$

This agrees with the limiting value as $\omega_E \to 0$, obtained through numerical integration in Fig. 3.4.

Since the exact results and perturbation theory agree for the effective mass in very weak-coupling, the latter calculations can be trusted in this regime. Therefore we plot in Fig. 3.4 only the perturbation theory results for the effective mass vs. ω_E/t to highlight the differences between the extended and standard models (for definiteness, we use $\lambda_{\rm tot} = 0.1$). At low values of ω_E/t the extended model's effective mass decreases monotonically with increasing ω_E/t while the on-site model has a peak near $\omega_E/t = 1$. Both models have an effective mass ratio of unity ($m^*/m = 1$) in the anti-adiabatic limit, $\omega_E \to \infty$.

Quantitatively, the extended Holstein model has a larger effective mass at weak-coupling, and a smaller effective mass at strong coupling compared

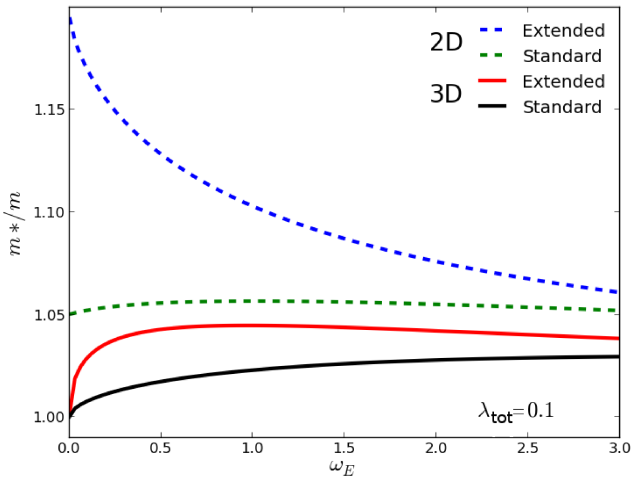

Figure 3.4: m^*/m from 2^{nd} order perturbation theory vs ω_E. For definiteness, the value of $\lambda_{\rm tot}$ is 0.1. In the large ω_E limit all the curves approach 1.0 but the Extended model always has a larger m^*/m than the Standard model in both two and three dimensions.

to the standard Holstein model (for the same phonon frequency). Previous researchers[58, 53, 28] have examined both the ordinary and/or extended models in the past, but due to computational considerations did not examine the model in the most physically important parameter regime. In many real materials the electronic bandwidth is in the eV range while the phonon modes tend to be in the meV range, so the physical adiabatic ratio regime is $\omega_E/t \lessapprox 0.2$.

For reasons stated earlier, calculations with small phonon frequencies are difficult to converge, so we have utilized a number of small frequencies. As a compromise, we will present most results for $\omega_E/t = 0.2$, as these are well converged, and also representative of the low frequency regime. In Figs. 3.5a and 3.5b we show the effective mass ratio vs coupling strength for $\omega_E/t = 0.2$ and $\omega_E/t = 1.0$, respectively, for the standard vs extended Holstein models. Several points should be made. First, the crossover from the so-called weak to the so-called strong coupling regime for both standard and extended models is not so clear when $\omega_E/t \approx 1$, especially for the extended model. In contrast,

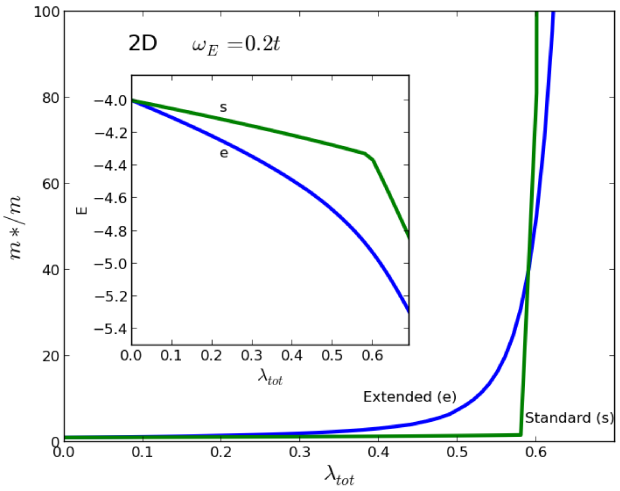

Figure 3.5a: For the two dimensional model, m^*/m as a function of λ_{tot} up to strong coupling with $\omega_E = 0.2t$. Note that beyond $\lambda_{\text{tot}} = 0.6$ the effective mass of both models is practically infinite, but at intermediate coupling strengths the extended model shows a significantly higher effective mass. *Inset:* Ground state energy vs. λ_{tot}.

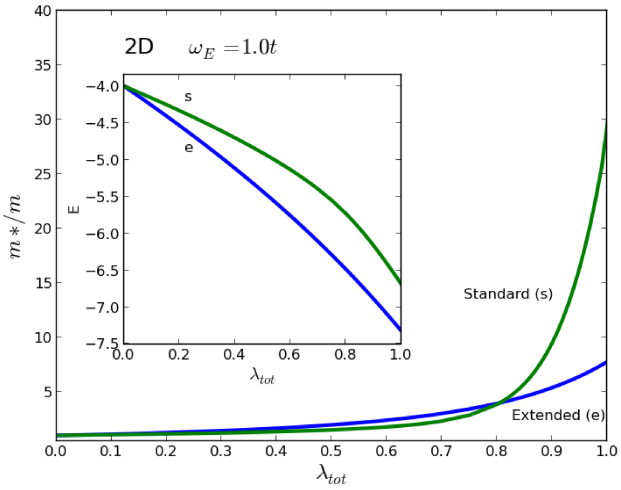

Figure 3.5b: For the two dimensional model, m^*/m as a function of λ_{tot} up to strong coupling with $\omega_E = t$. Note that the effective masses are all much smaller and at intermediate coupling strengths the extended model shows an effective mass only slightly higher than the standard model. The coupling strength is also much larger before the effective masses rise to unphysical values. *Inset:* Ground state energy vs. λ_{tot}.

the crossover is much better delineated for low phonon frequencies, as is clear in Fig. 3.5a. The point made in Ref. [53], that the extended model results in a lower effective mass is also clear, for λ values beyond some intermediate coupling strength. At high phonon frequency (Fig. 3.5b) this means a reduction from $m^*/m \approx 30$ to $m^*/m \approx 7$, for example. By any measure this reduction is significant, but somewhat irrelevant, since the effective masses involved, even after reduction, are too high to describe normal state properties. However, for more realistic (lower) phonon frequencies (Fig. 3.5a), both crossovers are sharpened as a function of coupling strength, although less so for the extended model, with the net result that a regime of effective mass reduction remains, and the reduction is enormous, but now the mass is 'lowered' to values of 40 or higher. In fact, the clear effect of extended interactions is to *raise* the effective mass for most of the parameter regime that is physically relevant.[59]

To summarize this subsection, the extended Holstein model is more realistic than the standard model insofar as it includes interactions extended beyond on-site. This does give rise to a coupling regime where the effective mass is lowered, compared to the standard model, but we argue that lowering the effective mass ratio from 100 to 40 is not so relevant. Instead, the clear result of increasing the range of interaction is to *enhance* the effective mass so that in the so-called weak-coupling regime the effective mass is increased due to the longer range interactions. Extended range interactions is therefore *not* seen as a means to lower the electron effective mass to reasonable levels in the two dimensional polaron problem. However, the effect of long range interactions can be different in three dimensions, and we turn to that question next.

3.4 Results in Three Dimensions

We applied the same technique to an extended Holstein model in three dimensions. We limited ourselves again to nearest neighbour and on site electron-

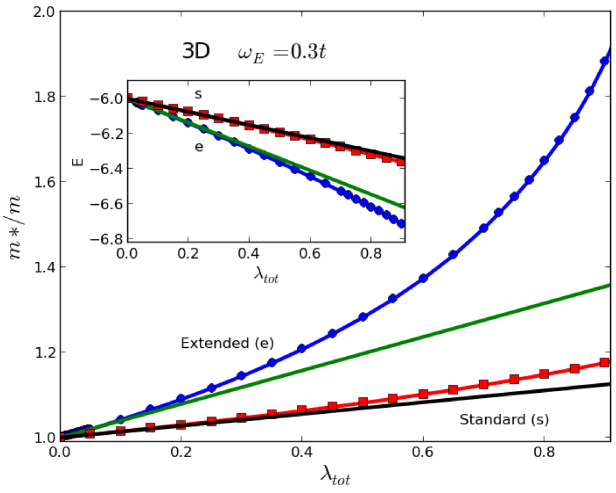

Figure 3.6: For the three dimensional model, m^*/m as a function of $\lambda_{\rm tot}$, with $\omega_E = 0.3t$, to compare exact and perturbative results. Similar to the two dimensional the region of validity for perturbation theory is much smaller in the extended model though it is not particularly large for the standard model either. *Inset:* Ground state energy vs. $\lambda_{\rm tot}$. Again, perturbation theory works better for the ground state energy than for the effective mass.

phonon coupling, simply extending the two-dimensional Hamiltonian to three dimensions. We then computed the ground state energy and effective mass with perturbation theory and with the numerical method outlined above.

The perturbation theory was done with straightforward Rayleigh-Schrödinger perturbation theory with the integrals performed numerically as in the two dimensional case. We used $\omega_E/t = 0.3$, since the electronic bandwidth with nearest neighbour hopping only is $12t$ in three dimensions (as opposed to $8t$ in two dimensions). As in the two dimensional case there is good agreement between the exact results and perturbation theory only for a small region of weak-coupling, $\lambda_{\rm tot} \lesssim 0.4$, for the standard model, as seen in Fig. 3.6. In the extended model, the good agreement is only achieved for an even more restricted range of $\lambda_{\rm tot} \lesssim 0.2$, as seen in the same figure.

These results are plotted for a 'low' phonon frequency, $\omega_E/t \approx 0.3$; however, in three dimensions there is no ambiguity about the adiabatic limit. Perturba-

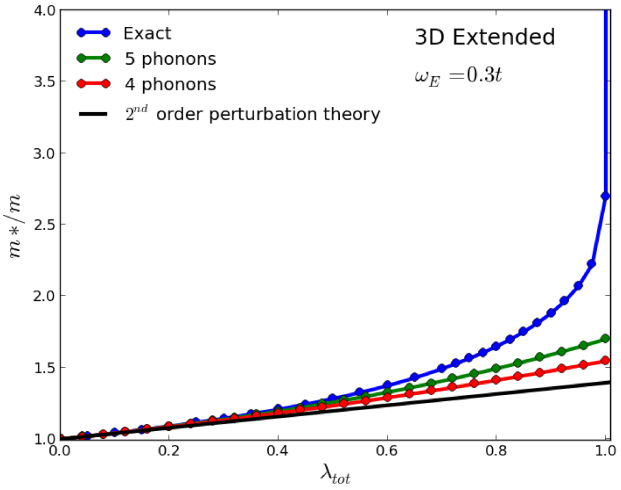

Figure 3.7: For the three dimensional case, m^*/m vs. λ_{tot}, with $\omega_E = 0.3t$. The effective mass increases as more and more states with more than one phonon excitation are included. The curves with 4 and 5 phonons include states with phonons far from the electron, but there are never more than a total of 4 or 5 phonons, respectively. The calculation with 2^{nd} order perturbation theory includes basis states with at most a single phonon.

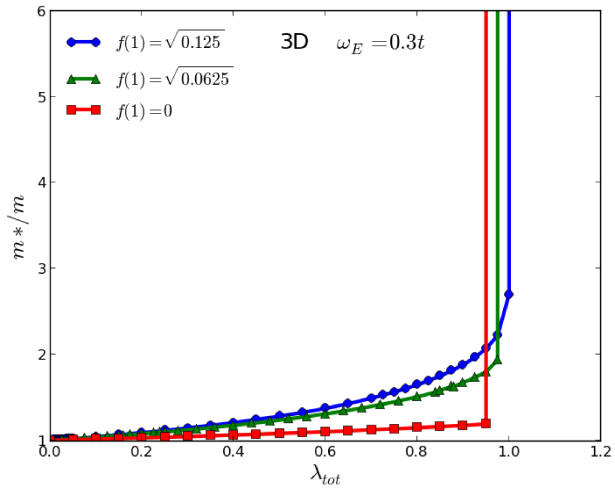

Figure 3.8: For the three dimensional case, m^*/m vs. λ_{tot} with various values of $f(1)$. These results are from numerically exact calculations. The extended model can shift the onset of unphysically high effective masses to stronger coupling, though the extra range of tenable coupling strengths is rather small.

tion theory, semi-classical adiabatic calculations[57] and limiting trends from exact diagonalization all agree that for small λ, the effective mass ratio approaches unity, i.e. $m^*/m \to 1$ as $\omega_E \to 0$, and there is no polaron formation in this limit. In Fig. 3.4 it is clear from the three dimensional results that the behaviour of the effective mass ratio for the extended model is quite similar to that for the standard Holstein model. Quantitatively, the effective mass is somewhat larger for the extended model, but not enormously so. The results in Fig. 3.6 are both representative of the adiabatic limit, which has no polaron formation.

In Fig. 3.7 we show the so-called perturbative regime to illustrate that also in three dimensions this regime is confined to very small values of λ only. The crossover region, shown for the effective mass in Fig. 3.8, becomes very sharp as the phonon frequency is decreased[30, 31], to coincide with the point in semi-classical calculations where the ground state abruptly becomes polaronic, after being free-electron-like up to that point. The impact of extended interactions is clear from the figure; the crossover region is definitely moved to higher coupling strengths as the range and strength of the nearest neighbour interaction increases. An obvious limiting case is where the interaction becomes infinitely long ranged, with the same strength independent of distance from the electron. In this case the electron will remain free-electron-like for all coupling strengths. Note that for realistic nearest neighbour interactions there is now a small range of coupling strengths where the effective mass is indeed reduced to realistic values through extended interactions, consistent with the original conclusions of Ref. [53]. That is, in contrast to the two-dimensional case, extended range interactions seem to shift the regime of coupling strengths wherein the effective mass is low, *without at the same time increasing significantly the effective mass in this regime.*

3.5 Summary

We have presented exact and perturbative results for the extended Holstein model. This model was conceived[53] in an effort to realize the Fröhlich model on a lattice. Our primary purpose was to re-assess the conclusions of Ref. [53] when a smaller and more realistic adiabatic ratio, ω_E/t, is used. We found that, in two dimensions, the effective mass in the so-called weak-coupling regime is enhanced by extended interactions, while the effective mass in strong coupling is suppressed. This is in agreement with the results of Ref. [53], but we nonetheless find this assessment misleading. In particular, in strong coupling, being able to achieve an effective mass reduction from 100 to 40 is wonderful, but does not serve to reconcile the qualitative results of the Migdal description with the single polaron results. It still remains that, over most of the range of coupling strengths, the effective mass is *increased* by longer range interactions. Moreover, it is clear that a perturbative description, which, for a single electron problem actually coincides (in a technical sense) with the Migdal approximation, is woefully inaccurate when it comes to describing the details (wavefunction, electron effective mass, etc.) of the solution, even for much weaker coupling strengths. In three dimensions this problem is slightly ameliorated, in that, at least for a very limited range of coupling strengths, the effective mass can be vastly reduced by many orders of magnitude by longer range interactions (see Fig. 3.8, just to the right of the standard Holstein results, i.e. the left-most almost vertical line). Even in three dimensions, however, the perturbative weak-coupling regime seems to require considerably more phonon excitations than second order perturbation theory would suggest.

Further attempts to reconcile Migdal-based approximations vs. exact single electron calculations can proceed along a number of paths, several of which are currently under investigation. For example, one can attempt to develop controlled approximations for more than one electron (the bipolaron, for example,

has been already investigated).[18, 32] One would expect phonon and coupling strength renormalization to occur as the increasing number of electrons will have a more significant impact on the phonons. Another direction involves more sophisticated electron-phonon couplings, and the possible importance of acoustic modes.

Chapter 4

The BLF-SSH Model in the Adiabatic Limit

We surveyed polaron formation in the BLF-SSH model using acoustic phonons in the adiabatic limit. Multiple different numerical optimization routines and strong-coupling analytical calculations are used to find a robust ground state energy for a wide range of coupling strengths. The electronic configuration and accompanying ionic distortions of the polaron were determined, as well as a non-zero critical coupling strength for polaron formation in two and three dimensions.

4.1 Introduction

Many-body calculations of electrons coupled to acoustic phonon modes were first proposed by Barisić, Labbé, and Friedel (BLF)[6] in the context of understanding transition metal superconductivity in 1970. The same coupling was subsequently reintroduced by Su, Schrieffer, and Heeger (SSH)[60, 7] 10 years later to model soliton modes in long polyacetylene chains. More recently there has been a revival of interest in these types of models to describe superconductivity in the cuprate materials, though typically only the so-called

BLF-SSH form of the coupling is adopted. For both physical and technical reasons, the acoustic phonons are usually modeled as Einstein oscillators, i.e. optical modes. We refer to this modification as the Capone, Stephan, Grilli (CGS) model to avoid confusion.[61] The BLF-SSH model has also been used recently in problems concerning conducting polymers for electronic and solar-cell applications,[62] as well as problems in biophysics.[63]

The BLF-SSH model differs from the commonly used Holstein model[5] in two main ways. First, as already mentioned, it uses acoustic phonon modes, thus maintaining relevance for materials without optical modes. This includes all elemental metals. Most significantly, superconductivity in elemental metals occurs via interactions between electrons and acoustic phonons, so the basic building block in this case is the BLF-SSH polaron. Moreover, in the case of the Holstein model, polaronic effects were most pronounced for low frequency phonons; since the BLF-SSH model has a dispersive phonon mode that approaches zero frequency in the long wavelength limit, we expect that these modes could alter the polaron characteristics. In other words, the Holstein spectrum is gapped whereas the acoustic spectrum is not.

Second, the electron-phonon interaction in the BLF-SSH model modifies the electron hopping term, not the on-site energy as in the Holstein model. Both these modifications makes the BLF-SSH model technically more difficult, but they also potentially alter the physics somewhat, as the lowering of energy due to the electron-phonon coupling is associated with *movement* of the electron, and not with the (Coulombic) potential energy between the electron and the displaced ionic charge. The so-called CSG model[61] shows somewhat unusual properties, even for the single polaron, presumably due to the optical mode simplification.

Much of the work done on this model is in the one dimensional adiabatic approximation, i.e. the phonons are treated classically.[60, 7] Barisić, Labbé, and Friedel[6] used BCS and diagrammatic methods to address superconductivity,

but after the SSH revival, the effects of quantum fluctuations were examined through quantum Monte Carlo and renormalization group studies,[12, 13] and these authors focused on half-filling. They found that the lattice ordering (in one dimension) was reduced by quantum fluctuations.

Further studies were performed for a single polaron, based on variational calculations,[50] for the Fröhlich Hamiltonian in the continuum with acoustic phonons and with a wave vector cutoff to mimic lattice effects. These authors generally found a phase transition to a "self-trapping" state, as a function of coupling strength.

For the BLF-SSH model, however, very little work has been done in the quantum regime for a single electron. We have studied the BLF-SSH polaron using perturbation theory, and were unable to find, for example, a perturbative regime in one dimension where polaron effects are absent.[23] In Ref. 64 the properties of a single polaron in the BLF-SSH model have been studied in one and two dimensions, using the adiabatic approximation. Unfortunately, we believe this two dimensional study has serious errors, and their results display unphysical emergent phenomena (see below). Here we will present a comprehensive survey of the adiabatic BLF-SSH model in one, two and three dimensions.

In the adiabatic limit the electrons are treated quantum mechanically, while the ions are treated semi-classically. The ions are considered to have no kinetic energy and their displacements from equilibrium are treated as input parameters to the Hamiltonian. Since the electronic bandwidth in real materials is often very large compared to the phonon energy scale, this limit is expected to be physically relevant. On the other hand certain pathologies have come to be associated with the adiabatic limit. For example, as will be reported below, we found a critical coupling strength in dimensions higher than one, beyond which the electron forms a polaron-like ground state, and below which the electron is decoupled from the lattice. From studies of the Holstein

model,[57, 28, 44, 10, 65] the existence of a critical coupling strength is expected to not survive away from the adiabatic limit. Nonetheless, studies of the adiabatic limit give a good picture of what will occur in the near-adiabatic limit, particularly in the strong-coupling limit.

This chapter is organized as follows: in the next section we define the model and the adiabatic approximation, and follow this with a short discussion concerning our methods. We then display some analytical results, and follow up with numerical results in the ensuing section. In the final section we provide a brief summary.

4.2 The Model

We begin by writing down the Hamiltonian for a two dimensional system - this is readily generalized to the one and three dimensional cases that are also treated in this chapter:

$$\begin{aligned} H &= -\sum_{\langle \mathbf{i},\mathbf{j}\rangle} t_{\mathbf{ij}}\left(c^{\dagger}_{\mathbf{i}\sigma}c_{\mathbf{j}\sigma} + h.c.\right) + \sum_{\mathbf{i}}\left[\frac{p^2_{x\mathbf{i}}}{2M} + \frac{p^2_{y\mathbf{i}}}{2M}\right] \\ &+ \frac{1}{2}K\sum_{\langle \mathbf{i},\mathbf{j}\rangle}\left[\left(u_{x\mathbf{i}} - u_{x\mathbf{j}}\right)^2 + \left(u_{y\mathbf{i}} - u_{y\mathbf{j}}\right)^2\right], \end{aligned} \tag{4.1}$$

where angular brackets denote nearest neighbours only without double counting, and the **i** and **j** indices are written in boldface to emphasize that for the D-dimensional case they are D-dimensional vectors. The operators and parameters are as follows: $c^{\dagger}_{\mathbf{i}\sigma}$ ($c_{\mathbf{i}\sigma}$) creates (annihilates) an electron at site **i** with spin σ. The x-components for the ion momentum and displacement are given by $p_{x\mathbf{i}}$, and displacement $u_{x\mathbf{i}}$, respectively (similarly for the y-components), and the ions have mass M and spring constant K connecting nearest neighbours

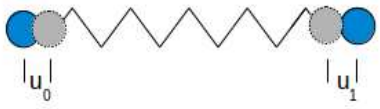

Figure 4.1: A one dimensional depiction of the variables used to describe ionic motion. The full blue circles are ions at their equilibrium positions, and the grey dotted circles are ions displaced from their equilibrium positions. The $u_{x\mathbf{i}}$ variables are then seen to be the displacements from equilibrium and $\tilde{x}_{\mathbf{0}} = u_{x\mathbf{0}} - u_{x\mathbf{1}}$ so $\tilde{x}_{x\mathbf{0}}$ can be thought of as the distance change between the two ions after subtracting the equilibrium distance spacing.

only. Furthermore,

$$t_{\mathbf{ij}} = t - \alpha(u_{x\mathbf{i}} - u_{x\mathbf{j}})\delta_{\mathbf{i,j}\pm\hat{\mathbf{a}}_{\mathbf{x}}} - \alpha(u_{y\mathbf{i}} - u_{y\mathbf{j}})\delta_{\mathbf{i,j}\pm\hat{\mathbf{a}}_{\mathbf{y}}}. \tag{4.2}$$

Note that the parameter α (the bare interaction strength) can be written as a derivative of the hopping amplitude with respect to displacement. Here it is simply treated as a parameter. Moreover, the electron hopping is modified only by ionic motions in the same direction, i.e. longitudinal coupling only, consistent with an expansion of the coupling term to linear order only in the displacements.[66] The adiabatic approximation is achieved by dropping the kinetic energy term for the ions:

$$\begin{aligned} H &= -\sum_{\langle \mathbf{i,j}\rangle} t_{\mathbf{ij}}\left(c^{\dagger}_{\mathbf{i}\sigma}c_{\mathbf{j}\sigma} + h.c.\right) \\ &+ \frac{1}{2}K\sum_{\langle \mathbf{i,j}\rangle}\left[\left(u_{x\mathbf{i}} - u_{x\mathbf{j}}\right)^2 + \left(u_{y\mathbf{i}} - u_{y\mathbf{j}}\right)^2\right]. \end{aligned} \tag{4.3}$$

This means that we can treat the ionic displacements as c-numbers, and the electronic part of the Hamiltonian remains as an eigenvalue problem. We change variables for the ions, since the Hamiltonian depends only on the separation between the ion sites. Thus we define $\tilde{x}_{\mathbf{i}} = u_{x\mathbf{j}} - u_{\mathbf{i}+\delta_{\mathbf{x}}}$ and $\tilde{y}_{\mathbf{i}} = u_{y\mathbf{i}} - u_{y\mathbf{i}+\delta_{\mathbf{y}}}$.

This simplifies the calculations and somewhat changes the nature of the

boundary conditions. We will use periodic boundary conditions; in the original $u_{x\mathbf{i}}$ and $u_{y\mathbf{i}}$ variables, this would mean that if a disruption occurred somewhere in the lattice (say, near the electron), then this 'disruption' would have to 'heal' itself at the boundary. By switching to the $\tilde{x}$ and $\tilde{y}$ variables this is no longer true. A separation of ions near the electron would simply 'push' the remaining ions further out. We have effectively eliminated the mode that corresponds to uniform translation of all the ions and introduced a stretching mode that allows the entire lattice to expand or contract (this is not possible with conventional periodic boundary conditions). In the thermodynamic limit this choice of variable and boundary conditions does not effect the physical result (an electron distorting the ions in its vicinity), but use of the $\tilde{x}_{\mathbf{i}}$ and $\tilde{y}_{\mathbf{i}}$ variables greatly reduces finite size effects for systems smaller than the thermodynamic limit.

It is advantageous to rescale the ion displacement parameters as dimensionless variables. To this end we define

$$\tilde{x}_{\mathbf{i}} = \frac{\alpha}{K} x_{\mathbf{i}} \tag{4.4}$$

$$\tilde{y}_{\mathbf{i}} = \frac{\alpha}{K} y_{\mathbf{i}} \tag{4.5}$$

As is customary we define a dimensionless electron-phonon coupling strength λ:

$$\lambda = \frac{\alpha^2}{\omega_0^2 M W}, \tag{4.6}$$

where $W \equiv 4Dt$ is the electronic bandwidth for a 'cubic' lattice in D-dimensions, and

$$\omega_0 = \sqrt{\frac{4K}{M}}. \tag{4.7}$$

Thus the adiabatic Hamiltonian becomes:

$$\begin{aligned} H &= \sum_{\mathbf{i}} [-t + 4\lambda W x_{\mathbf{i}}][c^{\dagger}_{\mathbf{i}} c_{\mathbf{i}+\delta_{\mathbf{x}}} + h.c.] \\ &+ \sum_{\mathbf{i}} [-t + 4\lambda W y_{\mathbf{i}}][c^{\dagger}_{\mathbf{i}} c_{\mathbf{i}+\delta_{\mathbf{y}}} + h.c.] \\ &+ \sum_{\mathbf{i}} 2\lambda W (x^2_{\mathbf{i}} + y^2_{\mathbf{i}}). \end{aligned} \tag{4.8}$$

Consideration of only longitudinal modes keeps the directions independent of each other, consistent with what is generally done in the fully quantum mechanical treatment.[23] This also neglects changes in y-distances that could come from changing nearby x-distances through triangulation. This is justifiable since the change in the hopping due to the electron-phonon interaction is itself a linear approximation and these definitions are consistently linear in the changes in bond length.

The adiabatic BLF-SSH model (with coupling to longitudinal modes as described here) has been studied in one dimension[60] and two dimensions.[64] More recent studies are motivated by biophysical and polymer applications and are generally done in one dimension.[67, 63, 62] Calculations in the adiabatic limit are useful since they allow us to understand the physical structure of a polaron, both electronically, and through the accompanying ionic displacements.

4.3 Methods

With the Hamiltonian defined in Eq. (4.8), for a given electronic wave function the ground state energy can be determined and minimized with respect to the ionic displacements. Solving the semi-classical adiabatic model is therefore a problem of function minimization. In this formulation, the bond length parameters are the variational input parameters. Given their values, the electron energy can be evaluated by evaluating the tight-binding electronic Hamiltonian

matrix elements with the $t_{\mathbf{i}}$ values calculated from the bond lengths. The ionic energy is a simple classical sum of the bond lengths squared and together these terms give the binding energy of the polaron. The number of parameters then scales as the number of ion sites and also dimension.

The multivariable minimization problem is in general much easier than the full quantum many-body problem, but remains a very difficult problem in its own right. Finding a solution with a low energy is not particularly difficult, but knowing that one has the lowest possible solution is virtually impossible. This is at the root of the confusion in the field — there is no good way to distinguish whether one has found the global minimum, or simply a low local minimum. For many applications, such as the traveling salesman problem, finding a solution that is quite close to the absolute minimum is acceptable. However, for the polaron, two solutions with similar energies may have a very different physical structure; thus finding the global minimum is important for a proper physical understanding.

There are many different algorithms for multivariable minimization, and to establish confidence in our results we have implemented several different ones, verifying that we have the correct answer. Each has its own strengths and weaknesses and by combining them we have a much better understanding of the energy landscape.

The state of the art in multivariable minimization with no a priori knowledge is the genetic algorithm. [68] This algorithm is very effective at searching through the entire space for low energy solutions, but is rather slow for large numbers of parameters and has a hard time "fine tuning" a solution. The basic method is to create a population of points in the N-dimensional space, then allow them to breed, where they swap coordinates, and small random variations are introduced. These new points are then ranked by evaluating their energies, and the best half are allowed to breed and compose the next iteration's population.

Alternatively, one may use minimization algorithms using the gradient. By using the Hellman-Feynman theorem, the gradient can be computed as a function of the bond lengths and the eigenvector of the tight-binding Hamiltonian can be constructed by using those bond lengths. We have

$$\frac{\partial E}{\partial y_{\mathbf{i}}} = \langle\psi|\frac{\partial H_{elec}}{\partial y_{\mathbf{i}}}|\psi\rangle + 4\lambda W y_{\mathbf{i}}. \tag{4.9}$$

and similarly for the $x_{\mathbf{i}}$ parameters. There are two ways to use this information. First, one can set up a self-consistent set of equations and iterate through these. Second, one can use a conjugate gradient optimization routine. Both of these methods run much faster than the genetic algorithm, but they do not sample more than one point in configuration space at a time. This makes them more prone to falling into local minima.

We implemented all of these algorithms and found the best performance from the conjugate gradient method. It found the same configuration as the genetic algorithm on small systems given random initial conditions, and could handle larger systems with ease. It was, however, more sensitive to errors in the eigenvalue and eigenvector of the diagonalization routine than the iterative method.

Preliminary calculations showed that the polaron would be very small at strong-coupling, so we first performed searches of the solution for strong-coupling parameters on small clusters. We used both the differential algorithm and conjugate gradient algorithm using random starting conditions. This generally produced a few low energy configurations. We then used these configurations as starting conditions for a sweep towards zero coupling strength. We would find the lowest energy configuration for a given λ, and then use that configuration as the starting point for the next lower λ calculation. This prevented getting lost in multi-dimensional phase space. We did other surveys for starting configurations that were not low energy solutions at strong-coupling,

but in these cases only the trivial solution of a free electron immersed in a lattice of unstretched bonds was found.

4.4 Analytical Results

Before we present data from our numerical simulations, it is instructive to examine analytically the case of strong-coupling. Here the polaron is very small, and thus we can perform a simple analytical calculation to obtain the optimum solution.

In one dimension, instead of following the numerical procedure of periodic boundary conditions, we adopt open boundary conditions, since we are anticipating a very small polaron. There is a general distinction between chains with an even or odd number of sites. For example, in the two-site model the electron wave function is expected to be a symmetric linear combination of the electron on both sites, i.e. $|\psi_2\rangle = (c_0^\dagger|0\rangle + c_1^\dagger|0\rangle)/\sqrt{2}$. The subscript 0 (1) refers to the left (right) site. The problem is immediately diagonal, and the electronic energy from the electronic Hamiltonian is $\epsilon_{\rm el} = -(t - 4\lambda W x)$, where x represents the dimensionless 'stretch' of the one bond in the problem. Combined with the ionic part of the Hamiltonian we obtain a total energy of $E = -t + 4\lambda W x + 2\lambda W x^2$. Minimization gives $x = -1$ and $E_{\rm min} = -t - 2\lambda W$.

For three sites there are two independent normalized wave functions,

$$\begin{aligned} |\phi_0\rangle &= c_0^\dagger|0\rangle \\ |\phi_1\rangle &= \frac{1}{\sqrt{2}}\big(c_{-1}^\dagger + c_1^\dagger\big)|0\rangle, \end{aligned} \tag{4.10}$$

where -1, 0 and 1 represent the site indices, and the electron wave function $|\psi_3\rangle$ is given in terms of these two basis states:

$$|\psi_3\rangle = a_0|\phi_0\rangle + a_1|\phi_1\rangle \tag{4.11}$$

We therefore have an eigenvalue problem for the two coefficients and the electronic energy, ϵ_{el}, as

$$\begin{pmatrix} 0 & -\sqrt{2}(t - 4\lambda W x_0) \\ -\sqrt{2}(t - 4\lambda W x_0) & 0 \end{pmatrix} \begin{pmatrix} a_0 \\ a_1 \end{pmatrix} = \epsilon \begin{pmatrix} a_0 \\ a_1 \end{pmatrix}, \tag{4.12}$$

where, due to the symmetry of the problem, the dimensionless bond stretches on the left and on the right will be equal (denoted here by x_0). The eigenvalues are readily determined, with the electronic ground state energy given by $\epsilon_{\text{el}} = -\sqrt{2}(t - 4\lambda W x_0)$; then the total energy

$$E_{\text{tot}} = -\sqrt{2}(t - 4\lambda W x_0) + 4\lambda W x_0^2 \tag{4.13}$$

is minimized by $x_0 = -1/\sqrt{2}$; this gives

$$E_{\text{GS}} = -\sqrt{2}t - 2\lambda W. \tag{4.14}$$

This represents a lower energy than the two-site model, and in general the solution with an odd number of sites partially occupied by the electron will have a lower energy than that with an even number of sites. The eigenvector corresponding to this energy is

$$|\phi_{\text{GS}}\rangle = \frac{1}{2} c_{-1}^\dagger |0\rangle + \frac{1}{\sqrt{2}} c_0^\dagger |0\rangle + \frac{1}{2} c_1^\dagger |0\rangle, \tag{4.15}$$

and corresponds to a central maximum electron amplitude with two smaller amplitudes on either side. One relative ion displacement is required, with $x_0 = -1/\sqrt{2}$. This corresponds to the ions on either side of the central maximum moving closer to the centre, with all other ions on either side following suit, meaning that there are no further relative displacements. For reasons further explained in the final section, we expect this solution to properly represent the strong-coupling solution, even for the quantum case. To verify this for the

adiabatic limit, at least, we expand the Hilbert space.

With five sites, we use an additional electron basis state,

$$|\phi_2\rangle = \frac{1}{\sqrt{2}}\left(c^\dagger_{-2} + c^\dagger_2\right)|0\rangle, \tag{4.16}$$

and an additional stretch denoted by x_1, between site 1 and site 2 (or site -1 and site -2). The equations are slightly more complicated, as a 3×3 matrix must be diagonalized,

$$\begin{pmatrix} 0 & -\sqrt{2}t_0 & 0 \\ -\sqrt{2}t_0 & 0 & -t_1 \\ 0 & -t_1 & 0 \end{pmatrix} \begin{pmatrix} a_0 \\ a_1 \\ a_2 \end{pmatrix} = \epsilon \begin{pmatrix} a_0 \\ a_1 \\ a_2 \end{pmatrix}, \tag{4.17}$$

where a_0 and a_1 are amplitudes of the two basis states in Eq. (4.10) as before and a_2 is the amplitude for the basis state $|\phi_2\rangle$, and $t_k \equiv t - 4\lambda W x_k$ for $k = 0, 1$. A straightforward diagonalization gives

$$\epsilon_{\text{el}} = -\sqrt{2(t - 4\lambda W x_0)^2 + (t - 4\lambda W x_1)^2}, \tag{4.18}$$

so that the total energy is well-defined in terms of x_0 and x_1. Taking partial derivatives with respect to these two parameters and setting them to zero then gives two equations that cannot be solved in closed form. However, an expansion in increasing powers of $t/(\lambda W)$ gives a minimum energy

$$E = -2\lambda W - \sqrt{2}t - \frac{t^2}{4\lambda W} + \frac{\sqrt{2}t^3}{8(\lambda W)^2} + \; O(\frac{t}{\lambda W})^3. \tag{4.19}$$

Note that the corresponding eigenvector is given by Eq. (4.15), *plus* corrections of order $O(1/\lambda)$, including the amplitude on the two sites furthest from the centre. Furthermore $x_1 = O(1/\lambda)$, and $x_0 = -1/\sqrt{2} + O(1/\lambda)$. This confirms Eqs. (4.15) and (4.14) as the strong-coupling solutions. Figure 4.2 shows these solutions along with our numerical solution for the thermodynamic limit, and

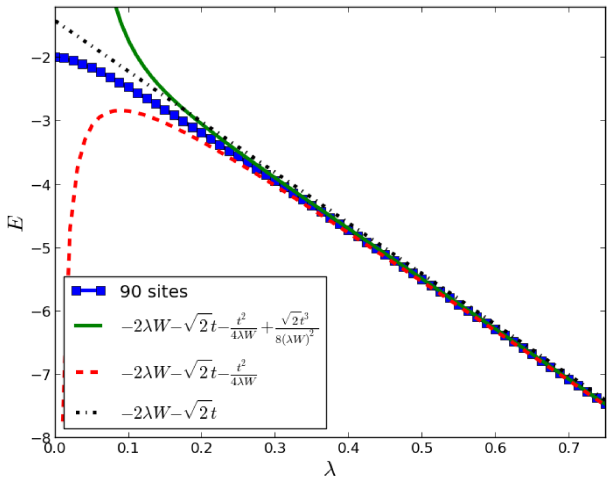

Figure 4.2: The ground state energy for the one dimensional BLF-SSH model in the adiabatic limit. The solid curve with (blue) squares is the numerical solution, while the various strong-coupling expansions are shown as indicated in the legend. The divergence in weak-coupling is due to the finite expansion in $t/\lambda W$ and not from some effect of the model itself.

the agreement is very good for strong-coupling.

Since all the corrections beyond the three-site model are of order $t/\lambda W$ or higher we are assured that the three-site solution represents the true strong-coupling limit. There are no finite size effects that need to be included and the minimization is analytical and thus this solution is not subject to being trapped in a local minimum as numerical methods can be.

Using the same analytical methods we can find the strong-coupling limit for the two and three dimensional cases as well. We restrict ourselves to solutions that have the same symmetries as the lattice since a symmetric Hamiltonian is expected to have symmetric solutions. Nonetheless, there are alternative analogues to the two- and three-site configurations that we considered in one dimension. The two general types of configurations are those in which a polaron is centred on a site, or those in which a polaron is centred at a location which is not a site; instead it is centred on a point equidistant from all neighbouring

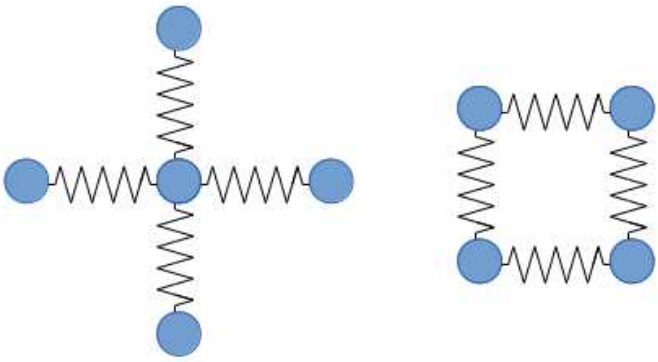

Figure 4.3: The two possible configurations for stretched bonds in the two dimensional strong-coupling limit. The square has the electron amplitude equal on all four sites while the star configuration has half of the electron probability on the centre site and one eighth on each of the four surrounding sites.

sites. In one dimension these configurations were the cases with an odd or even number of sites with significant amplitude, respectively. Some details along the lines given above for the one dimensional case are given in the final section. Here we simply present the final energies and configurations. The calculations are straightforward; numerical results are obtained by diagonalization of finite systems until convergence is achieved, and analytical results can be done very quickly with the help of a computer algebra system like Mathematica.

In two dimensions a curious degeneracy occurs — the two potential configurations (Fig. 4.3) have the same energy in the extreme strong coupling limit (see final section),

$$E = -2\lambda W - 2t \tag{4.20}$$

However, it should be noted that this degeneracy is really a special case applicable to the simple square lattice. For example, the two dimensional honeycomb lattice also has two analogous solutions, but they are not degenerate (see final section). For the two dimensional square lattice this degeneracy remains for all coupling strengths, as our numerical results showed no discernible difference once converged for finite size effects. This appears to come from

the fact that both solutions have the same number of bonds stretched on the square lattice so the energy cost is the same, and they have the same electron energy even though they have different electron configurations in real space. The existence of two solutions may be more important in many-electron calculations since they have different physical sizes, but for single electron studies they seem to be interchangeable.

In three dimensions there are again two types of solutions, those centred on an actual site of the lattice (so-called 'star' configuration) and and those centred on a point which would be the centre of a cube of eight sites. We found the 'star' configuration to always have the lowest energy; in strong-coupling the two energies are given by Eqs. (4.29):

$$\begin{aligned} E_{\text{star}} &= -2\lambda W - \sqrt{6}t \qquad \text{(3D)} \\ E_{\text{cube}} &= -\frac{3}{2}\lambda W - 3t, \qquad \text{(3D)} \end{aligned} \tag{4.21}$$

and clearly the first is lower for large values of λ. As we see in the next section, this remains true for all coupling strengths for which a polaronic solution exists.

4.5 Numerical Results

While the small polaron corresponding to the strong-coupling limit can be solved analytically, as the coupling strength decreases the electron spreads out over many lattice sites. Many different bonds are stretched or compressed to form the accompanying lattice distortion and this necessitates numerical calculations to find the lowest energy solution away from strong-coupling. The important question at weak-coupling is to determine if there is a critical coupling strength needed for polaron formation. To answer this we started with a calculation at strong-coupling and then slowly lowered the coupling strength in small increments, calculating the low energy ion configuration at each step.

Each subsequent minimization was seeded with the previous slightly higher lambda configuration and we repeated the process for many cluster sizes to converge finite size effects. Even in situations where the polaron configuration remains a local minimum in the energy landscape, if the polaron energy is higher than the electronic energy in the presence of an undistorted lattice, this signals the presence of a critical coupling strength below which the electron prefers to reside in a Bloch wave state surrounded by an undistorted ion lattice.

In one dimension, as shown in Fig. (4.2), we found that there was no critical coupling for polaron formation, i.e. the polaron energy remains lower than the bare tight-binding energy (for $k = 0$) for all coupling strengths down to $\lambda = 0$. Note that we used several lattice sizes, and for sizes beyond 30 or so, finite size effects have disappeared.

The two dimensional results are shown in Fig. (4.4) for a variety of lattice sizes, as indicated. Here there is no question that a critical point occurs, at $\lambda_c = 0.045$. Note that the energies for the two configurations ('star' and 'square') remain degenerate down to this critical coupling strength. This critical point therefore occurs for both polaron configurations discussed above (and in the final section). A snapshot of the electron and ion configuration for a modest coupling strength ($\lambda = 0.1$) is shown in Fig. (4.5)(a)and (b) for the 'star' and 'square' configuration, respectively. Even though these configurations have the same energy, they represent quite different electron and ion distortion patterns. Note, however, that both these solutions have the full symmetry of the underlying lattice, and differ considerably from the solution reported in Ref. (64).

There are significant finite size effects but we were able to model large enough clusters to eliminate these. When the cluster size is small a notable distortion remains, even in the weak-coupling limit. This can be understood by using the following energy, written for the case where all the bonds in the cluster are slightly stretched by the same amount (written as y in dimensionless

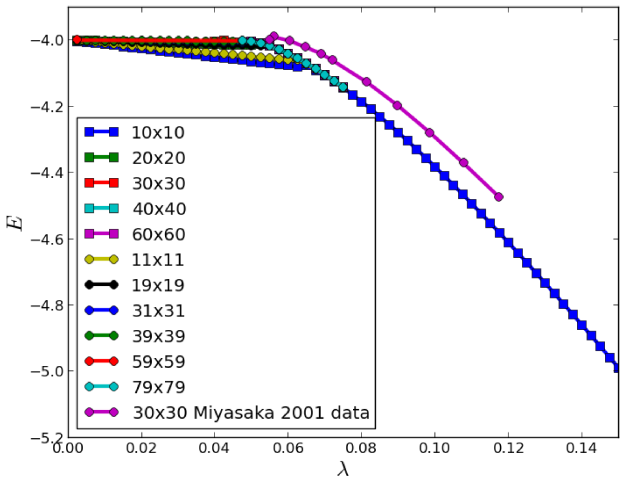

Figure 4.4: The energy for the two dimensional BLF-SSH model from numerical calculations (periodic boundary conditions) for a wide range of coupling strengths and using both possible starting configurations. Finite size effects have been converged to the thermodynamic limit by using larger and larger clusters. The previous results of Miyasaka and Ono[64] have been extracted from their 2001 paper to show that our energies are somewhat lower.

units):

$$E = 4(-t + 4\lambda W y) + 4N\lambda W y^2 \tag{4.22}$$

Minimization with respect to y yields $y = -2/N$, and results in a minimum energy

$$E = \frac{-16\lambda W}{N} - 4t. \tag{4.23}$$

Of course in the thermodynamic limit, $N \to \infty$ so the distortion goes to zero, as is apparent in Fig. (4.4).

In three dimensions, finite size effects are not so pronounced. We show results for the ground state energy in Fig. (4.6) for several lattice sizes. We extract a critical coupling strength of $\lambda_c = 0.11$. In some sense the polaron in three dimensions remains small over all coupling strengths beyond this critical value, as even for a $7 \times 7 \times 7$ cluster, finite size effects are almost negligible, and this lattice size is sufficiently large to contain all the ionic distortions present.

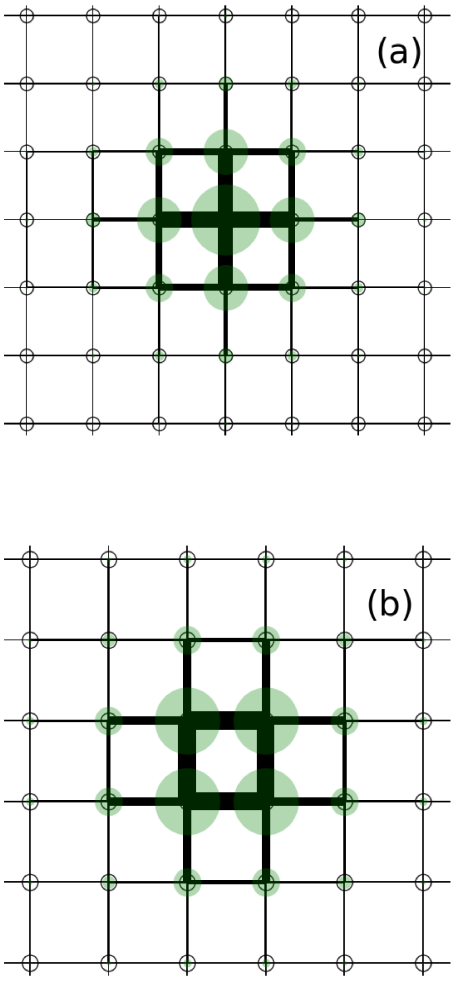

Figure 4.5: The electron and ion distortion configuration at $\lambda = 0.1$ for the two configurations discussed in the text. In (a) and (b) we show the 'star' and 'square' configurations, respectively. The energies of both these configurations are degenerate. The width of the black rectangles connecting the ion sites is proportional to the amount that a bond is compressed. The green circles have an area proportional to the electron density on that site. Both of these configurations differ qualitatively from the quasi-one-dimensional configuration found in Ref. (64).

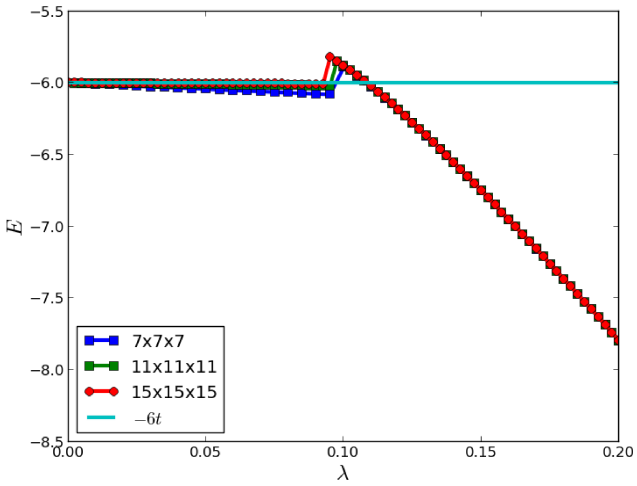

Figure 4.6: The energy for the three dimensional SSH model from numerical calculations (periodic boundary conditions) for a wide range of coupling strengths.

4.6 Summary

We have presented results for the one, two, and three dimensional BLF-SSH model in the adiabatic limit. The nature of these solutions is not so different from what they were for the Holstein model.[57] In one dimension the solution is always polaronic; no matter how weak the electron-ion coupling, a lattice distortion always accompanies the electron, even though it exists in a Bloch state. In two and three dimensions there exists a critical coupling strength, λ_c, below which there is no longer an ionic distortion, i.e. the electron is completely independent of the ions. This is exactly what happened with the Holstein model,[57] and as in that case, we fully expect the quantum solution to *not* display this same behaviour, i.e. we expect that the quantum solution does not have a critical point. Instead, we expect that a crossover will occur. It remains to be seen how sharp this crossover will be as the characteristic phonon energy becomes much smaller than the characteristic electron energy. For reference, in the Holstein model it remained *very* sharp.[23]

The function optimization required here, with many parameters, is quite a difficult problem, more difficult than was the case with the Holstein problem, which we have also solved. We have taken a number of important steps to obtain the true global minimum solutions, and have found lower energy configurations than previous works.[64] Hopefully these precise solutions will help to inform further quantum mechanical studies of the BLF-SSH model and many-electron calculations in the adiabatic limit. The small polaron formation in three dimensions is particularly interesting since many studies in semiconductors have used large polarons and Fröhlich-like models. However, for atomic semiconductors such as silicon, the Einstein oscillators or optical phonons used in most of the Fröhlich-like models simply do not exist. Further research and full quantum mechanical solutions are necessary to resolve the role of small vs large polarons, to see if the 'sharpness' of the crossover from weak to strong-coupling present in the Holstein model[23] remains for the BLF-SSH model. In any event, we fully expect the strong-coupling solutions obtained here to faithfully reflect the fully quantum mechanical solutions in strong-coupling, via coherent states.

4.7 Supplemental Calculations for the adiabatic strong coupling limit in two and three dimensions

In two dimensions the possible configurations are as shown in Fig. (4.5). For the first (star), the electronic wave function is given as a linear combination of the central site and the symmetric combination of the four surrounding sites,

$$|\phi_{\rm star}\rangle = a_0 c_{00}^\dagger|0\rangle + a_1\frac{1}{2}(c_{10}^\dagger + c_{-10}^\dagger + c_{01}^\dagger + c_{0-1}^\dagger)|0\rangle. \tag{4.24}$$

Evaluating the relevant matrix elements results in a 2×2 eigenvalue problem,

$$\begin{pmatrix} 0 & -2(t - 4\lambda W u_0) \\ -2(t - 4\lambda W u_0) & 0 \end{pmatrix} \begin{pmatrix} a_0 \\ a_1 \end{pmatrix} = \epsilon_{\text{el}} \begin{pmatrix} a_0 \\ a_1 \end{pmatrix}, \tag{4.25}$$

where, due to the symmetry of the problem, the dimensionless stretches on the left and right of the centre will be equal to the stretches above and below the centre (denoted here by u_0). The eigenvalues are readily determined, and when combined with the ionic energy, results in $u_0 = -1/2$, so that the total energy is

$$E_{\text{star}} = -2\lambda W - 2t \qquad \text{(2D)} \tag{4.26}$$

This constitutes the strong-coupling solution for the star configuration in two dimensions. We now turn to the 'competing' symmetry, the so-called 'square' configuration, as depicted also in Fig. (4.5). Here symmetry dictates that there is only one electronic wave function, a linear combination of the electron located at each of the four corners:

$$|\phi_{\text{square}}\rangle = \frac{1}{2}(c_{00}^{\dagger} + c_{10}^{\dagger} + c_{11}^{\dagger} + c_{01}^{\dagger})|0\rangle. \tag{4.27}$$

Where the hopping is modulated by an longitudinal ionic distortion which we will denote by v_0 and which is the same in all directions. We find an electronic energy $\epsilon_{\text{el}} = -2(t - 4\lambda W v_0)$. When combined with the ion energy, minimization leads to $v_0 = -1/2$ and

$$E_{\text{square}} = -2\lambda W - 2t \qquad \text{(2D)} \tag{4.28}$$

This is in complete agreement with the energy of the star configuration. One can proceed further with bond distortions in either case extending further from the central region, but neither configuration can be solved in closed form. Remarkably, numerical diagonalization leads to results that are numerically in-

distinguishable nonetheless.

A similar exercise for the honeycomb lattice, however, results in a strong-coupling solution of $E_{\rm star} = -2\lambda W - \sqrt{3}t$ and $E_{\rm hex} = -\frac{4}{3}\lambda W - 2t$, where the 'star' configuration, with one centrally located electron amplitude (like the 'star' configuration noted above), has a lower energy than the 'hexagonal' configuration, which has six sites occupied by the electron with equal amplitude. Once again, these strong-coupling solutions can be further developed as a power series in $1/\lambda$ by including more sites.

Finally, the same exercise can be performed in three dimensions, for a cubic system; the two competing configurations are the 'star' configuration with one central electron amplitude surrounded by six nearest neighbour amplitudes, and the 'cube' configuration, consisting of the eight sites constituting the corners of the cube having an equal amplitude for the electron (so, as in the two dimensional 'square' and 'hexagonal' configurations, the centre of the polaron is *not* a lattice site). One finds, for three dimensions in the strong-coupling limit,

$$\begin{aligned} E_{\rm star} &= -2\lambda W - \sqrt{6}t \qquad \text{(3D)} \\ E_{\rm cube} &= -\frac{3}{2}\lambda W - 3t, \qquad \text{(3D)} \end{aligned} \tag{4.29}$$

so, in the strong-coupling limit the 'star' configuration has lower energy than the 'cube' configuration. As described in the text, by solving the problem numerically, we have found that this remains true over all coupling strengths for which a polaronic configuration with accompanying lattice distortions is the ground state.

Chapter 5

Weak Coupling Perturbation Theory for the BLF-SSH Model

We used both a perturbative Green's function analysis and standard perturbative quantum mechanics to calculate the decrease in energy and the effective mass for an electron interacting with acoustic phonons. The interaction is between the difference in lattice displacements for neighbouring ions, and the hopping amplitude for an electron between those two sites. The calculations where performed in one, two, and three dimensions, and comparisons are made with results from other electron-phonon models. We also computed the spectral function and quasiparticle residue, as a function of characteristic phonon frequency. There are strong indications that this model is always polaronic in one dimension, where an unusual relation between the effective mass and the quasiparticle residue is also found.

5.1 Introduction

When electrons interact strongly with phonons, the electrons acquire a polaronic character. That is, they move around the lattice much more sluggishly than non-interacting electrons would, because a phonon cloud must accompany

them as they move. A measure of the strength of the coupling between the electron and the phonons is the degree to which the ground state energy is lowered. For example, previous studies for the Holstein model[5] have indicated that the decrease in energy is proportional to the bare coupling strength (λ) in strong-coupling,[43] independent of the value of the phonon frequency. On the other hand, in weak-coupling, while the proportionality to λ remains, there is some dependence on phonon frequency, and the decrease in energy is greater for higher phonon frequency.[43, 10]

A much more indicative measure of the polaronic character of an electron is the effective mass. In the Holstein model, a glimpse of polaronic tendencies, even within perturbation theory, can be attained by examining the effective mass, particularly in one dimension. Usually an increasing effective mass is accompanied by a decrease in quasiparticle residue, although this is not always the case, as described below.

The Holstein model describes electrons interacting with optical phonons; the coupling is via the electron charge density, and, in this sense, the Holstein model is the simplest model for electron-phonon interactions just like the celebrated Hubbard model [69, 70] is the simplest description of electron-electron interactions. Many of the basic features of this model are now fairly well understood — see Ref. [44, 27] along with more recent work in Ref. [10, 29]. However, just as important is the electron interaction with acoustic phonons; typically the ionic motions couple to the electron motion, as opposed to its charge density. A very simple model to describe this kind of electron-phonon interaction within a tight-binding framework is given by

$$\begin{aligned} H &= -\sum_{\langle i,j\rangle} t_{ij}\left(c^{\dagger}_{i\sigma}c_{j\sigma} + h.c.\right) + \sum_{i}\left[\frac{p^2_{xi}}{2M} + \frac{p^2_{yi}}{2M}\right] \\ &+ \frac{1}{2}K\sum_{\langle i,j\rangle}\Big[\left(u_{xi}-u_{xj}\right)^2 + \left(u_{yi}-u_{yj}\right)^2\Big], \end{aligned} \tag{5.1}$$

where angular brackets denote nearest neighbours only, and

$$t_{ij} = t - \alpha(u_{xi} - u_{xj})\delta_{i,j\pm\hat{a}_x} - \alpha(u_{yi} - u_{yj})\delta_{i,j\pm\hat{a}_y}. \tag{5.2}$$

This Hamiltonian has been written specifically for two dimensions, but the generalization to three dimensions (or back to one dimension) is evident from Eqs. (5.1) and (5.2). The operators and parameters are as follows: $c^\dagger_{i\sigma}$ ($c_{i\sigma}$) creates (annihilates) an electron at site i with spin σ. The x-components for the ion momentum and displacement are given by p_{xi}, and displacement u_{xi}, respectively (similarly for the y-components), and the ions have mass M and spring constant K connecting nearest neighbours only. The electron-ion coupling is linearized in the components of the displacement, and we choose to include only longitudinal coupling.

This Hamiltonian is commonly known as the Su-Schrieffer-Heeger (SSH) model, [60, 7] because it was used for seminal work describing excitations in polyacetylene by these authors. However, it was also introduced and studied a decade earlier by Barišić, Labbé, and Friedel [6] to describe superconductivity in transition metals, so we will refer to it as the BLF-SSH model. Much of the work done on this model is in the adiabatic approximation, i.e. the phonons are treated classically.[60, 7] This was followed by an examination of quantum fluctuations through quantum Monte Carlo and renormalization group studies,[12, 13] and these authors focused on half-filling. They found that the lattice ordering (in one dimension) was reduced by quantum fluctuations.

Very little work has been done, however, in the quantum regime for a single electron. Capone and coworkers studied a model similar to this one, except that they utilized optical phonons instead of acoustic ones.[71, 72, 73, 74] We will refer to this model as the Capone-Stephan-Grilli (CGS) model to avoid confusion with the model with acoustic phonons. This leads to some significant differences, about which we will comment below.

In the past decade Zoli has studied the BLF-SSH polaron using perturbation theory, and found, for example, a perturbative regime in one dimension where polaron effects are absent.[75, 76, 77] This result happened to agree with the conclusions of Capone et al.[71] in the perturbative regime of the CSG model.[74] In this chapter we focus on 2^{nd} order perturbation theory, and find results in disagreement with Ref. 75, 76, 77. These results also disagree *qualitatively* with the results from the CSG model. That is, in one dimension, for example, perturbation theory breaks down as the characteristic phonon frequency decreases. In two dimensions there is a modest mass enhancement for all characteristic phonon frequencies, while in three dimensions the mass enhancement approaches unity in the adiabatic limit. We also note that the quasiparticle residue does not necessarily follow the trend of the inverse effective mass, as the characteristic phonon frequency varies.

This chapter is organized as follows: in the first section we outline the calculation, both using perturbation theory, and using Green function techniques. For some of our work (especially in one dimension), the calculation can be done analytically, and we derive these results where applicable. We then show some numerical results and compare our results with previous work and other electron-phonon models. We close in the final section with a summary.

The main conclusion is that, as far as one can tell from weak-coupling perturbation theory, the BLF-SSH model has a stronger tendency to form a polaronic state than is the case with the Holstein model. In one dimension this is most evident in the effective mass, and not at all evident in the quasiparticle residue.

5.2 Perturbation Theory

5.2.1 Hamiltonian

The Hamiltonian Eq. (5.1), Fourier-transformed to wavevector space, and utilizing phonon creation and annihilation operators, is written (again in two dimensions),

$$\begin{aligned} H &= \sum_{k\sigma} \epsilon_{k\sigma} c^{\dagger}_{k\sigma} c_{k\sigma} \\ &+ \sum_{q} \hbar\omega(q) \left[a^{\dagger}_{xq} a_{xq} + a^{\dagger}_{yq} a_{yq} \right] \\ &+ \sum_{\substack{kk' \\ \sigma}} g_x(k,k') \left[a_{x(k-k')} + a^{\dagger}_{x(-k+k')} \right] c^{\dagger}_{k\sigma} c_{k'\sigma} \\ &+ \sum_{\substack{kk' \\ \sigma}} g_y(k,k') \left[a_{y(k-k')} + a^{\dagger}_{y(-k+k')} \right] c^{\dagger}_{k\sigma} c_{k'\sigma}. \end{aligned} \tag{5.3}$$

Here,

$$\epsilon_k \equiv \epsilon(k_x, k_y) = -2t[\cos(k_x) + \cos(k_y)] \tag{5.4}$$

is the dispersion relation for non-interacting electrons with nearest neighbour hopping, and

$$\omega(q) \equiv \omega_0 \sqrt{\sin^2(q_x/2) + \sin^2(q_y/2)} \tag{5.5}$$

is the phonon dispersion for acoustic phonons with nearest neighbour spring constants K, and $\omega_0 \equiv \sqrt{4K/M}$ is the characteristic phonon frequency. The phonon creation and annihilation operators are given by $a^{\dagger}_{xq}$ and a_{xq}, respectively, and similarly for those in the y-direction. The coupling constants are given by

$$g_x(k,k') \equiv i\alpha \sqrt{\frac{2}{MN\omega(k-k')}} \Big[\sin(k'_x) - \sin(k_x) \Big], \tag{5.6}$$

with a similar expression for the y direction, and M is the mass of the ion and N is the number of lattice sites.

5.2.2 Green's function analysis

We carried out a Green's function analysis using the free electron and phonon parts of the Hamiltonian as the unperturbed part. The self energy of a single electron to lowest (2^{nd}) order in the coupling α gives,

$$\begin{aligned}&\Sigma(k,\omega+i\delta) = \\ &-\sum_{k'}\left[|g_x(k,k')|^2+|g_y(k,k')|^2\right]G_0(k',\omega+i\delta-\omega(k-k')),\end{aligned} \tag{5.7}$$

where $G_0(k,\omega+i\delta)\equiv\left[\omega+i\delta-\epsilon_k\right]^{-1}$ is the non-interacting electron retarded propagator.

One way to determine the effect of interactions on the electron dispersion is to compute the renormalized energy for the ground state (here, $k_x=k_y=0$), and the effective mass. The effective mass has long been used as the primary indicator for polaronic behaviour [44, 27], and though within 2^{nd} order perturbation we can only get an indication of this crossover, we use it here nonetheless. The renormalized energy is given by the solution for the pole location in the interacting electron Green's function, $G(k,\omega+i\delta)\equiv\left[\omega+i\delta-\epsilon_k-\Sigma(k,\omega+i\delta)\right]^{-1}$,

$$E_k=\epsilon_k+\mathrm{Re}\Sigma(k,E_k). \tag{5.8}$$

To determine the effective mass, defined by the expectation that $E_k\equiv\hbar^2k^2/(2m^*)$, we take two derivatives[78] of Eq. (5.8), and, using the fact that $(dE_k/dk)|_{k=0}=0$, we obtain

$$\begin{aligned}\frac{m^*}{m} &= \frac{1-\frac{\partial\Sigma(k,\omega)}{\partial\omega}|_{\omega=E_k}}{1+\frac{1}{2t}\frac{\partial^2\Sigma(k,\omega)}{\partial k^2}|_{\omega=E_k}} \\ &= 1-\frac{\partial\Sigma(k,\omega)}{\partial\omega}|_{\omega=E_k}-\frac{1}{2t}\frac{\partial^2\Sigma(k,\omega)}{\partial k^2}|_{\omega=E_k}.\end{aligned} \tag{5.9}$$

Here we have used the fact that the band mass given by the electron dispersion in Eq. (5.4) is $m = 1/(2t)$. Note that it is common (and advisable) to replace the substitutions for ω required in Eq. (5.9) with ϵ_k, rather than with E_k. This is due to the fact that the former substitution keeps the evaluation for every term at $O(\alpha^2)$, whereas the latter substitution includes some (inconsistently) higher order contributions. The former substitution is known as Rayleigh-Schrödinger perturbation theory while the latter is known as Brillouin-Wigner perturbation theory.[79] This means that we will use the following equation,

$$\frac{m^*}{m} = 1 - \frac{\partial \Sigma(k,\omega)}{\partial \omega}|_{\omega=\epsilon_k} - \frac{1}{2t}\frac{\partial^2 \Sigma(k,\omega)}{\partial k^2}|_{\omega=\epsilon_k}, \tag{5.10}$$

to define the effective mass.

In contrast, the quasiparticle residue is defined as the weight that remains in the δ-function-like portion of the spectral weight. The spectral weight is defined as

$$\begin{aligned} A(k,\omega) &\equiv -\frac{1}{\pi}\mathrm{Im}G(k,\omega+i\delta) \\ &= -\frac{1}{\pi}\mathrm{Im}\frac{1}{\omega+i\delta-\epsilon_k-\Sigma(k,\omega+i\delta)}. \end{aligned} \tag{5.11}$$

For a given momentum, as the energy of the pole given by Eq. (5.8) is approached, the imaginary part of the self energy tends towards zero; this produces a δ-function contribution in Eq. (5.11) , at the pole energy, but with weight z_k defined by

$$z_k = \frac{1}{1 - \frac{\partial \Sigma(k,\omega)}{\partial \omega}|_{\omega=E_k}}. \tag{5.12}$$

The relationship amongst these various quantities — effective mass in Eq. (5.9), effective mass in Eq. (5.10), and quasiparticle residue in Eq. (5.12) — is discussed further in the last section.

5.2.3 Standard Perturbation Theory

Eq. (5.10) (or Eq. (5.9)) requires a numerical evaluation of Eq. (5.7), and then the required derivatives can be (numerically) determined. Because the positions of the singularities in Eq. (5.7) are difficult to determine in advance, it is customary to introduce a small (numerical) imaginary part corresponding to the infinitesimal δ, and then the numerical integration is more stable. This trick remains problematic, as we discuss further below. Alternatively, we can simply perform a 2^{nd} order perturbation theory expansion, as outlined in every undergraduate quantum mechanics textbook. The result is

$$E_k^{(2)} = \frac{2\alpha^2}{M}\frac{1}{N}\sum_{k'}\frac{\left(\sin k'_x - \sin k_x\right)^2 + \left(\sin k'_y - \sin k_y\right)^2}{\omega(k-k') \quad [\epsilon_k - \epsilon_{k'} - \omega(k-k')]}, \tag{5.13}$$

where we remember that the first order (in α) contribution is zero, and the superscript (2) indicates the 2^{nd} order contribution. Comparison with Eq. (5.7) shows that this corresponds to Rayleigh-Schrödinger perturbation theory with the self energy, evaluated at $\omega = \epsilon_k$ corresponding to the 2^{nd} order energy correction. Eq. (5.13) can be evaluated numerically, and then two derivatives with respect to k are required. However, the same numerical problems mentioned above will arise; fortunately, at least in one dimension, Eq. (5.13) can be evaluated analytically, whereas we were unable to do the same with Eq. (5.7).

5.3 Results and Discussion

5.3.1 Analytical Results in One Dimension

The result of an analytical evaluation[80] of Eq. (5.13) is, in one dimension,

$$E^{(2)}(k) = -\frac{32t}{\pi}\lambda_{\mathrm{BLF}}\tilde{\omega}_0\left\{-2\cos k + \pi\tilde{\omega}_0 + C_k(\tilde{\omega}_0)\right\}, \tag{5.14}$$

where $\tilde{\omega}_0 \equiv \omega_0/(4t)$, and a dimensionless coupling parameter $\lambda_{\rm BLF}$ is defined, in analogy to the dimensionless coupling parameter defined in the Holstein model, as

$$\lambda_{\rm BLF} \equiv \frac{\alpha^2}{M\omega_0^2}\frac{1}{W}, \tag{5.15}$$

where here the bandwidth $W = 4t$ for one dimension. Note that this coupling parameter has nothing to do physically with the coupling parameter defined in the Holstein model, so we will treat them as completely independent.[81] The function $C_k(\tilde{\omega}_0)$ must be evaluated separately in the two regimes:

$$C_k(\tilde{\omega}_0) = 2\sqrt{\tilde{\omega}_0^2 - 1}\Big(h(k) + h(-k) - 2h(\pi/2)\Big), \quad \tilde{\omega}_0 > 1, \tag{5.16}$$

where

$$h(k) = \tan^{-1}\left(\frac{\tilde{\omega}_0 \tan\frac{k}{2} + 1}{\sqrt{\tilde{\omega}_0^2 - 1}}\right) \tag{5.17}$$

and

$$C_k(\tilde{\omega}_0) = \sqrt{1 - \tilde{\omega}_0^2}\Big(s(k) + s(-k) - 2s(\pi/2)\Big), \quad \tilde{\omega}_0 < 1, \tag{5.18}$$

where

$$s(k) = \log\left(\frac{\tilde{\omega}_0 \tan\frac{k}{2} + 1 + \sqrt{1 - \tilde{\omega}_0^2}}{\tilde{\omega}_0 \tan\frac{k}{2} + 1 - \sqrt{1 - \tilde{\omega}_0^2}}\right). \tag{5.19}$$

Eq. (5.14) is readily evaluated at $k = 0$ to determine the ground state energy. Evaluating the second derivative with respect to wavevector k is equally straightforward, and determination at $k = 0$ yields the rather simple result for the effective mass,

$$\frac{m^*}{m} = 1 + \frac{32}{\pi}\frac{\lambda_{\rm BLF}}{\tilde{\omega}_0}, \tag{5.20}$$

valid for all values of $\tilde{\omega}_0$.[82]

5.3.2 Comparison with other models

An analytical result is readily available for the Holstein model; there, the ground state energy (in one dimension) was given by[43]

$$E_{\mathrm{H}} = -2t\left(1 + \lambda_{\mathrm{H}}\sqrt{\frac{\tilde{\omega}_E}{\tilde{\omega}_E + 1}}\right), \tag{5.21}$$

where $\tilde{\omega}_E \equiv \omega_E/(4t)$ is the Einstein phonon frequency normalized to the bandwidth, and, as explained earlier, the dimensionless coupling constant λ_{H} cannot be compared directly to the corresponding quantity for the BLF-SSH model. The effective mass is given by

$$\left(\frac{m^*}{m}\right)_{\mathrm{H}} = 1 + \frac{\lambda_{\mathrm{H}}}{4\sqrt{\tilde{\omega}_E}}\frac{1 + 2\tilde{\omega}_E}{\left(1 + \tilde{\omega}_E\right)^{3/2}}. \tag{5.22}$$

In both cases, as the phonon frequency approaches zero (adiabatic limit) the ground state energy approaches the non-interacting value; however, the effective mass diverges in this same limit. So, while the first statement would appear to justify perturbation theory in this limit, the second statement clearly indicates a breakdown in the adiabatic limit. It is known in both cases that the adiabatic approximation leads to a polaron-like solution for all coupling constants,[57, 22] and clearly these two observations are consistent with one another. In fact, the divergence is stronger in the BLF-SSH model, and goes beyond the inverse square-root behaviour observed for the Holstein model and attributed to the diverging electron density of states in one dimension;[71] this indicates that the BLF-SSH model, at least in the adiabatic limit in one dimension, has a stronger tendency for polaron formation than the Holstein model.

In the model studied by Capone et al.[71], where optical phonons were used, the opposite behaviour was obtained; they found that the effective mass ratio approached unity as the phonon energy approached zero.[83] In the opposite limit Capone et al.[71] found an effective mass ratio that did not approach

unity as the phonon frequency increased (anti-adiabatic limit). In the BLF-SSH model, however, this ratio does approach unity as the phonon frequency increases beyond the electron bandwidth, in one dimension, in agreement with the Holstein result in all dimensions. As we will see below, however, in the BLF-SSH model in two and three dimensions the effective mass ratio remains above unity in the anti-adiabatic limit. This is not surprising, since here the interaction modulates the hopping, and we expect a non-zero correction in this limit.[83] In the adiabatic limit, the BLF-SSH mass ratio approaches a constant value in two dimensions, and falls to unity in three dimensions, similar to the behaviour of the Holstein model.

Our results disagree with those of Zoli[75, 76, 77] for reasons that are not entirely clear. We have utilized both the straightforward perturbation theory method (analytically and numerically), and the Green's function formalism (numerically). In the latter case we required a numerically small imaginary part for the frequency significantly smaller than the value quoted in Ref. (75, 76, 77) (we used $\delta = 10^{-9}$ whereas he used $\delta = 10^{-4}$. However, as is clear from our analytical result, Eq. (5.20), our effective mass diverges at low phonon frequency, and decreases monotonically to unity as the phonon frequency increases. The result in Ref. (75, 76, 77) peaks sharply near $\tilde{\omega}_0 \approx 1$, and, as noted above, decreases to unity at low phonon frequency.

5.3.3 Numerical Results

In Fig. 5.1 we plot the reduction in the ground state energy due to the second order correction (for the BLF-SSH model, this is given by Eq. (5.13)), normalized to λ_{BLF} (or λ_H). This is also written as $\Sigma(k = 0, \omega = \epsilon_k)/\lambda$, where the self energy is given by the expression in Eq. (5.7). Also plotted for comparison are the corresponding quantities for the Holstein model. Note that both models share a few features in common: (i) they both go to zero as the characteristic phonon energy decreases to zero, regardless of the dimensionality, (ii) they all

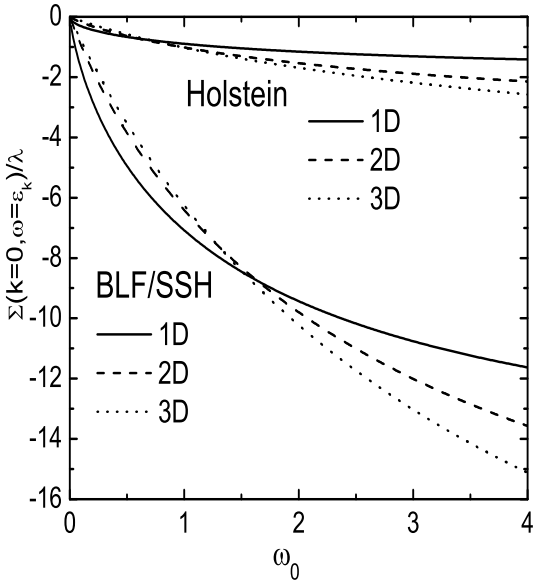

Figure 5.1: Electron self energy for the ground state ($k = 0$), normalized to λ (or λ_H) vs. characteristic phonon frequency ω_0 (this is ω_E for the Holstein model), for both the BLF-SSH and Holstein models, in one, two, and three dimensions, as indicated. Alternatively, the ordinate is simply the second order (in g) correction to the ground state energy within Rayleigh-Schrödinger perturbation theory. In all cases the magnitude of the correction increases with increasing ω_0. At low ω_0 the magnitudes of the the results are ordered three, two, and one dimensions (lowest to highest) whereas at high frequency the ordering is just the opposite. All six cases have non-zero limiting values as $\omega_0 \to \infty$, given in Table 1.

approach a non-zero negative (and finite) value as the characteristic phonon frequency grows, and (iii) they cross one another in strength as a function of dimensionality as ω_0 increases, i.e. at low phonon frequencies the self energy has the highest magnitude for one dimension, whereas for high phonon frequency the highest magnitude is achieved in both models for three dimensional systems. Also note that the BLF-SSH results are well separated from Holstein results. In particular, there appears to be more 'bang for the buck' with the BLF-SSH model, i.e. for a given value of λ_{BLF} and the same characteristic phonon frequency, the energy reduction is almost an order of magnitude higher for the BLF-SSH model as compared with the Holstein model. Again, we remind the reader that the value of λ_H in the Holstein model has nothing to do with the value of λ_{BLF} in the BLF-SSH model, so this comparison is unwarranted.

For this reason we will use the value for the self energy, in weak-coupling, as the phonon frequency increases to infinity, as the energy scale that provides a measure of the energy lowering expected for a given model and a given dimensionality. These numbers, mostly determined analytically, are provided in Table 5.1.

Table 5.1: Self energy in the anti-adiabatic limit divided by coupling strength or: $\lim_{\omega_0 \to \infty} \Sigma(k = 0, \omega = \epsilon_k)/(\lambda t)$

Dim.	BLF-SSH	Holstein
1D	-16	-2
2D	-23.3	-4
3D	-30.2	-6

In Fig. 5.2 we plot the effective mass ratio (minus unity), normalized to the self energy evaluated for infinite characteristic phonon frequency. This normalization is important to divide out enhancements that are solely due to definitions. Moreover, in this way, we are determining the mass enhancement for a given 'coupling strength', where this strength is now a measure of the

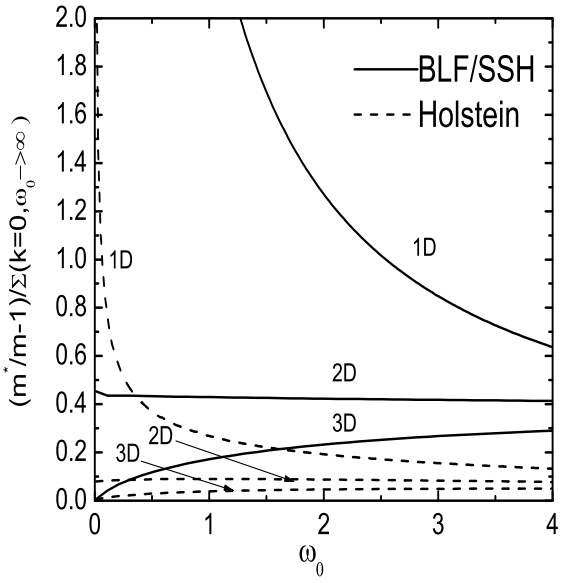

Figure 5.2: The electron effective mass, normalized to the 2^{nd} order correction to the energy for the anti-adiabatic limit, vs. characteristic phonon frequency, ω_0, for both the BLF-SSH and Holstein models, in one, two, and three dimensions, as indicated. In one dimension the effective mass diverges for both models, though the divergence is stronger for the BLF-SSH model, as indicated by Eq. (5.20). In two dimensions the effective mass approaches a constant as $\omega_0 \to 0$ for both models, while in three dimensions the effective mass ratio approaches unity in the same limit. At the opposite extreme, both one dimension results give $m^*/m \to 1$ as $\omega_0 \to \infty$, while in both two and three dimensions the effective mass remains above unity in this limit. Note that in all three dimensions, for a given reduction in energy as given by the 2^{nd} order correction to the energy, the BLF-SSH model results in significantly higher effective masses.

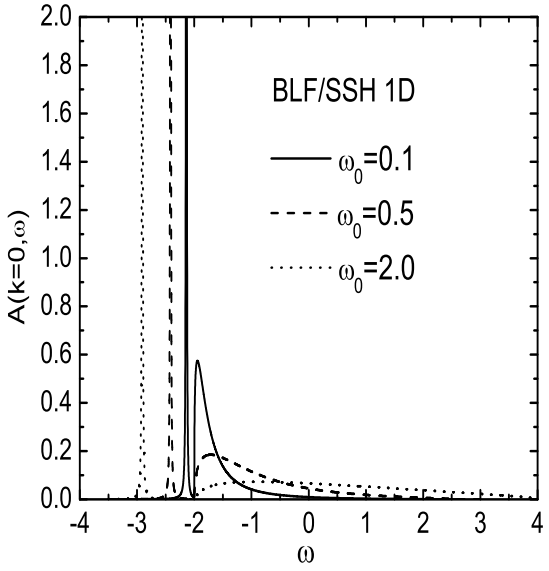

Figure 5.3: Spectral function for the BLF-SSH model, for $\lambda_{BLF} = 0.2$ for three different characteristic phonon frequencies, as a function of frequency. All three spectra are similar as one would find for the Holstein model, and consist of quasiparticle peak with weight $z_0 = 0.766, 0.727, 0.724$, for $\omega_0/t = 0.1, 0.5, 2.0$, respectively, followed by an incoherent piece.

energy lowering caused by a certain amount of coupling to phonons, regardless of the origin of that coupling. This plot now makes clear that the BLF-SSH model, within weak-coupling perturbation theory, has more 'polaronic' tendency than the Holstein model. Note in particular that the divergence (in one dimension) at low characteristic phonon frequency is much stronger for the BLF-SSH model, as Eq. (5.20) already indicated. Thus, as discussed above, we predict that in the one dimension adiabatic approximation, the system will always be polaronic, regardless of the coupling strength. This is borne out in by the full adiabatic calculations for the BLF-SSH model in the previous chapter. This is similar to the Holstein model,[57] and in disagreement with the result from the hybrid model defined in Ref. 71.

Otherwise, the behaviour of the effective mass in the two models is very

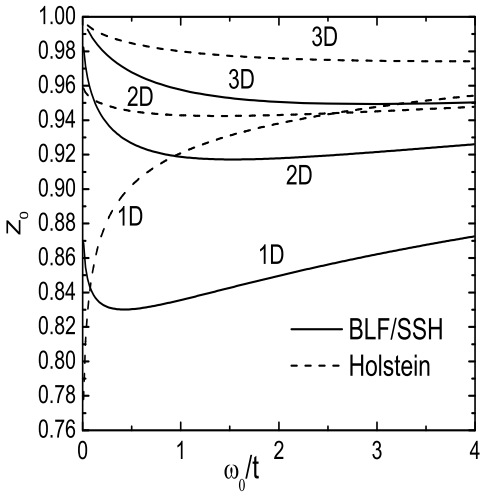

Figure 5.4: Quasiparticle residue, z_0 vs. ω_0/t for both the BLF-SSH and Holstein models in all three dimensions. Note that while the result for the Holstein model tends to be inversely proportional to the effective mass, this is not the case for the BLF-SSH model at low phonon frequency in one and two dimensions. In one dimension in particular, the effective mass diverges, while z_0 also turns upward.

similar, as a function of characteristic phonon frequency, for the various dimensions shown. The effective mass can be made arbitrarily close to unity, for any non-zero phonon frequency, for sufficiently weak-coupling. Numerical calculations indicate a free electron-like to polaron crossover,[22] similar to what was found for the Holstein model at least in the adiabatic limit.

5.3.4 Spectral function

It is interesting to examine the spectral function, defined by Eq. (5.11) (see also the discussion in the last section). For simplicity we show the result in one dimension, in Fig. 5.3, for the ground state ($k = 0$) as a function of frequency.

The results for two or three dimensions do not differ in any significant way from these results. The results for three different characteristic phonon frequencies are shown. In each case a quasiparticle δ-function is present (here

artificially broadened so as to be visible), followed by an incoherent piece; the incoherent part has energies ranging approximately from $-2t < \omega < +2t + \omega_0$. The quasiparticle residue, z_0 must be determined numerically, and is given in the figure caption for each of the cases considered (see also Fig. 5.4). We have verified that the remaining weight (the spectral functions each have weight unity) is present in the incoherent part. The result shown is not too different from what is found in the Holstein model;[58] the singularities from the one dimensional electron density of states are now smeared out in the incoherent piece, as a result of the coupling and phonon energy having some frequency dependence. Note that because we use perturbation theory, a gap appears between the quasiparticle part and the incoherent part. This is due to the fact that the incoherent part is entirely perturbative; hence, it starts at the *unperturbed* ground state energy, $-2t$, while the actual ground state energy (the location of the quasiparticle peak), within 2^{nd} order perturbation theory, is pushed to a lower value (see also Fig. 5.1). This would be the case even in the Holstein model, where the spectral function shows a gap exceeding ω_E in that case. In Fig. 3 of Ref. 58 the gap is *precisely* ω_E, in agreement with the exact result (shown in Fig. 2 of that reference), because that calculation is for *self-consistent* perturbation theory, where the *interacting* Green's function is used in the expression for the self-energy (in contrast, in our Eq. (5.7) we use the non-interacting Green's function in the expression for the self-energy). So in the BLF-SSH model, the exact result is expected to not have a gap between the coherent and incoherent parts of the spectral function, as the phonon frequencies in this model cover a range starting at zero energy. Note however, that the coupling goes to zero as the phonon frequency goes to zero, a sufficient condition to maintain a robust quasiparticle peak.

In Fig. 5.4 we show the quasiparticle residue as a function of ω_0 for both the Holstein and BLF-SSH models. The Holstein results tend to follow the inverse of the result for the inverse effective mass; this is as expected. This is not the

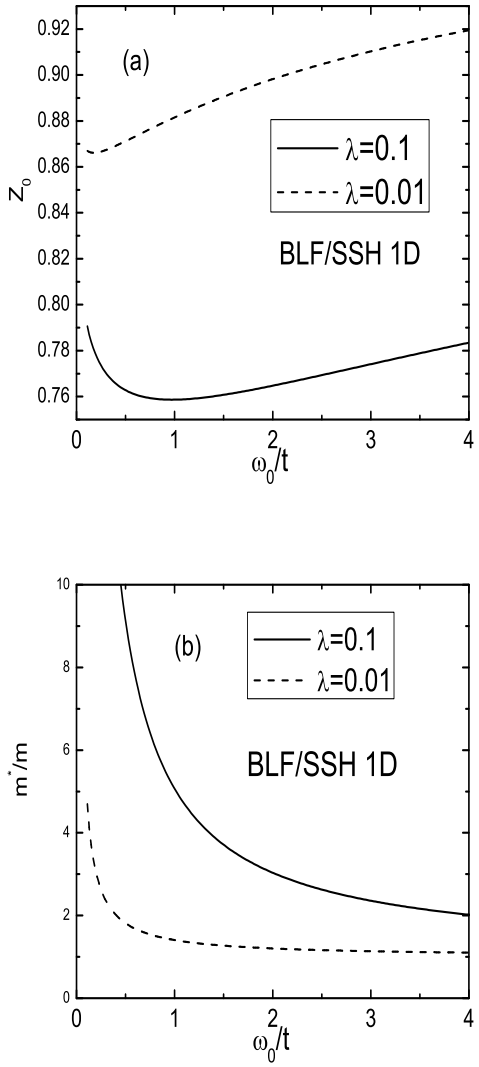

Figure 5.5: Comparison of the quasiparticle residue (upper panel) with the electron effective mass (lower panel) as a function of ω_0/t, for the BLF-SSH model in one dimension. The behaviour noted in Fig. 5.4 is clear here. Moreover, note the scales; while the effective mass ratio is very large (≈ 4) for $\lambda_{BLF} = 0.01$ and small values of ω_0/t, the quasiparticle residue remains within 15% of unity.

case with the BLF-SSH, but for more subtle reasons than the fact that the self energy is now momentum dependent. The more important effect, which shows up in both one and two dimensional results, is that the quasiparticle weight requires an evaluation of the frequency derivative of the self energy at the energy of the pole, whereas the effective mass in Rayleigh-Schrödinger perturbation theory requires the same derivative at the *non-interacting* ground state energy. Most noteworthy is that the quasiparticle residue shows a clear upturn at low characteristic phonon frequencies, while the inverse effective mass clearly approaches zero (see Fig. 5.2) as this characteristic frequency is taken to zero.

To see this more clearly we show in Fig. 5.5 a comparison of the residue (upper panel) vs. effective mass (lower panel), as a function of ω_0, for two (weak) strengths of electron-phonon coupling. At high phonon frequency, as the former decreases, the latter increases with decreasing phonon frequency, but at low phonon frequency, the two properties no longer behave in inverse fashion with respect to one another.

5.4 Summary

The BLF-SSH model appears to have very strong polaronic tendencies, stronger than those of, say, the Holstein model, especially in one dimension. This conclusion is based on the 2^{nd} order perturbative calculation performed in this chapter, but also has corroborative evidence from calculations in the strong-coupling regime. In one dimension we have been able to obtain an analytical solution for the ground state energy and the effective mass. The conclusion concerning polaronic behaviour is an important one, as much of what we know about polarons arises from Holstein-like models.[84] In particular, for a coupling strength that leads to a fixed amount of energy lowering (in 2^{nd} order), the effective mass can become an order of magnitude larger than the bare

mass, a clear indicator that perturbation theory breaks down. This occurs in the BLF-SSH model at much weaker coupling than in the Holstein model. We have also noted that the relationship between effective mass and quasiparticle residue breaks down in one and two dimensions for the BLF-SSH model, not because of the momentum dependence in the self energy, but because the two properties involve evaluation of the frequency derivative of the self energy at different energies. Future work will address the strong-coupling regime and these clarified calculations will assist in the develompent of algorithms for the full BLF-SSH model.

5.5 Supplemental Perturbation Theory Calculations

It is sometimes stated that for a momentum-independent self energy, the quasiparticle residue is equal to the inverse of the effective mass. This follows simply by comparing Eqs. (5.9) and (5.12). On the other hand, we have argued that Eq. (5.10) is more appropriate for the effective mass, in which case this statement appears not to be true. A resolution of this difficulty is straightforward for the Holstein model, which we outline below, but, interestingly, not possible for the BLF-SSH model, at least in one dimension. The essential difference appears to be that in the Holstein model the (phonon) excitations are gapped, whereas they are not in the BLF-SSH model because of the low-lying acoustic modes at small momentum transfer. Here we focus attention on one dimension, where some subtleties arise.

For the Holstein model the computation of the self energy in weak-coupling is straightforward.[43] We obtain

$$\Sigma_H(\omega) = \frac{2t\omega_E\lambda_H \mathrm{sgn}(\omega-\omega_E)}{\sqrt{(\omega-\omega_E)^2-(2t)^2}}. \tag{5.23}$$

The location of the quasiparticle pole at zero momentum (ground state) is then given by

$$\omega + 2t = -\frac{2t\omega_E\lambda_H}{\sqrt{(\omega-\omega_E)^2-(2t)^2}}, \tag{5.24}$$

which can readily be determined numerically. Denoting the solution by writing $\omega \equiv -2t - E_b$ (so E_b is the 'binding' energy below the bottom of the band), we can then use this in the spectral function, Eq. (5.11), to determine the residue z_0 in the quasiparticle peak at $\omega = -2t - E_b$:

$$A(k=0,\omega) = z_0\delta(\omega + 2t + E_b) + \text{incoherent part.} \tag{5.25}$$

Straightforward calculation gives

$$z_0 = 1/\left(1 + \frac{2\lambda_H\tilde{\omega}_E\left[1+2\tilde{\omega}_E+2\tilde{E}_b\right]}{\left[(1+2\tilde{\omega}_E+2\tilde{E}_b)^2-1\right]^{3/2}}\right), \tag{5.26}$$

which is *not* in agreement with the inverse of Eq. (5.22), except when λ_H is truly very small. Here $\tilde{E}_b \equiv E_b/(4t)$.

In particular, for arbitrarily small λ_H, $\partial\Sigma(\omega)/\partial\omega|_{\omega=-2t}$, which is used in Eq. (5.22), diverges as $\omega_E \to 0$, leading to a divergent effective mass (and therefore associated residue of zero). On the other hand, from Eq. (5.24) one readily sees

$$\lim_{\omega_E\to 0} E_b = t\big(\lambda\omega_E/t\big)^{2/3}, \tag{5.27}$$

from which Eq. (5.26) yields the result

$$\lim_{\omega_E\to 0} z_0 = 2/3, \tag{5.28}$$

surprisingly a universal number. The actual weight in the quasiparticle peak of the spectral function given by Eq. (5.11) for any given (even very small) value of λ_H actually tracks Eq. (5.26), and not the inverse of Eq. (5.22).

Interestingly, for the Holstein model, one can take a different tack towards

calculating the spectral function: using perturbation theory to compute the perturbed wavefunction, which is then inserted into the calculation for the matrix elements required in the definition of the spectral function,[85] one obtains

$$\begin{aligned} A_{\rm pert}(k=0,\omega) &= z_0^{\rm pert}\delta(\omega+2t+\frac{\lambda_H\omega_E}{\sqrt{(1+2\tilde{\omega}_E)^2)-1}}) \\ &+ \frac{1}{\pi}\frac{2t\omega_E\lambda_H}{(\omega+2t)^2}\frac{\theta(2t-|\omega-\omega_E|)}{\sqrt{(2t)^2-(\omega-\omega_E)^2}}. \end{aligned} \tag{5.29}$$

Note that there is no difficulty in integrating over this function, as the divergence in the denominator $(1/(\omega+2t)^2)$ is not within (or bordering) the range of frequency given by the Heaviside function restriction in the numerator. This is due to the finite phonon frequency, ω_E. From this expression fulfillment of the sum rule determines that

$$z_0^{\rm pert} = 1/\left(1+\frac{2\lambda_H\tilde{\omega}_E\left[1+2\tilde{\omega}_E\right]}{\left[(1+2\tilde{\omega}_E)^2-1\right]^{3/2}}\right), \tag{5.30}$$

which *is in agreement* with the inverse of Eq. (5.22). The message is that, as long as we use the expression given by Eq. (5.11) for the spectral function, the area under the quasiparticle peak will correspond to Eq. (5.26), which is *not* the inverse of the effective mass, even if the self energy is independent of momentum.

In the BLF-SSH model, the self energy is evaluated numerically through Eq. (5.7). An attempt to follow the procedure just outlined, which leads to Eqs. (5.29) and (5.30) for this model fails; this is because the minimum phonon frequency is zero, so the restriction corresponding to the Heaviside function in Eq. (5.29) yields $-2t < \omega < 2t+\omega_0$; this in turn makes the divergence at $\omega = -2t$ non-integrable. One can only (in one dimension) define the spectral function through Eq. (5.11), in which case the inverse of the effective mass differs from the quasiparticle pole for two reasons: the usual reason that the explicit momentum dependence now plays a role (see Eq. (5.10)), and, in

addition, the derivative of the self energy with respect to frequency is evaluated at $\omega = -2t$ for the effective mass, whereas it is evaluated at the frequency corresponding to the pole for the quasiparticle residue.

Eq. (5.7) or Eq. (5.13) is written as a function of momentum k, and it is of interest to estimate the range of validity of perturbation theory, as a function of k. In the Holstein model, this is clear: we require that $\epsilon_k < \epsilon_{k=0} + \omega_E$, otherwise the unperturbed state (with momentum k) no longer has lower energy than the perturbed state, also with total momentum k (but with an electron part with zero momentum). This leads to the condition (in one dimension) $k < 2\sin^{-1}\sqrt{\omega_E/4t}$, and this is verified, for example, in Fig. 5 of Ref. (10). For the BLF-SSH model the same criterion is $\epsilon_k < \epsilon_{k=0} + \omega_k$, which leads to the condition $k < 2\sin^{-1}(\omega_0/(4t)$, which is much more restrictive than for the Holstein model, consistent with the results for the effective mass shown in Fig. 5.2.

Chapter 6

Conclusions

In this thesis various polaron models have been discussed in light of the polaron's role in phonon-mediated superconductivity, concentrating on calculating the effective mass of a single electron. The large effective mass (practically infinite, or immobile electrons) found in the Holstein model at strong-coupling is disturbing, since many real phonon-mediated superconducters have a very large electron-phonon coupling coefficient. Since the standard Holstein model is still a rather crude approximation to the Hamiltonian of real materials, this thesis comprises exploratory calculations for a number of more realistic and complex models. A summary of these models and conclusions follows, along with suggestions for future research directions.

6.1 Next Nearest Neighbour Hopping Holstein Model

Adding next nearest neighbour hopping is the first step to producing a band structure that matches real materials. The simple nearest neighbour tight-binding model band structure is a far cry from the complex band structures plotted in text books for even relatively simple materials such as silicon. With

next nearest neighbor hopping and beyond we can produce any band structure that we wish. This work shows that this is possible with our algorithms and is not too computationally expensive, even for 3 dimensions.

On a more practical level, we followed up on a previous study [33] that suggested that longer range hopping could dramatically reduce the effective mass, and thus solve the apparent inconsistency between the Holstein model at strong-coupling and real strong-coupling superconductors. We reproduced their results for one dimension and then continued on to model two and three dimensions. The effective mass does change, but when the proper scaling is taken into account the effects are smaller and in the opposite direction than initially reported by Chakraborty et al. With our heuristic scaling we see that in three dimensions the effect at large lambda will not be strong enough to reduce the effective mass to reasonable levels, thus this does not completely solve the question of large effective masses.

The lack of a physical explanation for the heuristic scaling factor discovered is intriguing, especially given it has excellent predictive power in three dimensions. A further study that explained this would be most interesting, however the main point remains that these longer range hoppings are not the unique answer to the question of electron mobility at strong-coupling. In this light it seems more profitable to concentrate on other aspects of the polaron model.

6.2 Extended Range Interaction Holstein Model

The standard Holstein model makes the assumption that the electron can only influence the ion position of the ion that it is currently on. This is a simplification, as even with shielding, the Coulomb interaction decays as the Yukawa potential. We used an extended range interaction instead which included an electron-phonon interaction with the next nearest neighbours. This model again paves the way for realistic modeling of real materials from first prin-

ciples since the interaction can be tuned to match that of any real material.

We followed up on a two dimensional calculation by Alexandrov and Kornilovitch [53] which examined this model and reproduced their results for two dimensions as well as performing calculations in three dimensions. We were also able to go to a smaller ion frequency, which is a more physical parameter regime. This allowed us to draw different conclusions from their two dimensional results. While the effective mass is decreased by the extended interaction at strong-coupling it is not a large enough effect to lower the effective mass at strong-coupling to reasonable levels. In three dimensions there is again a small effect, but not large enough to allow for mobile electrons at a physical level of strong-coupling.

Like the next nearest neighbour hopping, the Hamiltonian used here is undoubtedly better than the standard model and important for the accurate modeling of real materials. We have ruled it out as the solution to the problem of immobile electrons at strong-coupling, but the algorithm and results here can be used as a starting point for more realistic calculations.

6.3 Acoustic Phonons

The BLF-SSH model seems to us a much more promising model than the extensions to the Holstein model, if only because it enables the modeling of a polaron and Cooper pair in the simplest possible situation: an elemental superconductor. Here there are only acoustic phonon modes so the Holstein model is not relevant. Unfortunately, inclusion of acoustic phonons model makes it much more difficult to solve than the Holstein model. While a great deal of effort was put forth trying to apply the same elegant Krylov space exact diagonalization techniques of the Holstein model to the BLF-SSH, we failed to find a similar technique.

We were, however, able to clear up the erroneus literature on the weak-

coupling perturbation theory and adiabatic limits for the BLF-SSH model even without a full quantum mechanical algorithm for polarons with acoustic phonons. We applied state of the art optimization techniques to adiabatic limit and found superior ground state energies for 1,2, and 3 dimensions. Since we verified the strong-coupling solutions with analytical calculations we are reasonably confident that we have found the true ground state solution. We also corrected the previously published perturbation calculations again with verification of our results by independent analytical means. Finally, the appendix contains some previously unpublished notes for a variational quantum mechanical wavefunction for the near adiabatic BLF-SSH model.

The strong-coupling adiabatic limit seems to indicate that the BLF-SSH model will also have a very large effective mass in this regime by analogy to the adiabatic Holstein calculations by Kabanov and Mashtakov [57]. We cannot say definitively that this is the case, but it would not be surprising that the BLF-SSH model also is unable to explain the discrepancy of electron mobility at strong-coupling. The BLF-SSH is still deserving of attention however, as the most basic superconducting Hamiltonian. The non-local nature of the acoustic polarons also means that algorithms developed for the BLF-SSH model may also have wider applicability.

6.4 Common Misconceptions

Finally, there are a couple of themes throughout this thesis that warrant parting remarks and which encompass all the models discussed. The first is the importance of using a low ion frequency. Any real material normally has an electron energy scale that is orders of magnitude larger than the phonon energy scale. This means that the ion frequency should be very small compared to the electron hopping term, and in general this makes numerical calculations much more difficult. Even with the algorithms presented in this thesis, the

low frequencies were always the hardest. Regardless of the difficultly, this is the physical regime, and the polaron models can look very different when the ion frequency is commensurate with the hopping t. The issue of large effective masses and abrupt crossovers into a strong-coupling regime is all smoothed away when large ion frequencies are used.

Secondly, perturbation theory is a very limited tool for the polaron problem. The weak-coupling perturbation theory considers only states with one phonon excitation which is a tiny sliver of the phase space at weak-coupling. As we have shown in detail in chapter 2, this is a many-body problem from the very start with many phonons needed even before the crossover into strong-coupling like solutions. The BLF-SSH model also requires a very large number of phonons which is part of the reason why the Krylov space methods were unsuccessful. Strong coupling perturbation theory is even worse, providing a qualitatively correct strong-coupling wavefunction, but with energies that differ from the exact results by orders of magnitude in the Holstein model. The perturbation theory calculations are still important and are invaluable for verifying new exact methods, but cannot tell us much about the parameter regime of real materials.

6.5 Final Remarks and Future Research Directions

In this thesis we have examined several extensions to the Holstein model in greater depth and have performed the groundwork for the quantum mechanical solution to the BLF-SSH model. The smoking gun of why the effective mass at strong-coupling is so high in these models compared to real materials was not found, and it is the author's opinion that this will not be solved until calculations involving multi-polaron interactions are possible. Cluster DMFT looks promising, as do many-electron adiabatic calculations, since the region

of parameter space of interest is close to the adiabatic limit.

The work in this thesis should provide a carefully checked starting point for those calculations as we have corrected several previously published works, particularity for the BLF-SSH model. We hope that this thesis will inspire more research into the BLF-SSH model and acoustic polarons since this will pave the way for true ab-initio calculations of the simplest elemental superconductors.

Bibliography

[1] R. P. Feynman. *Physics Review*, (97):660, 1955.

[2] T. D. Schultz. *Polarons and Excitons*. Oliver and Boyd, 1962.

[3] G. R. Allcock. *Polarons and Excitons*. Oliver and Boyd, 1962.

[4] G. L. Sewell. *Physics Review*, (129):597, 1963.

[5] T. Holstein. *Annals of Physics (New York)*, (8):325, 1959.

[6] S. Barišić, J. Labbé, and J. Friedel. *Physics Review Letters.*, (25):919, 1970.

[7] W. P. Su, J. R. Schrieffer, and A. J. Heeger. *Physics Review B*, (22):2099, 1980.

[8] P. E. Kornilovitch. *Physics Review Letters.*, (84):1551, 2000.

[9] J. T. Devreese and A. S. Alexandrov. *Reports on Progress in Physics*, (72):066501, 2009.

[10] Z. Li, D. Baillie, C. Blois, and F. Marsiglio. *Physical Review B*, (81):115114, 2010.

[11] C. P. J. Adolphs and M. Berciu. *Europhysics Letters*, (102):47003, 2013.

[12] J. E. Hirsch and E. Fradkin. *Physics Review Letters.*, (49):402, 1982.

[13] E. Fradkin and J. E. Hirsch. *Physics Review B*, (27):1680, 1983.

[14] R. T. Scalettar, N. E. Bickers, and D. J. Scalapino. *Physics Review B*, (40):197, 1989.

[15] F. Marsiglio. *Physics Review B*, (42):2416, 1990.

[16] M. Hohenadler, H. G. Evertz, and W. Linden. *Physics Review B*, (69):024301, 2004.

[17] S. Biermann. *Journal of Physics: Condensed Matter*, (26):173202, 2014.

[18] J. Bonča and S. A. Trugman. *Physics Review B*, (64):094507, 2001.

[19] B. Boykin, G. Klimeck, and F. Oyafuso. *Physics Review B*, (69):115201, 2004.

[20] C. J. Chandler, C. Prosko, and F. Marsiglio.

[21] C. J. Chandler and F. Marsiglio. *Physics Review B*, (90):125131, 2014.

[22] C. J. Chandler and F. Marsiglio. *Physics Review B*, (90):245149, 2014.

[23] Z. Li, C. J. Chandler, and F. Marsiglio. *Physics Review B*, (183):045104, 2011. Note that this work disagrees qualitatively with M. Zoli, Physica C**384**, 274 (2003), and references therein.

[24] J. Bardeen, L. N. Cooper, and J. R. Schrieffer. Theory of superconductivity. *Physical Review*, (108):1175–1204, 1957.

[25] A. S. Alexandrov. High-temperature superconductivity: the explanation. *Physica Scripta*, (83):038301, 2011.

[26] J. E. Hirsch, M. B. Maple, and F. Marsiglio. *Physica C*, (514):1–443, 2015.

[27] A. S. Alexandrov, editor. *Polarons in Advanced Materials*, volume 103. Springer Netherlands, 2007. See the many articles within.

[28] J. Bonča, S. A. Trugman, and I. Batistíc. Holstein polaron. *Physical Review B*, (60):1633, 1999.

[29] A. Alvermann, H. Fehske, and S. A. Trugman. *Physical Review B*, (81):165113, 2010.

[30] L-C. Ku, S. A. Trugman, and J. Bonča. Dimensionality effects on the holstein polaron. *Physical Review B*, (65):174306, 2002.

[31] Z. Li and F. Marsiglio. The polaron-like nature of an electron coupled to phonons. *Journal of Superconductivity and Novel Magnetism*, (25):1313, 2012.

[32] A. R. Davenport, J. P. Hague, and P. E. Kornilovitch. *Physics Review B*, (86):035106, 2012.

[33] M. Chakraborty, A. N. Das, and A. Chakrabarti. *Journal of Physics: Condensed Matter*, (23):025601, 2011.

[34] G. Gladstone, M. A. Jensen, and J. R. Schrieffer. *Superconductivity*, pages 665–816. Marcel Dekker, Inc., New York, 1969.

[35] G. M. Eliashberg. *Zh. Eksp. Teor.Fiz.*, (38):966, 1960. see also english translation: Sov. Phys. JETP **11** 696 (1960).

[36] D. J. Scalapino. *Superconductivity*, page 44. Marcel Dekker, New York, 1969.

[37] P. B. Allen and B. Mitrović. *Solid State Physics*, volume 37, page 1. Academic, New York, 1982.

[38] J. P. Carbotte. *Reviews of Modern Physics*, (62):1027, 1990.

[39] F. Marsiglio and J. P. Carbotte. *Superconductivity, Conventional and Unconventional Superconductors*, chapter Electron-Phonon Superconductivity, pages 73–162. Springer-Verlag, Berlin, 2008.

[40] The isotope effect is a notable exception, and experiments on Hg and Pb in particular confirmed that the BCS prediction that $T_c \propto M^{-\alpha}$, with $\alpha \approx 0.5$ was correct. This was followed by a lack of confirmation on many other (lower critical temperature) superconductors; an explanation for this was forthcoming once the direct Coulomb repulsion was accounted for (see, Zhou Li, Carl Chandler, Frank Marsiglio, Physical Review B **83**, 045104 (2011), W. Garland, Jr. Physics Review Letters. **11** 111 (1963) and 114 (1963), and the dozen or so papers in the first five references of his first paper) **103**, Springer Verlag, Dordrecht (2007).

[41] J. Bauer, J. E. Han, and O. Gunnarsson. *Physics Review B*, (84):184531, 2011.

[42] A. S. Alexandrov, V. V. Kabanov, and D. K. Ray. *Physics Review B*, (49):9915, 1994.

[43] F. Marsiglio. *Physica C*, (244):21, 1995.

[44] H. Fehske and S. A. Trugman. *Polarons in Advanced Materials*, volume 103, pages 393–461. Springer Netherlands, 2007.

[45] The primary advocate for the viewpoint that properties of the Holstein model are irreconcilable with a description of the electron phonon interaction based on the Migdal approximation has been A.S. Alexandrov. Aside from the quoted references, see, for example, *Polarons & Bipolarons*, by A. S. Alexandrov , N. F. Mott (World Scientific, Singapore, 1996).

[46] H. Fröhlich. *Proceedings Royal Society A*, (16):230, 1937.

[47] H. Fröhlich. *Polarons and Excitons, Scottish Universities' Summer School*, pages 1–32. Oliver and Boyd, Edinburgh, 1963.

[48] J.T. Devreese. *Polarons in Advanced Materials*, volume 103, pages 3–61. Springer Netherlands, 2007.

[49] C. G. Kuper and G. D. Whitfield, editors. *Polarons and Excitons*. Oliver and Boyd, Edinburgh, 1963. See the many articles contained therein.

[50] F. M. Peeters and J. T. Devreese. *Physics Review B*, (32):3515, 1985.

[51] W. B. da Costa and F. M. Peeters. *Journal of Physics: Condensed Matter*, (8):2173, 1996.

[52] G. A. Farias, W. B. da Costa, and F. M. Peeters. *Physics Review B*, (54):12835, 1996.

[53] A. S. Alexandrov and P. E. Kornilovitch. *Physical Review Letters*, (82):807, 1999.

[54] J. P. Hague and P. E. Kornilovitch. *Physics Review B*, (82):094301, 2010.

[55] I. G. Lang and Yu. A. Firsov. *Journal of Experimental and Theoretical Physics*, (16):1301, 1963.

[56] I. G. Lang and Yu. A. Firsov. *Soviet Physics Solid State*, (5):2049, 1964.

[57] V. V. Kabanov and O. Yu. Mashtakov. *Physics Review B*, (47):6060, 1993.

[58] F. Marsiglio. *Physics Letters A*, (180):280, 1993.

[59] This fact was also pointed out in Ref. [53] — see their Fig. 4, for example, but was de-emphasized in their work in favour of the effective mass decrease at higher coupling strengths.

[60] W. P. Su, J. R. Schrieffer, and A. J. Heeger. *Physics Review Letters.*, (42):1698, 1979.

[61] This modelling with optical phonons seems to have started with 71, and more recently with 72 and 73.

[62] P. H. de Oliveira Neto, W. F. da Cunha, L. F. Roncaratti, R. Gargano, and G. M. e Silva. *Chemical Physics Letters*, (493):283287, 2010.

[63] G. Zhang, P. Cui, J. Wu, and C. Liu. *Physica B*, (404):14851489, 2009.

[64] N. Miyasaka and Y. Ono. *Journal of the Physical Society of Japan*, (70):2968–2976, 2001.

[65] L.-C. Ku, S. A. Trugman, and J. Boncá. *Physics Review B*, (65):174306, 2002.

[66] C. P. J. Adolphs and M. Berciu. *Europhysics Letters*, (102):47003, 2013. This article discusses the issues concerning the validity of a linear expansion.

[67] E. M. Conwell and S. V. Rakhmanova. *Proceedings of the National Academy of Science USA*, (97):4556, 2000.

[68] R. M. Storn K. Price and J. A. Lampinen. *Differential Evolution: A Practical Approach to Global Optimization*. Springer, 2005.

[69] J. Hubbard. *Proceedings Royal Society A*, (276):238, 1963.

[70] J. Hubbard. *Proceedings Royal Society A*, (277):237, 1964.

[71] M. Capone, W. Stephan, and M. Grilli. *Physics Review B*, (56):4484, 1997.

[72] D. J. J. Marchand, G. De Filippis, V. Cataudella, M. Berciu, N. Nagaosa, N. V. Prokof'ev, A. S. Mishchenko, and P. C. E. Stamp. *Physics Review Letters*, (105):266605, 2010.

[73] M. Berciu and H. Fehske. *Physics Review B*, (82):085116, 2010.

[74] After this work was essentially complete, two articles 72, 73, appeared on the cond-mat archive. In the first case in particular, the authors carry out a study of what they call the Su-Schrieffer-Heeger model. In fact, they study a model in which the coupling of the electrons is to optical phonons; the model resembles the BLF-SSH model insofar as the ions couple to the

electronic motion (as opposed to electron charge density). Moreover, this model was studied earlier in Ref. (71), so we will refer to it as the CSG model to avoid confusion. Capone et al71 did not recognize that the ground state momentum in the CSG model would become non-zero for sufficiently strong coupling; in fact they refer to this region as 'non-physical'. In any event, the two new references appear to be unaware of the work of Capone et al. As we demonstrate in this paper, some very important differences result from the use of acoustic phonons.

[75] M. Zoli. *Physics Review B*, (66):012303, 2002.

[76] M. Zoli. *Solid State Communications*, (122):531, 2002.

[77] M. Zoli. *Physica C*, (384):274, 2003.

[78] The effective mass will in general be anisotropic, so the direction in which these derivatives are to be taken would have to be specified; we nonetheless retain this simple notation and avoid some cumbersome indices.

[79] G. D. Mahan. *Many-Particle Physics*. Kluwer Academic/Plenum Publishers, New York, 3rd edition edition, 2000.

[80] One needs to use the identities $\sin a - \sin b = 2\sin\left[(a-b)/2\right]\cos\left[(a+b)/2\right]$ and $\cos a - \cos b = -2\sin\left[(a-b)/2\right]\sin\left[(a+b)/2\right]$, and then the integral is straightforward.

[81] However, since in this model the coupling is to the motion of the electron, for a given 'strength' of coupling as given by α in this model, we expect the overall contribution here to grow as the number of nearest neighbours increases, whereas the same is not true for the Holstein model.

[82] Within perturbation theory, and with preliminary exact calculations in the strong coupling regime, the ground state remains fixed at $k = 0$ over all coupling strengths, in contrast to what happens in the CSG model.[74].

[83] As explained in Ref. (71), we utilize limiting procedures for the characteristic phonon frequency while keeping the effective spring constant fixed. This means that as the phonon frequency approaches zero the ion mass increases to keep the product $M\omega_0^2$ constant.

[84] We include Fröohlich models in this category, as the lattice displacement couples to the charge density, as occurs in the Holstein model. The only difference is that in Fröhlich models interaction is simply long range.

[85] See, for example, Eq. (3.120) in Ref. 79.

[86] S. Sivakumar. *International Journal of Theoretical Physics*, (53):1697–1709, 2014.

Appendix A

Variational Wavefunction for BLF-SSH

Here we propose a fully quantum mechanical wavefuntion for the BLF-SSH model using the adiabatic limit as a guide. The phonon part of the wavefunction has been treated with coherent states and the electron part treated as in the Trugman method. A potential path towards an exact refinement of this wavefunction is suggested.

A.1 Introduction

While unconventional, we will include in this last section a bit of unfinished work on finding an exact solution to the BLF-SSH model. As discussed previously, the BLF-SSH model is important to our understanding of polarons as the simplest acoustic polaron model, just as the original Holstein model was the simplest model of optical polarons. Due to time constraints, we were unable to solve the BLF-SSH model exactly. We did develop a functional framework and a variational wavefunction that we think is important to document.

A.2 Model

As we have previously discussed in chapters 4 and 5, the BLF-SSH model is much more difficult to solve because the phonon modes are non-local. There is no perturbative strong-coupling result, despite our best efforts to find one. The weak-coupling perturbation theory is valid only at very weak-coupling strengths if the Holstein model is any guide, so this is not super helpful in looking for the full exact solution. Let us begin by examining the adiabatic Hamiltonian since this is a problem we can solve. We will then use this as inspiration for a variational wavefunction and look at ways of refining it even further. Recall the Hamiltonian is

$$H = \sum_n [c_n^\dagger c_{n+1} + c_{n+1}^\dagger c_n](-t + \alpha(X_{n+1} - X_n)) + \frac{1}{2}K(X_{n+1} - X_n)^2 + \frac{P_n^2}{2M} \ . \quad \text{(A.1)}$$

In the strong-coupling adiabatic limit, the wavefunction describes the electron spread out over three sites, and two bonds are compressed as discussed in chapter 4. The first problem with creating a variational wavefunction arises with periodic boundary conditions. In the adiabatic limit $\langle P_n \rangle$ is zero (the ions have no kinetic energy) and one can use $x_{n+1} - x_n$ as a parameter, and all of the x_n are classical parameters not operators. We can't do that once we step into variational wavefunction territory since the ion displacements must be described by k-space phonons, so we consider a cluster of N ions and N phonon modes.

We do want to keep the electrons in real space though as this is at the heart of the Trugman method using Bloch's theorem which will be explained later.

To do this, we modify the Hamiltonian so that only the phonon part is

written in k-space,

$$H = \sum_n [c_n^\dagger c_{n+1} + c_{n+1}^\dagger c_n] \left\{ -t + \sqrt{\frac{\lambda_{BLF}\omega_0 W}{2N}} \sum_k (a_k + a_{-k}^\dagger) \frac{e^{ika(n+1)} - e^{ikan}}{|\sin k/2|} \right\} + \sum_k \omega_k a_k^\dagger a_k \ , \tag{A.2}$$

where

$$\omega_k = \omega_0 |\sin k/2| \tag{A.3}$$

and

$$\lambda_{BLF} \equiv \frac{\alpha^2}{M\omega_0^2} \frac{1}{W} \ . \tag{A.4}$$

The adiabatic limit has classical ions with quantum mechanical electrons. Since classical mechanics is simply a special case of quantum mechanics, we can translate this solution into a wavefunction. The wavefunction for a classical simple harmonic oscillator is a coherent state, so the simplest possible variational wavefunction will look like:

$$c_0^\dagger \prod_k e^{g_k a_k^\dagger} e^{|g_k|^2/2} \ , \tag{A.5}$$

or

$$c_0^\dagger e^{\sum_k g_k a_k^\dagger - \frac{1}{2} g_k g_k^*} \ . \tag{A.6}$$

The g_k are the variational parameters, which define the expectation values of the ion displacements and the electron is in real space at site 0. We'd like to start with the g_k values that correspond to the ion displacements that we determined in the adiabatic limit, so we examine the expectation value of a single ion site, n,

$$\langle c_0 e^{\sum_{k'} g_{k'} a_{k'} - \frac{1}{2} g_{k'} g_{k'}^*} | X_n | c_0^\dagger e^{\sum_{k''} g_{k''} a_{k''}^\dagger - \frac{1}{2} g_{k''} g_{k''}^*} \rangle \ . \tag{A.7}$$

This is in real space with the phonon modes in k-space, so to go back and forth when using periodic boundary conditions we can use:

$$x_n = \frac{1}{\sqrt{N}} \sum_k x_k e^{ikan} \tag{A.8}$$

$$x_k = \frac{1}{\sqrt{N}} \sum_n x_n e^{-ikan} \tag{A.9}$$

$$x_k = \sqrt{\frac{\hbar}{2M\omega_k}}(a_k + a_{-k}^\dagger) \tag{A.10}$$

Here we let the lower case x_n , x_k refer to the classical adiabatic variational parameters. Uppercase X_n and X_k will be reserved for operators, with n and k referring to the real space and wavevector space respectively. We now can consider what the expectation value of X_k is, and then use those to find the expectation value of X_n.

$$\langle X_k \rangle = \langle c_0 e^{\sum_{k'} g_{k'} a_{k'} - \frac{1}{2} g_{k'} g_{k'}^*} | X_k | c_0^\dagger e^{\sum_{k''} g_{k''} a_{k''}^\dagger - \frac{1}{2} g_{k''} g_{k''}^*} \rangle \tag{A.11}$$

$$= \langle c_0 e^{\sum_{k'} g_{k'} a_{k'} - \frac{1}{2} g_{k'} g_{k'}^*} | \sqrt{\frac{\hbar}{2M\omega_k}}(a_k + a_{-k}^\dagger) | c_0^\dagger e^{\sum_{k''} g_{k''} a_{k''}^\dagger - \frac{1}{2} g_{k''} g_{k''}^*} \rangle \ . \tag{A.12}$$

We know that from the Baker-Campbell-Hausdorff theorem,

$$a_k e^{g_k a_k^\dagger - |g_k|^2/2} = g_k e^{g_k a_k^\dagger - |g_k|^2/2} \ . \tag{A.13}$$

So we can simplify this to be:

$$\langle X_k \rangle = \langle c_0 e^{\sum_{k'} g_{k'} a_{k'} - \frac{1}{2} g_{k'} g_{k'}^*} | \sqrt{\frac{\hbar}{2M\omega_k}}(g_k + g_{-k}^\dagger) | c_0^\dagger e^{\sum_{k''} g_{k''} a_{k''}^\dagger - \frac{1}{2} g_{k''} g_{k''}^*} \rangle \tag{A.14}$$

To simplify our notation we define:

$$| c_0^\dagger e^{\sum_k g_k a_k^\dagger - \frac{1}{2} g_k g_k^*} \rangle = | \psi \rangle \tag{A.15}$$

which gives:

$$\langle X_k \rangle = \langle \psi | X_k | \psi \rangle = \langle \psi | \psi \rangle \sqrt{\frac{\hbar}{2M\omega_k}} (g_k + g^*_{-k}) = \sqrt{\frac{\hbar}{2M\omega_k}} (g_k + g^*_{-k}) \quad \text{(A.16)}$$

At this point we start making assumptions, namely, that g_k is real and thus $g_k = g^*_k$. This is reasonable since the imaginary part of a coherent state is the momentum and in our adiabatic approximation we have said that ions are stationary, i.e. have no kinetic energy or momentum.

$$x_k \sqrt{2M\omega_k} = g_k + g^*_{-k} \quad \text{(A.17)}$$

We set $\hbar = 1$ from our choice of units so:

$$g_k \propto \frac{x_k \sqrt{2M\omega_k}}{2} \quad \text{(A.18)}$$

We say proportional to, since this derivation has $M\omega_0$ in it which is infinite in our adiabatic approximation. By trial and error we found an analytic form which makes our wavefunction give the same energies as the adiabatic calculation for small ω_0:

$$g_k = \frac{x_k 4 \sqrt{\omega_k \lambda 2}}{\omega_0} \quad \text{(A.19)}$$

We know that x_k and x_n are simply related as Fourier transforms presented above. Thus to find x_k for any k, we need to know all of the x_n for every n. We can take any adiabatic semi-classical arrangement of ions to find the x_n values and then find all of the g_k for given parameters of λ and ω_0.

However this only considers the electron at the origin. To make a variational wavefunction, it makes sense to use the Trugman Method idea of implicit Bloch's theorm. We will only consider wavefunctions with the electron at site 0 such as:

$$|\psi\rangle = c_0^\dagger | e^{\sum_k g_k a_k^\dagger - \frac{1}{2} g_k g_k^*} \rangle \quad \text{(A.20)}$$

This is implicitly short hand for the Bloch wavefunction:

$$|\psi\rangle = \frac{1}{\sqrt{N}} \sum_m e^{-ik_g am} c_m^\dagger |e^{\sum_k g_k a_k^\dagger - \frac{1}{2} g_k g_k^*}\rangle \tag{A.21}$$

where k_g is the total momentum of the polaron. Thus when we have an electron hop and have a state such as:

$$c_1^\dagger |e^{\sum_k g_k a_k^\dagger - \frac{1}{2} g_k g_k^*}\rangle \tag{A.22}$$

we can write instead:

$$e^{ik_g a} c_0^\dagger |e^{\sum_k g_{k,1} a_k^\dagger - \frac{1}{2} g_{k,1} g_{k,1}^*}\rangle \tag{A.23}$$

Here, since the electron was moved in the negative direction, the phonon distortion needs to be shifted plus one so that the distortion of ion 1 for the g_k is now the distortion of ion 2 for the $g_{k,1}$. In general:

$$g_{k,m} = \frac{1}{\sqrt{N}} (\sum_n x_{n+m} e^{ikan}) 4 \frac{\sqrt{2\lambda\omega_k}}{\omega_0} \tag{A.24}$$

This means only states with the electron at site zero need to be considered. With N states (N being the size of our finite cluster of ions), each using the adiabatic ion positions shifted, we can reproduce exactly the same energy as found with the semi-classical machinery with:

$$|\phi\rangle = \sum_m c_m c_0^\dagger e^{\sum_k g_{k,m} a_k^\dagger - \frac{1}{2} g_{k,m} g_{k,m}^*} \tag{A.25}$$

The c_m can be determined independently by diagonalizing the basis space of coherent states, but are also the electron wavefunction coefficients from the adiabatic calculation.

The question is now how to improve the wavefunction for a larger ω_0. While we used the adiabatic ion positions to come up with this variational wavefunction, we can try different g_k for other states to try to improve the wavefunction.

One may think of the N x_n or equivalently the x_k parameters as the variational parameters, and create many different basis states using different sets of x_n or x_k. Complex x_n are also permitted as these give states with a $\langle p \rangle \neq 0$ and $\langle x \rangle$ remains real.

Using coherent states means that there is no guarantee that basis states are orthogonal. In fact, there is always a non-zero overlap between two coherent states, but near the adiabatic limit basis states that represent very different ion configurations have an overlap that is negligible for double precision floating point calculations. States with very similar ion configurations, that is the x_n values are very close can have a large overlap approaching unity, so we need to consider how to treat a non-orthogonal basis.

The eigenvalue problem is:

$$H|\phi\rangle = E|\phi\rangle \tag{A.26}$$

Where $|\phi\rangle$ is the unknown ground state wavefunction. Since the coherent states form an overcomplete basis, we can expand in terms of those:

$$|\phi\rangle = \sum_n c_n |\psi_n\rangle \tag{A.27}$$

To obtain the energy we take the expectation value of the Hamiltonian:

$$\langle\phi|H|\phi\rangle = E\langle\phi|\phi\rangle = E\sum_{n,m} c_n c_m^* \langle\psi_m|\psi_n\rangle \tag{A.28}$$

S is the overlap matrix, where:

$$S_{m,n} = \langle\psi_m|\psi_n\rangle \tag{A.29}$$

We can also write out H in matrix form:

$$H_{m,n} = \langle \psi_m | H | \psi_n \rangle \tag{A.30}$$

In the basis of $|\psi_n\rangle$ we have:

$$\sum_{n,m} c_m^* c_n H_{m,n} = E \sum_{n,m} c_m^* S_{m,n} c_n \tag{A.31}$$

This is the generalized eigenvalue problem:

$$\sum_{n} H_{m,n} c_n = E \sum_{n} S_{m,n} c_n \tag{A.32}$$

Thus once our basis of $|\psi_n\rangle$ has been decided on, H and S matrices can be calculated, and the ground state energy found by using the appropriate algorithm for the generalized eigenvalue problem.

To set up the Hamiltonian for use with coherent states, consider:

$$\langle h | H | p \rangle \tag{A.33}$$

$$|p\rangle = c_0^\dagger e^{\sum_k p_k a_k^\dagger - \frac{1}{2} p_k p_k^*} \tag{A.34}$$

$$|h\rangle = c_0^\dagger e^{\sum_k h_k a_k^\dagger - \frac{1}{2} h_k h_k^*} \tag{A.35}$$

We break down the Hamiltonian into three parts for simplicity, first is the ordinary electron hopping:

$$H_t = -t(c_n^\dagger c_{n+1} + c_{n+1}^\dagger c_n) \tag{A.36}$$

The phonon mediated electron hopping:

$$H_{interaction} = [c_n^\dagger c_{n+1} + c_{n+1}^\dagger c_n] \left\{ \sqrt{\frac{\lambda_{BLF}\omega_0 W}{2N}} \sum_k (a_k + a_{-k}^\dagger) \frac{e^{ika(n+1)} - e^{ikan}}{|\sin k/2|} \right\} \tag{A.37}$$

The bare phonon hamiltonian:

$$H_{phonon} = \sum_k \omega_k a_k^\dagger a_k \tag{A.38}$$

These are quite complicated, so it helps to introduce:

$$\langle h|\alpha X_n|p\rangle = 8\lambda(x_{n,p} + x_{n,h}^*)\langle h|p\rangle \tag{A.39}$$

The extra subscript on the x_n is for determining which state it came from, though the complex conjugate on the second hints that it came from the bra.

We set $M = 1, \hbar = 1$ in these calculations, which gives a reasonable scale to the expectation values for our parameters. Then $H_{interaction}$ can be viewed as we initially introduced it:

$$H_{interaction} = [c_n^\dagger c_{n+1} + c_{n+1}^\dagger c_n](\alpha(X_{n+1} - X_n)) \tag{A.40}$$

Also helpful to keep the equations tidy are the definitions of the coherent states that are produced from the electron hopping.

$$|\overrightarrow{p}\rangle = |c_0^\dagger e^{\sum_k p_{k,+1} a_k^\dagger - \frac{1}{2} p_{k,+1} p_{k,+1}^*}\rangle \tag{A.41}$$

$$|\overleftarrow{p}\rangle = |c_0^\dagger e^{\sum_k p_{k,-1} a_k^\dagger - \frac{1}{2} p_{k,-1} p_{k,-1}^*}\rangle \tag{A.42}$$

Thus after some algebra one may obtain:

$$\langle h|H_t|p\rangle = -te^{-ik_g a}\langle h|\overrightarrow{p}\rangle + -te^{ik_g a}\langle h|\overleftarrow{p}\rangle \tag{A.43}$$

$$\langle h|H_{interaction}|p\rangle = e^{-ik_g a}8\lambda[(p_{1,+1}+h_1^*)-(p_{0,+1}+h_0^*)]\langle h|\overrightarrow{p}\rangle + e^{ik_g a}8\lambda[(p_{0,-1}+h_0^*)-(p_{-1,-1}+h_{-1}^*)]\langle h|\overleftarrow{p}\rangle \quad \text{(A.44)}$$

Note that the p_n values are taken from the original $|p\rangle$ state and thus after the electron pushes and remapping the indices are not the same as for $\langle h|$.

$$\langle h|H_{phonon}|p\rangle = \sum_k \omega_k (\sum_n h_n g(k)_n)(\sum_{n'} p_{n'} g(k)_{n'})\langle h|p\rangle \quad \text{(A.45)}$$

The Trugman Method added basis states using a Krylov method where the Hamiltonian acting on a given basis state produced new basis states which where added to the basis space. With coherent states this is not so simple. When the Hamiltonian produces a state like:

$$a_q^\dagger c_0^\dagger e^{\sum_{n,k} c_n g(n)_k a_k^\dagger} \quad \text{(A.46)}$$

There is no way to simplify in terms of coherent states. This has overlap with every other coherent state due to their non-orthogonality. One can keep the state un-simplified as what is called an Agarwal state or phonon-added state. This makes dot products and expectation values complicated, but a system along these lines was implemented by the author. A good explanation of these states can be found in Ref. [86] .

The main problem with this is that the newly created phonon-added states are very similar to the original state, and the overlap is very close to unity. This means that the S matrix is almost singular and as the states are added S quickly becomes intractable with standard floating point arithmetic. Thus this approach did not lead to any improvement upon the original variational wavefunction.

Instead of strictly following the Krylov space method for adding states, a

different approach was tried to find new coherent state basis states. The ideal coherent state is one that has a large overlap with the phonon-added state discussed above but is also significantly different from the other states already included in the basis space so that S remains invertible. S is never actually inverted, a generalized eigensolver routine is used. This routine fails at about the same point that inversion does and for the same reason; that S has off diagonal elements very close to one.

New states are chosen then with a conjugate gradient optimization routine that tries to maximize the overlap of the new state with the phonon-added state previously discussed, while at the same time a penalty function is included to keep the new state from having too much of an overlap with other states. This is a variable that has to be adjusted heuristically. If the penalty is too severe and the new state is very far from the phonon-added state, it will not improve the wavefunction much. If the penalty is too small, all the problems of singular S arise again.

Thus the optimization equation for electron-phonon interaction looks like:

$$O = |\langle B|H_{interaction}|C\rangle| + P(|B\rangle) \tag{A.47}$$

for

$$P(|B\rangle) = F\sum_{n} f(|\langle B|C_n\rangle|) \tag{A.48}$$

v is the overlap limit, a parameter that needs to be adjusted for the optimum basis space creation. F is a constant that is used to control the magnitude of the penalty. This is another variable but generally the optimization is done multiple times with F increasing each time so that optimizer is sure to avoid the existing states $|C_n\rangle$. In practice, optimization routines are not super reliable as noted in the previous discussion of the adiabatic BLF-SSH model. This means that the overlap with other states is often larger than desired or that a poor solution is found that is not close to what a full Krylov space would produce.

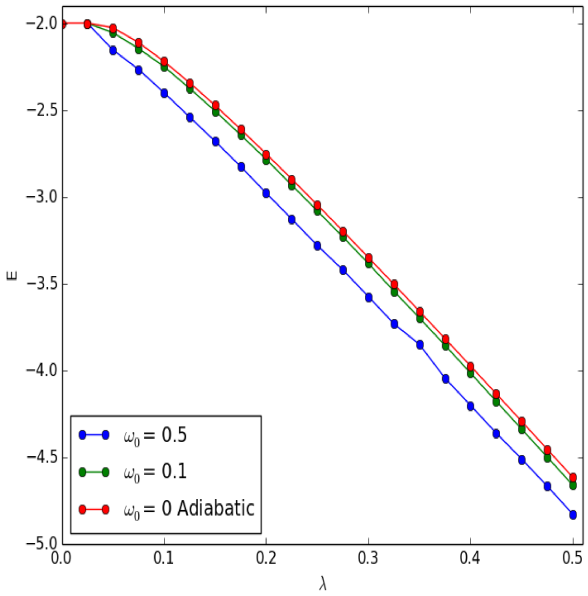

Figure A.1: Here we plot the variational energies for $\omega_0 = 0.1$ and $\omega_0 = 0.5$ along with the adiabatic results for a 10 site cluster. The general trend is similar to the Holstein model, the energy decreasing with increasing ω_0 and it appears to be always polaronic, in agreement with the perturbation results. Note that the variational method fails at low lambda, that is, for the data point at $\lambda = 0.02$ the variational energies are not lower than the adiabatic. This means a comparison with the perturbation theory is unhelpful.

The optimization here was implemented with both the conjugate gradient method and the differential evolution algorithm. The differential evolution algorithm is in general more robust when finding the true global minimum or maximum, however it is also much slower. The speed is important since each energy calculation requires hundreds of optimizations. A comparison of the two methods at $\lambda = 0.5$ showed the same variational energy and thus the conjugate gradient method is probably sufficient.

A.3 Future Directions

The uncertain nature of the variational process makes it hard to draw any firm conclusions from these calculations. Their usefulness is limited to a starting point for better exact approaches such as projector methods. One starts with a good estimation of the ground state $|\theta\rangle$ which could be the wavefunction from the semi-classical adiabatic calculations or the product of the further optimizations discussed previously. In the (unknown) eigenbasis of the Hamiltonian, this is:

$$|\theta\rangle = \sum_n c_n |\phi_n\rangle \ , \tag{A.49}$$

where $|\phi_n\rangle$ are the eigenvectors of the Hamiltonian and c_n are the coefficients. Since $|\psi\rangle$ is only a guess at the ground state, all of the eigenvectors will probably contribute. The closer our guess however, the larger the c_0 coefficient will be. We then act on $|\theta\rangle$ with $D = -H - A$ where H is the Hamiltonian and A is a constant:

$$D \sum_n c_n |\phi_n\rangle = \sum_n c_n \cdot (-E_n - A)|\phi_n\rangle \tag{A.50}$$

We pick A such that $(-E_0 - A)$ is the largest of all relevant $(-E_n - A)$. Thus acting with D^m progressively favours the ground state, and in the limit of large m:

$$D^m \sum_n c_n |\phi_n\rangle \approx c_0(-E_0 - A)^m |\phi_0\rangle \tag{A.51}$$

With this approach the hard part is calculating $\langle\psi|H^m|\psi\rangle$ and the other large powers of H. On may insert identities to transform it into a multi-dimensional integral:

$$\langle\theta|H^m|\theta\rangle = \int \cdots \int dx_1 \ldots dx_m \langle\theta|H|x_1\rangle\langle x_1|H|x_2\rangle \ldots \langle x_m|\theta\rangle \tag{A.52}$$

This can then in theory be solved using Monte Carlo integration in the basis of one's choice. There still exists a sign problem, but it may be tractable if

the initial guess is good enough. In our implementation, we were unable to find convergence. This does not mean that this is impossible, however, since we are not Monte Carlo experts. However, it does mean that the variational wavefunction must be very good to begin with. We thank Dr. Kevin Beach for his help with the theory of Projector Monte Carlo.

A more straightforward, if time consuming, approach is to analytically write out the expressions for H^2 , H^3 etc. using the commutation relations to simplify their use with coherent states. Then a projector method can be used to find the ground state energy, effective mass, and other observables. The Hamiltonian has 5 basic parts: 2 t electron hopping parts, 2 interaction electron hopping parts, and a phonon part. For H^m this is then an operator with 5^m terms, each of which needs to be simplified. This means that realistically a computer algebra system would be needed to go beyond H^2. It's possible that then 10's of thousands of terms would be doable leading to perhaps H^7 which might be enough to converge the energy and effective mass. Unfortunately due to time constraints this approach was not tried.